POLISH MARITIME RESEARCH

No 2(65)   2010   Vol 17

CONTENTS

POLITECHNIKA GDAŃSKA / POLYTECHNICA GEDANENSIS
PATRIAE MARIQUE FIDELIS

Editorial

POLISH MARITIME RESEARCH is a scientific journal of worldwide circulation. The journal appears as a quarterly four times a year. The first issue of it was published in September 1994. Its main aim is to present original, innovative scientific ideas and Research & Development achievements in the field of :

Engineering, **Computing & Technology**, **Mechanical Engineering**,

which could find applications in the broad domain of maritime economy. Hence there are published papers which concern methods of the designing, manufacturing and operating processes of such technical objects and devices as : ships, port equipment, ocean engineering units, underwater vehicles and equipment as well as harbour facilities, with accounting for marine environment protection.

The Editors of POLISH MARITIME RESEARCH make also efforts to present problems dealing with education of engineers and scientific and teaching personnel. As a rule, the basic papers are supplemented by information on conferences , important scientific events as well as cooperation in carrying out international scientific research projects.

Scientific Board

Preliminary Designing Method of External Pressure Vessels for Sea Subsurface Applications

Jan P. Michalski, Assoc. Prof.
Gdansk University of Technology
Polish Naval University

ABSTRACT

This paper describes a unique engineering method intended for the preliminary designing of marine echo-location systems. The solved designing problem consists in determining geometrical parameters and selecting structural materials for a vessel of a buoyancy necessary to contain measuring instruments of a given mass, as well as its maximum gabarites and operational submersion depth. The assumed variability range of the system's parameters determines a space of permissible applicability parameters of the method. Stress level related to permissible and critical stresses was assumed to be safety criterion for the vessel. The method may be applied also to solving converse problems consisting in determining maximum permissible submersion depth for a vessel made of assumed structural materials and having given geometrical parameters. The presented description of the method is illustrated by an example of its application.

Keywords: subsurface buoy mooring systems; external pressure vessels

INTRODUCTION

Tight submerssible vessels intended for the fulfilling of assumed functions deep in water, capable of carrying large external hydrostatic loads find many civil and military applications such as submarines and submersible vehicles, bathyscaphes, crude-oil and gas storage tanks, or casings for measurement apparatus to conduct underwater oceanological experiments [3]. For example, the measuring, recording and investigating of physical fields of seas and oceans is conducted by means of echo-location systems (*Subsurface buoy mooring systems*) composed of such elements as:
− floats (buoys of a required buoyancy)
− vessels containing measuring and recording apparatus
− vessels containing electric storage batteries
− anchoring device in the form of ballast
− tension members joining elements of a module.

The system's elements are connected to each other by means of elastic tension members, i.e. cables or chains. The vessel's shell plating is loaded by hydrostatic pressure proportional to submersion depth, sometimes also by a hydrodynamic load due to water current or surface wave motion. Also, concentrated loads generated by tension members are applied to the vessel. For functional reasons the vessel's structure should ensure its buoyancy, shape and watertightness to be maintained.

This paper contains a description of the engineering method for the preliminary designing of echo-location system, which serves to determining design solutions satisfying a set of functional, technological and mechanical assumptions. Original algorithms for the determining of parameters of vessels subjected to action of external pressure – in the aspect of their buoyancy, shell structure strength and form stability – are also presented in it.

Applicability of the method is determined by ranges of permissible values of vessel's form parameters, external pressure values as well as a kind of structural material. The method may be useful in particular for the preliminary designing of echo-location systems (*Subsurface buoy mooring systems*) within the area of:
− designing their geometrical configuration
− designing geometrical parameters of their vessels
− selection of their structural materials
− assessment of quantity of their mass
− determining optimum design solutions in an assumed sense.

FORMULATION OF DESIGNING PROBLEM

The designing problem consists in determining geometrical parameters and selection of a structural material for a vessel of a given effective buoyancy, capable of accommodating measurement apparatus of a given mass and dimensions, at a given operational submersion depth. Variability range of parameters for which calculation algorithms of the method have been elaborated, determines a space of permissible parameters for its application. The method makes it possible to solve also converse problems, namely determination of a maximum

permissible submersion depth of a vessel made of a given structural material and having given geometrical parameters.

An axially symmetrical vessel is considered of empty interior (a float) or containing measurement apparatus of the mass m_a and maximum linear dimension l_a; a part of the vessel can be filled with a lightweight material, e.g. polyurethane foam in order to maintain buoyancy of the vessel in the case of flooding its interior by water due to damage or loss of watertightness of its shell plating. The effective displacement D_e of the vessel of the volume V, plating surface area S and constant shell plating thickness h, immersed in water of the constant density ρ_w, is described by the buoyancy equation in which:

− $\alpha = 0$ - in the case of keeping the vessel tight
− $\alpha = 1$ - in the case of flooding the vessel entirely

$$D_e = (1-\alpha) \cdot \rho_w \cdot V + \alpha \cdot \rho_w \cdot \left(\frac{m_a}{\rho_a} + \frac{m_f}{\rho_f} + S \cdot h \right) +$$
$$- (m_v + m_a + m_f) \pm \frac{F_z}{g} \quad (1)$$

where:
g - gravity acceleration
m_v - mass of vessel plating
ρ_v - density of vessel plating material
m_a - mass of apparatus
ρ_a - average density of apparatus
m_f - mass of filler
ρ_f - density of filler (foam)
F_z - value of external concentrated load

Balance of components of mass and displacement of vessel in Eq. (1) can be described by the following important design parameters of the system:
− the geometrical parameters of the vessel, V, S, h
− the density of structural material of its shell plating, ρ_v
− the mass of apparatus inside the float, m_a, and its average density ρ_a
− the maximum linear dimension of the apparatus, l_a
− the filler volume V_f and its density ρ_f
− value of the external load F_z

The balance equation is then expressed by the equivalent relation as follows:

$$D_e = (1-\alpha) \cdot \rho_w \cdot V + \alpha \cdot \rho_w \cdot \left(\frac{m_a}{\rho_a} + V_f + S \cdot h \right) +$$
$$- S \cdot h \cdot \rho_p - m_a - V_f \cdot \rho_f \pm \frac{F_z}{g} \quad (2)$$

Positive value of the right-hand side of Eq.(2) as well as positive sign of the external load Fz stands for senses of forces opposite to gravity force. In Eq. (2) the belonging of parameters either to the set of the parameters to be determined or that of given ones constitutes a tag of variant of the method for preliminary designing the float. To achieve an effective solution of Eq. (2) it is necessary to add complementary equations whose set and genealogy constitute another tag of the designing method. In the case of the method formulated in the form of an optimization problem Eq. (2) should be complemented by:
− a criterion of choice of an optimum solution
− a set of inequalities which restrain allowable solutions.

The elaborated calculation algorithms of the method concern the designing process of vessels having axially symmetrical shells of circular cross-section, made of:

− NW 210 steel of normal strength
− AL 5085 aluminium alloy usually applied in shipbuilding.

The range of permissible parameters of the method in question was so selected as to make it possible to obtain geometrical dimensions, form proportions, structural material as well as maximum operational submersion depth which would satisfy requirements for echo-location research systems for Baltic Sea environment.

A hazard to structural safety of a vessel subjected to action of high external pressure may result either from exceedance of reduced permissible stresses or critical stresses leading to loss of form stability (buckling) of its shell plating [1, 2, 4], in consequence to loss of its functional qualities. The method in question covers the whole range of elastic deformations up to the material yield point R_e; the vessel's parameters are so determined as to obtain reduced stresses as well as critical stresses which do not exceed their permissible values at an external load enlarged by safety factor.

ASSUMPTIONS AND GEOMETRICAL DESCRIPTION OF FORM OF VESSEL

Vessel's shell plating is composed of a cylindrical casing of circular cross-section closed by two bottoms of a specific form which ensures moment-less state of stresses in the shell plating. The choice of such form of the vessel results from its usefulness to accommodate measurement apparatus and a simpler process of its manufacturing in contrast to spherical vessels. In accordance with the linear theory of stability of thin-walled elastic shells permissible values of the vessel plating thickness h were assumed much smaller than the curvature radius R of shell casing. Effects of possible geometrical imperfections of shell form were taken into account by safety factor increasing calculation external loads. The shell surface area of the vessel is assumed the same as the middle surface area of the shell plating. Structural mathematical models for determining structural strength and stability of shells as well as reccomended values of safety factors were taken from the respective subject-matter literature sources [1, 2, 3, 4].

Form of bottom's surface

The bottoms constitute support for vessel casing loaded by constant pressure. The desired momentless state of internal forces in shell plating will occur at an appropriate form of the bottoms. In the case of convex bottoms such form can be described by an appropriate plane curve (directrix) whose rotation around cylinder's axis generates, at vessel's bottom/ shell casing contact, a surface of the circumferential curvature radius $R_\varphi = R$ and axial curvature radius $R_z = \infty$, which are consistent with curvatures of the shell casing. The requirement is fulfilled by the bottom surface of the directrix described by the following relation [4]:

$$\zeta = (1-\xi^2)^{\frac{1}{t}} = \left[1 - \left(\frac{r}{R} \right)^2 \right]^{\frac{1}{t}} \quad (3)$$

where:
$t \in \mathbf{R} > 2.0$ - index exponent - a real number
$\xi = \frac{r}{R}$ - dimensionless radius of vessel, $0 \leq \xi \leq 1$
$\zeta = \frac{z}{l_d}$ - dimensionless camber of bottom, $1 \leq \xi \leq 0$
l_d - camber of bottom.

Area of bottom's surface

Bottom's surface area constitutes a part of vessel's shell area and affects quantity of shell plating mass. The bottom's surface area S_d can be expressed by using Guldin theorem:

$$S_d = 2 \cdot \pi \cdot \int_0^R r \cdot \sqrt{1 + \left(\frac{dz}{dr}\right)^2} \cdot dr \qquad (4)$$

and after substituting dimensionless variables:

$$S_d = 2 \cdot \pi \cdot R^2 \cdot \int_0^1 \xi \cdot \sqrt{1 + \left(\frac{l_d}{R}\right)^2 \cdot \left(\frac{d\zeta}{d\varsigma}\right)^2} \cdot d\xi =$$
$$= 2 \cdot \pi \cdot R^2 \cdot \int_0^1 s(\xi; R, l_d, t) \cdot d\xi \qquad (5)$$

Inverse function of the integral is not known hence it cannot be expressed by an analytical formula. In order to elaborate a simple approximating formula useful in formulating Eq. (2), parametric investigations of numerical values of the integral were conducted within the following ranges of the parameters: $0 \leq l_d/R \leq 0.5$ and $2.5 \leq t \leq 4.5$, by using the quadrature [6]:

$$S_d\left(R, \frac{l_d}{R}, t\right) \cong 2\pi \frac{\Delta R}{2}\left(s_{\xi=0} + s_{\xi=1} + 2\sum_{i=1}^N s_{\xi=i\frac{\Delta R}{R}}\right) \quad (6)$$

The best obtained analytical approximation of discrete values of the quadrature is represented by the expression [6]:

$$S_d\left(R, \frac{l_d}{R}, t\right) \cong \pi \cdot R^2 \cdot \left[1 + c_1 \cdot \left(\frac{l_d}{R}\right)^{c_2} \cdot t^{c_3}\right] =$$
$$= \pi \cdot R^2 \cdot \left[1 + 0.4281 \cdot \left(\frac{l_d}{R}\right)^{1.411} \cdot t^{0.4862}\right] \qquad (7)$$

Within the considered variability range of the investigated parameters the relative percentage error of values of the integral determined by means of Eq. (7) and the quadrature (6), does not exceed 0.3%.

Bottom's volume

Volume of the bottoms which constitutes a part of the vessel volume, affects value of its displacement. The bottom volume can be determined by using the Guldin theorem:

$$V_d = 2\pi \cdot l_d \cdot \int_0^R r \cdot \left(1 - \left(\frac{r}{R}\right)^2\right)^{\frac{1}{t}} dr \qquad (8)$$

In the case of the considered form of the bottom the integral is non-infinitesimal, as its primitive function is not known. By substituting the dimensionless variables $r = R \cdot \xi$ and $dr = R \cdot d\xi$ the following is achieved:

$$V_d = 2\pi \cdot l_d \cdot R^2 \cdot \int_0^1 \xi \cdot (1 - \xi^2)^{\frac{1}{t}} d\xi =$$
$$= 2 \cdot \pi \cdot \frac{l_d}{R} \cdot R^3 \cdot \int_0^1 v(\xi, t) \cdot d\xi \qquad (9)$$

In order to elaborate a simple approximating formula useful in formulating Eq. (2), parametric investigations of numerical values of the integral were conducted within the following ranges of the parameters: $0 \leq l_d/R \leq 0.5$ and $2.5 \leq t \leq 4.5$, by using the quadrature [6]:

$$V_d\left(R, \frac{l_d}{R}, t\right) \cong 2 \cdot \pi \cdot \frac{\Delta R}{2} \cdot \left(v_{\xi=0} + v_{\xi=1} + 2\sum_{i=1}^N v_{\xi=i\frac{\Delta R}{R}}\right)(10)$$

On the basis of the obtained numerical values, by testing various hypotheses on a form of approximating functions, the following analytical formula for approximate determination of values of bottom's volume was elaborated [6]:

$$V_d\left(R, \frac{l_d}{R}, t\right) \cong c_1 \cdot \pi \cdot \frac{l_d}{R} \cdot t^{c_2} \cdot R^3 =$$
$$= 0.5747 \cdot \pi \cdot \frac{l_d}{R} \cdot t^{0.2339} \cdot R^3 \qquad (11)$$

Within the considered variability range of the investigated parameters the relative percentage error of values of the integral determined by means of Eq. (11) and the quadrature (10), does not exceed 0.3%.

The complementary part of the whole volume of the vessel, V, is the following volume of its cylindrical part, V_c, of the length L:

$$V_c = 2\pi R L \ \wedge \ V = 2 V_d + V_c \qquad (12)$$

CRITERION OF STRUCTURAL STRENGTH SAFETY

As a measure of material effort of structure under external load the reduced stresses are assumed usually in compliance with Mises-Huber hypothesis expressed as follows:

$$\sigma_{red} = \frac{1}{\sqrt{2}} \cdot$$
$$\cdot \sqrt{(\sigma_x - \sigma_y)^2 + (\sigma_y - \sigma_z)^2 + (\sigma_z - \sigma_x)^2 + 6 \cdot (\tau_{xy}^2 + \tau_{yz}^2 + \tau_{zx}^2)} \quad (13)$$

In the case of thin-walled shells (of R/h > 20) under momentless load their state of stress can be considered two-dimensional, in this case the reduced stresses can be expressed by the principal stresses: axial ones, σ_z, and circumferential ones, σ_φ, [4]:

$$\sigma_{red} = \sqrt{\sigma_z^{22} + \sigma_\varphi - \sigma_z \cdot \sigma_\varphi} \qquad (14)$$

Structural strength safety is determined by the condition of maintaining the reduced stresses in the shell plating smaller than the permissible ones. Value of the permissible stresses related to the structural material yield point R_e, was obtained by assuming the safety factor $n_s > 1$ of a value determined according to a standard, rules, or on the basis of experimental knowledge or empirical practice:

$$\sigma_{max} \leq \sigma_{per} = \frac{R_e}{n_s} \qquad (15)$$

Depending on a required reliability of a device, value of the safety factor is contained within the range of: $n_s = 1.1 \div 20$, and usually: $n_s = 2.5 \div 4.0$ [1, 2, 3, 4]. Hence the structural strength safety condition takes the following form:

$$\sigma_{red\,max} = \max\left(\sqrt{\sigma_z^{22} + \sigma_\varphi - \sigma_z \cdot \sigma_\varphi}\right) \leq \sigma_{per} = \frac{R_e}{n_s} \quad (16)$$

In momentless state of stress vessel's shell plating is compressed simultaneously by uniformly distributed axial and circumferential forces. Unit compression forces in vessel's casing are determined by the following relations:
− axial force per unit length of vessel's circumference:

$$N_z = \frac{F}{2 \cdot \pi \cdot R} = \frac{\pi \cdot R^2 \cdot p - F_z}{2 \cdot \pi \cdot R} \cong 0.5 \cdot R \cdot p \quad (17)$$

− circumferential force per unit length of vessel's directrix:

$$N_\varphi = \frac{F}{2 \cdot R} = \frac{2 \cdot R \cdot L \cdot p}{2 \cdot L} = R \cdot p \quad (18)$$

The principal axial stresses are determined by the relation:

$$\sigma_z = \frac{\pi \cdot R^2 \cdot p - F_z}{2 \cdot \pi \cdot R \cdot h} \cong 0.5 \cdot \frac{R}{h} \cdot p \quad (19)$$

The principal circumferential stresses by the relation:

$$\sigma_\varphi = \frac{2 \cdot R \cdot p \cdot L}{2 \cdot L \cdot h} = \frac{R}{h} \cdot p \quad (20)$$

If vessel load changes occur slowly then dynamic and fatigue loads can be neglected, and the structural strength safety criterion for vessel under uniform external pressure is determined by the relation:

$$\sigma_{red\,max} = \max(\sqrt{\sigma_z^2 + \sigma_\varphi^2 - \sigma_z \cdot \sigma_\varphi}) =$$
$$= \frac{\sqrt{3}}{2} \cdot \frac{R}{h} \cdot p_{max} \leq \sigma_{per} = \frac{R_e}{n_s} \quad (21)$$

CRITERION OF FORM STABILITY SAFETY

Static stability of shell form means that there is an equilibrium state in a position neighbouring to the considered. The state of static equilibrium of form of axially symmetrical vessel under constant external load at momentless state of stress and linear elastic strain is described by the deformation form function w = w(z, φ) which is solution of shell form stability equation. Depending on parameters of a vessel, loss of form stability may take mode of axial or circumferential buckling. Form deformation depends on values of geometric and material parameters of a vessel and mode of its loading. The parameters constitute arguments of differential equation of shell stability. Under certain simplifying assumptions the form stability equation of cylindrical shell takes the following form [4]:

$$D \cdot \nabla^8 w + \frac{E \cdot h}{R^2} \cdot \frac{\partial^4 w}{\partial z^4} + \frac{1}{2} \cdot p \cdot R \cdot \nabla^4 \left(\frac{\partial^2 w}{\partial z^2} \right) +$$
$$+ p \cdot R \cdot \nabla^4 \left(\frac{\partial^2 w}{R^2 \cdot \partial \varphi^2} \right) = 0 \quad (22)$$

where:

$$D = \frac{E \cdot h^3}{121 \cdot (1 - v^2)} \text{ - shell stiffness}$$

$$\nabla^4 w = \frac{\partial^4 w}{\partial z^4} + \frac{2}{R^2} \frac{\partial^4 w}{\partial z^2 \cdot \partial \varphi^2} + \frac{1}{R^4} \cdot \frac{\partial^4 w}{\partial \varphi^4}$$

Eq. is solved by assuming *a priori* a form of allowable function which satisfies relevant boundary conditions of deformation:

$$w = \overline{w} \cdot \sin \frac{\pi \cdot m \cdot z}{L} \cdot \cos n \cdot \varphi \quad (23)$$

where:
$\overline{w}$ - shell deflection
m   - number of longitudinal half-waves of shell deformation
n   - number of circumferential waves of shell deformation.

On substitution of the allowable function to Eq. (22) the algebraic equation of deformations is obtained as follows:

$$\frac{\overline{w}}{R^{62}} \left\{ \frac{D}{R} \cdot \left[\left(\pi \cdot m \frac{R}{L} \right)^2 + n^2 \right]^4 + E \cdot h \left(\pi \cdot m \frac{R}{L} \right)^4 + \right.$$
$$\left. - p \cdot R \cdot \left[\frac{1}{2} \left(\pi \cdot m \frac{R}{L} \right)^2 + n^2 \right] \cdot \left[\left(\pi \cdot m \frac{R}{L} \right)^2 + n^2 \right]^2 \right\} \cdot$$
$$\cdot \sin \frac{\pi \cdot m \cdot z}{L} \cdot \cos(n \cdot \varphi) = 0 \quad (24)$$

The pressure at which the equation is fulfilled, is determined by the relation [4]:

$$p_{m,n} = \frac{\dfrac{(s^{22} + n)^4}{121(1 - v^2)} + s^4 \cdot \left(\dfrac{R}{h} \right)^2}{\left(\dfrac{s^2}{2} + n^2 \right) \cdot (s^2 + n^2)^2} \cdot E \cdot \left(\frac{h}{R} \right)^3 \quad (25)$$

where:

$$s = \pi \cdot m \cdot \frac{R}{L}$$

The critical pressure at which a shell under uniform external load loses its form stability within elastic deformation range (i.e. suffers buckling), is equal to the smallest value of the pressures $p_{m,n}$ determined at the successively assumed integer numbers m of longitudinal half-waves and n numbers of circumferential waves, at fixed R/L and R/h ratios and the parameters E, v, at which relevant modes of form deformations take place, namely the critical pressure p_{cr}:

$$p_{cr} = \min_{m,n} \{ p_{m,n} \} \quad (26)$$

where:
$m \wedge n \in \mathbf{N}$.

MINIMUM OF CRITICAL PRESSURE FUNCTIONAL

Value of the critical pressure p_{cr} is equal to the global minimum value of critical pressure relevant to all possible modes of shell form deformations within permissible variability range of design parameters:

$$p_{cr} = \min_{m,n \in \mathbf{N}} p \left(m, n, \frac{R}{L}, \frac{R}{h}, v, E \right) \quad (27)$$

The presented method concerns vessels of specific geometrical and material features which have been *a priori* assumed to be functionally useful [5], and the below given range of their variability determines the allowable applicability space of the method:
− the range of allowable values of the ratio R/L:
   $0.25 \leq R/L \leq 1$ {0.25, 0.5, 1.0};

- the range of allowable values of the ratio R/h:
  $25 \leq R/h \leq 150$ {25, 50, 150}
- Poisson number v (for NW-steel and AL-5083 alloy):
  $v = 0.3$ and $v = 0.33$
- Young modulus E (for NW-steel and AL-5083 alloy):
  $E = 2.1 \cdot 10^5$ and $E = 0.72 \cdot 10^5$ [Mpa]
- the number of considered axial half-waves of deformation:
  $m = 1$
- the number of considered circumferential waves of deformation: $n = 3 \div 12$.

For the above given combinations of parameters the following was elaborated:
- discrete values of the critical pressure:

$$p_{cr} = \min_{\substack{m=1 \\ n \in \{1 \div 12\}}} p_{cr}\left(m, n, \frac{R}{L}, \frac{R}{h}, v, E\right)$$

- diagrams of (continuous) functions of critical pressures [6], exemplified in Fig. 1
- from the diagrams was read a number of circumferential waves at which the critical pressure p_{cr} reaches its smallest value, at constant values of the remaining parameters.
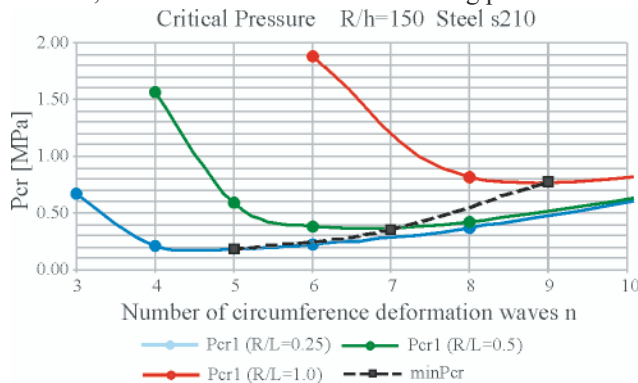
Fig. 1. *Example of envelopes of the minimum critical pressure values [6]:*

$$p_{cr} = p_{cr}\left(\frac{R}{L}, n; m = 1, \frac{R}{h} = 150, E = 2.1 \cdot 10^5 MPa, v = 0.3\right)$$

APPROXIMATION OF CRITICAL PRESSURE

On the basis of the set of discrete critical pressure values an analytical approximation formula minimizing the sum of squares of deviations, was elaborated. In the case of vessels made of NW-steel the best approximation of critical pressure is represented by the following expression [6]:

$$p_{cr} = 0.0806 + 414330 \cdot \left(\frac{R}{h}\right)^{-2.66} \cdot \left(\frac{R}{L}\right)^{1.11} \text{ [MPa] (28)}$$
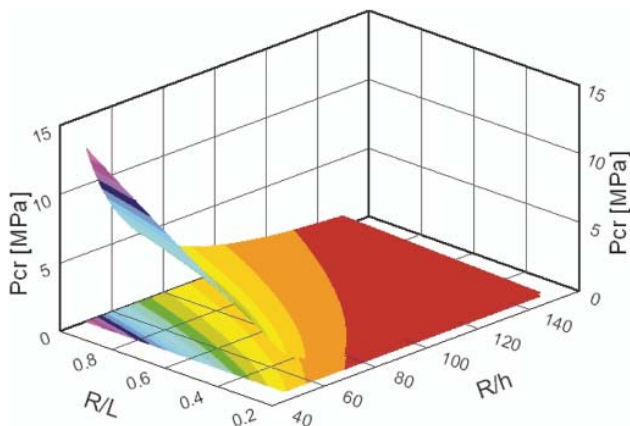
Fig. 2. *Diagram of the relation* $p_{cr} = f\left(\frac{R}{h}, \frac{R}{L}\right)$
– for structural material: NW-steel

In the case of AL-5083 alloy the best approximation of critical pressure is represented by the following expression [6]:

$$p_{cr} = 0.0262 + 139640 \cdot \left(\frac{R}{h}\right)^{-2.66} \cdot \left(\frac{R}{L}\right)^{1.11} \text{ [MPa] (29)}$$
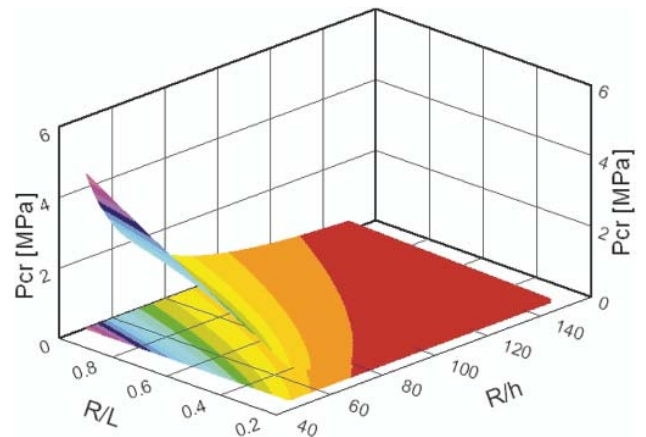
Fig. 3. *Diagram of the relation* $p_{cr} = f\left(\frac{R}{h}, \frac{R}{L}\right)$
– for structural material: AL-5083 alloy

APPROXIMATION OF MINIMUM VALUE OF SHELL THICKNESS

On the basis of Eq. and was obtained the set of discrete values of the converse problem consisting in determining geometrical parameters of vessel at an assumed operational submersion depth:

$$\left(\frac{R}{h}\right)_i = f\left((p_{cr})_i, \left(\frac{R}{L}\right)_i\right) \quad (30)$$

On the basis of the set of discrete values achieved from the relation (30) an analytical formula was elaborated by applying the method of least squares of deviations. In the case of steel vessels the best obtained approximation of critical pressure is represented by the following expression [6]:

$$\frac{R}{h} = 144745 - 5538 \cdot p_{cr}^{0.009869} +$$
$$- 139075 \cdot \left(\frac{R}{L}\right)^{-0.00040244} + 3.670 \cdot p_{cr}^{1.0916} \cdot \left(\frac{R}{L}\right)^{-1.1045} \quad (31)$$

where:
p_{cr} - given in [MPa].
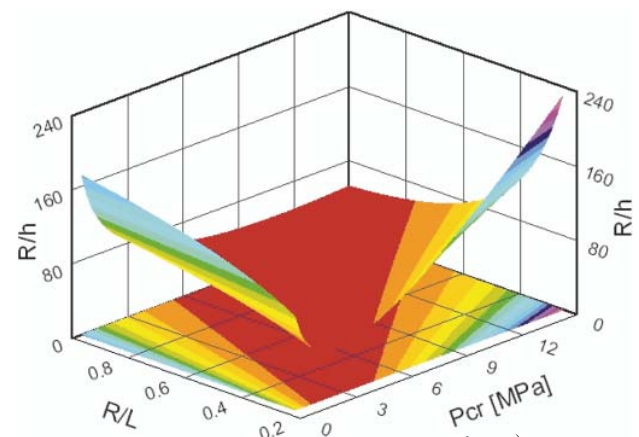
Fig. 4. *Diagram of the relation* $\frac{R}{h} = f\left(p_{cr}, \frac{R}{L}\right)$
– for structural material: NW-steel

PARAMETER		Variant I	Variant II	Variant III	Variant IV
Assumptions	Unit of measure	Value	Value	Value	Value
Structural material	–	Al-5083	Al-5083	St-235	St-235
0 - tight; 1 - flooded	–	0	1	0	1
Material density	[t/m³]	2.7	2.7	7.85	7.85
Submersion depth	[m]	200	200	200	200
Mass of apparatus	[t]	0.15	0.15	0.15	0.15
Average density of apparatus	[t/m³]	1.5	1.5	1.5	1.5
Effective displacement	[t]	0.1	0.1	0.1	0.1
R/L ratio	[-]	1	1	1	1
ld/R ratio	[-]	0.5	0.5	0.5	0.5
Exponent t >2	[-]	2.5	2.5	2.5	2.5
Young modulus	[MPa]	72000	72000	210000	210000
Poisson ratio	[-]	0.33	0.33	0.3	0.3
Safety factor	[-]	3	3	3	3
Life time	[year]	5	5	5	5
Water density	[t/m³]	1.025	1.025	1.025	1.025
Foam density	[t/m³]	0	0.05	0	0.05
Results of calculations	Unit of measure	Value	Value	Value	Value
Design pressure	[MPa]	6.03	6.03	6.03	6.03
Vessel diameter	[m]	0.754	0.895	0.820	1.293
Casing height	[m]	0.377	0.447	0.410	0.647
Shell plating thickness	[mm]	8.5	10.1	7.0	11.0
Vessel height	[m]	0.754	0.895	0.820	1.293
Bottom height	[m]	0.189	0.224	0.205	0.323
Bottom surface area	[m2]	0.56	0.79	0.66	1.64
Casing surface area	[m2]	0.894	1.258	1.056	2.627
Vessel surface area	[m2]	2.012	2.831	2.379	5.914
Volume of two bottoms	[m³]	0.120	0.200	0.154	0.605
Vessel volume	[m³]	0.289	0.482	0.371	1.454
Vessel displacement	[kg]	295.8	337.1	380.1	788.7
Mass of vessel shell plating	[kg]	46.2	77.1	129.8	508.5
Mass of foam	[kg]	0.0	10.0	0.0	30.2
Total mass	[kg]	196.2	237.1	279.8	688.7
Effective displacement	[kg]	99.6	100.0	100.3	100.0
Axial stresses	[MPa]	133.8	133.9	178.0	178.1
Circumferential stresses	[MPa]	267.53	267.8	355.9	356.2
Reduced stresses	[MPa]	231.7	231.9	308.2	308.4
Permissible stresses	[MPa]	235.0	235.0	235.0	235.0
Minimum strength-based thickness	[mm]	8.4	9.9	9.1	14.4
Minimum permissible thickness	[mm]	8.5	10.1	9.1	14.4
Corrosion allowance	[mm]	0.25	0.25	0.25	0.25
Allowance for plate thickness manufacturing tolerance	[mm]	0.8	0.8	0.8	0.8
Allowance for other stresses	[mm]	0.25	0.25	0.25	0.25
Technological plating thickness	[mm]	10.0	11.0	10.0	16.0
Mass of vessel after thickness correction	[kg]	54.3	84.1	138.0	546.2
Total mass after thickness correction	[kg]	204.3	234.1	288.0	696.2
Effective displacement after thickness correction	[kg]	96.3	107.7	95.1	101.4

In the case of vessels made of AL-5083 alloy the best approximation of critical pressure, within the range of considered design parameters, is represented by the following expression [6]:

$$\frac{R}{h} = 5.682 + 82.78 \cdot p_{cr}^{-0.4234} \cdot \left(\frac{R}{L}\right)^{0.4533} \quad (32)$$

where:
p_{cr} - given in [MPa].
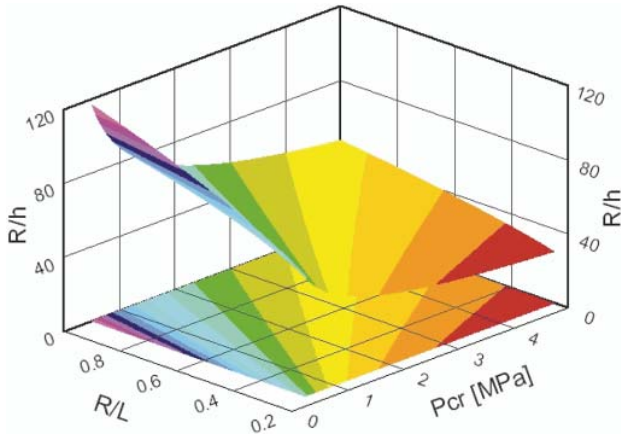
Fig. 5. *Diagram of the relation* $\frac{R}{h} = f\left(p_{cr}, \frac{R}{L}\right)$
– for structural material: AL-5083 alloy

RECAPITULATION AND EXAMPLE OF APPLICATION OF THE METHOD

By substituting, to the buoyancy equation , the approximation formulae for $V(R_p, L_p, L_d)$, $S(R_p, L_p, L_d)$, $h(R_p, L_p, p_{cr})$ and $p_{cr}(R/h, R/L)$, the balance is obtained of mass and displacement components of vessel, expressed *explicite* by its design parameters and design assumptions, as follows:

$$(1-\alpha) \cdot \rho_w \cdot V(R, L, L_d) - S(R, L, L_d) \cdot$$
$$\cdot h(R, L, p_{cr}) \cdot \rho_v - m_a - V_f \cdot \rho_f + \alpha \cdot \rho_w \cdot$$
$$\cdot \left(\frac{m_a}{\rho_a} + V_f + S(R, L, L_d) \cdot h(R, L, p_{cr})\right) - D_e = 0$$
$$(33)$$

Solution of the design problem in question is reached by numerical solving the buoyancy equation supplemented by relevant assumptions on requirements and conditions for a given case.

Example of application of the method

It has to be designed a vessel made of AL-5083 alloy or NW steel, capable of accommodating apparatus of the average density of 1.5 t/m³ and 100 kg mass, intended for operation at 200 m submersion depth in the water of 1.025 t/m³density, so as to obtain the vessel's effective displacement of about 100 kg. Alternatively it should be considered the case of a vessel of foam-filled bottoms, so as to obtain, but after flooding its interior, the same effective displacement of about 100 kg.

The supplementary assumptions and determined values of the design parameters are contained in Tab. 1.

NOMENCLATURE

D_e - effective displacement
E - Young modulus
F_z - value of external concentrated load
g - gravity acceleration
h - shell plating thickness
L - length of casing (cylindrical part of a vessel)
l_d - bottom camber
m_a - mass of apparatus
m_f - mass of filler (foam)
m_v - mass of vessel shell plating
N_φ - circumferential force per unit of vessel directrix length
N_z - axial force per unit of vessel circumference length
n_s - value of safety factor
R - casing curvature radius
R_e - material yield point
R_φ - circumferential curvature radius
R_z - axial curvature radius
r - radial variable
S - vessel surface area
S_d - bottom surface area
t - power exponent
V - vessel volume
z - axial variable
α - index of vessel's variant (tight or flooded)
ΔR - quadrature step
v - Poisson ratio
σ_{red} - reduced stresses
σ_z - axial stresses
σ_φ - circumferential stresses
ρ_a - average density of apparatus
ρ_f - filler density
ρ_v - vessel plating density
ρ_w - water density
ξ - dimensionless radial variable
ζ - dimesionless axial variable.

BIBLIOGRAPHY

1. Timoshenko S.: *Theory of elastic stability*. McGraw-Hill Book Co. New York 1936
2. Bochenek B., Krużelecki J.: *Optimization of stability of structures* (in Polish). Wydawnictwo Politechniki Krakowskiej (Publishing House of Cracow University of Technology), Cracow 2007
3. Rowiński L.: *Underwater vehicles – construction and equipment* (in Polish). „WiB" Publishers, Gdańsk 2008
4. Magnucki K.: *Strength and optimization of pressure vessels* (in Polish). Wydawnictwo Naukowe PWN (Polish Scientific Publishing House). Warsaw 1998
5. Michalski J.P.: *A study on identification of elements of a set of design assumptions for an autonomous echo-location module* (in Polish). Prace Naukowo-Badawcze W.O.i O. PG No.03/PR/2010 (Scientific reports of Faculty of Ocean Engineering and Ship Technology, Gdańsk University of Technology), Gdańsk 2010
6. Michalski J.P.: *Elaboration and testing of calculation algorithms useful in formulating a method for the preliminary designing of structure of echo-location module* (in Polish). Prace Naukowo-Badawcze W.O.i O. PG No.04/PR/2010 (Scientific reports of Faculty of Ocean Engineering and Ship Technology, Gdańsk University of Technology), Gdańsk 2010.

CONTACT WITH THE AUTHOR

Assoc. Prof. Jan P. Michalski
Faculty of Ocean Engineering
and Ship Technology
Gdansk University of Technology
Narutowicza 11/12
80-233 Gdansk, POLAND
e-mail: janmi@pg.gda.pl

A method for the accurate numerical prediction of the tip vortices shed from hydrofoils

P. Flaszyński, Ph. D.
J. A. Szantyr, Prof.
R. Biernacki, Ph. D.
Gdansk University of Technology
P. Dymarski, Ph. D.
M. Kraskowski, M. Sc.
Ship Design and Research Centre CTO SA

ABSTRACT

The possibly accurate numerical prediction of the detailed structure of vortices shed from the tips of hydrofoils is an important element of the design process of marine propellers. The concentrated tip vortices are responsible for the propeller cavitation erosion and acoustic emission. The purpose of the project described in this paper was to develop the numerical method for prediction of the tip vortex structure. In the course of the project the numerical calculations were confronted with the results of experimental measurements. This led to creation of the specific method of construction of the computational grid and to selection of the optimum turbulence model. As a result the reliable method for the accurate numerical prediction of the concentrated tip vortices for different hydrofoil geometry and flow conditions has been developed and validated. This method enables elimination of the unfavourable phenomena related to the tip vortices in the course of the propeller design calculations.

Keywords: marine propulsors, vortex generation, numerical methods, experimental techniques

INTRODUCTION

The concentrated tip vortices shed from the tips of the marine propeller blades are responsible for many unfavourable phenomena. Due to the strongly reduced pressure in their centres they generate cavitation, which in turn leads to destructive cavitation erosion of the propeller and the rudder, generation of the intensive acoustic signals and induction of vibration in the elements of ship structure (cf. Fig. 1). These phenomena should be accurately predicted at the design stage of the propeller, in order to eliminate them completely or at least to limit their intensity to a harmless level. This can be done by a sufficiently accurate and widely experimentally validated numerical method, which responds correctly to even small modifications of the propeller blade geometry and to small changes in the flow conditions. Such a method may be used for numerical optimization of the marine propeller geometry and its operating conditions.

The first step in numerical prediction of the tip vortex cavitation is the possibly accurate determination of the tip vortex structure, i.e. the spatial distribution of the flow velocity and pressure in the vicinity of the vortex, including its centre. The accurate determination of location and magnitude of the minimum pressure is of particular importance, because this pressure is the decisive factor in cavitation inception. The region in question is dominated by the high velocity transverse flow generated by the vortex. Consequently, the resultant local velocity vectors deviate strongly from the direction of the

Fig. 1. *Cavitating tip vortices shed from the blades of the marine propeller model and interacting with the ship rudder (courtesy of the Ship Design and Research Centre CTO S.A. in Gdansk, Poland)*

general flow. This creates special problems for the numerical methods, for example the most frequently used methods based on numerical solution of the Reynolds Averaged Navier Stokes equations. These problems concern the adequacy of the computational grid structure and the accuracy of the turbulence models, which have been calibrated for much simpler flows. The accumulated practical experience of the past shows, that

in most cases the numerical methods tend to underestimate the degree of concentration and the minimum pressure of the tip vortices. Consequently, their ability to predict accurately the tip vortex cavitation inception was regarded as questionable.

The purpose of the research project described in this paper was to develop a computational method, which makes use of the special structure of the computational grid and which employs the specific turbulence models, especially suited for the vortex-dominated flows. This method is based on the combined numerical and experimental research, presented in detail in [1, 2, 3] and described briefly in the following section.

DESCRIPTION OF THE NUMERICAL AND EXPERIMENTAL RESEARCH

The research forming the basis for the development of the new method included experiments [4] and calculations [5, 6, 7, 8, 9, 10]. The experiments were conducted in the cavitation tunnel of CTO S.A. and they were concerned with the measurements of the velocity field in three cross-sections of the tip vortex generated by hydrofoils of different geometry in different flow conditions (cf. Fig. 2). The measurements were performed using the Laser Doppler Anemometer. The geometry of the hydrofoils was selected in such a way that it resembled the blades of contemporary marine propellers. Three variants of the hydrofoil were tested: one with optimum distribution of the hydrodynamic loading along its span, one with hydrodynamically unloaded tip and one with hydrodynamically loaded tip. Each of these hydrofoils was tested at three different angles of attack: +2.5 degrees, 0 and -2.5 degrees. It was expected that the variation of the hydrodynamic loading along the span of the hydrofoils may influence the process of formation of the tip vortices and it may lead to generation of vortices of different strength. The sufficiently accurate numerical method should be able to detect these small differences.
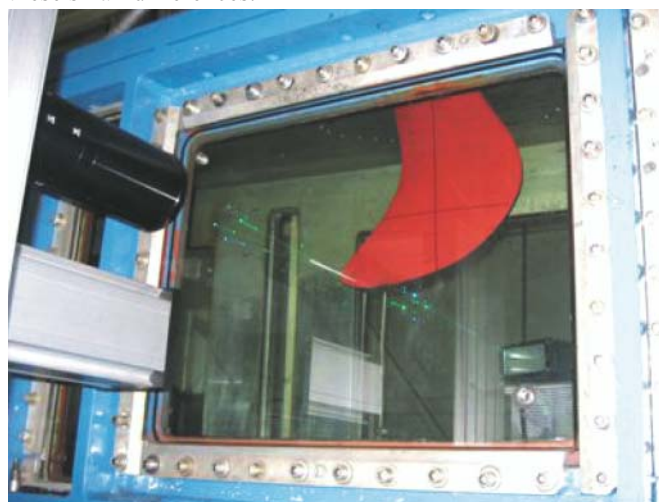
Fig. 2. *Hydrofoil model mounted in the measuring section of the cavitation tunnel of CTO S.A.*

The numerical calculations were arranged in such a way that they reproduced the experiments as closely as possible. The details of the computational flow domain, based on the geometry of the measuring section of the cavitation tunnel, are shown in Fig. 3.

The calculations were performed using three different CFD codes (commercial codes Fluent and Comet together with the code Solaga developed at CTO S.A.) and in all six turbulence models (Spalart-Allmaras, k-ω, k-ε, RSM, k-ω SST, k-ε RNG). The accuracy of the results of calculations for such a complicated, vortex-dominated flow, depends on the detailed

structure of the computational grid and on the adequacy of the applied turbulence models. The purpose of calculations was to develop a method for construction of the optimum grid for this specific type of flow and to select a turbulence model which is best suited to simulate the process of turbulence generation, transport and dissipation in this type of flow. This was performed on the basis of comparison of the experimental and computational results in three cross-sections of the vortex, located respectively 10 mm, 70 mm and 300 mm behind the hydrofoil tip, as shown in Fig. 4.
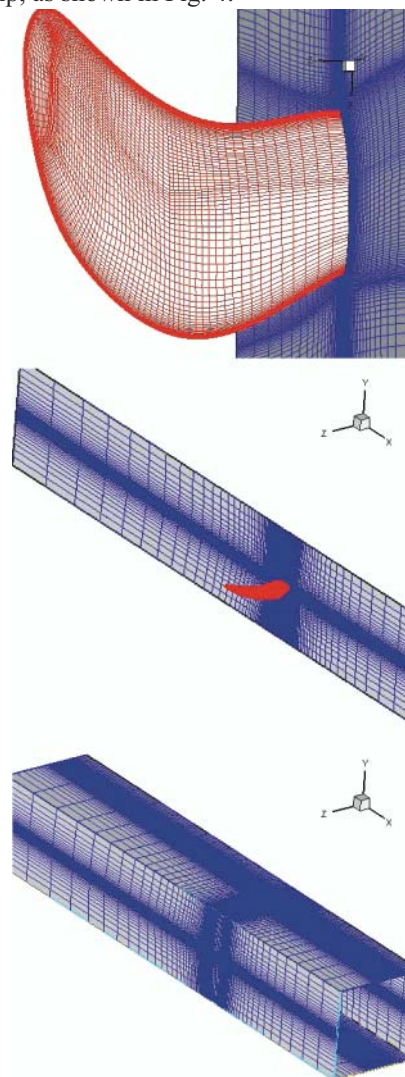
Fig. 3. *The discrete mesh for numerical calculations on the hydrofoils surface (top) and on the external surfaces of the flow domain (bottom)*
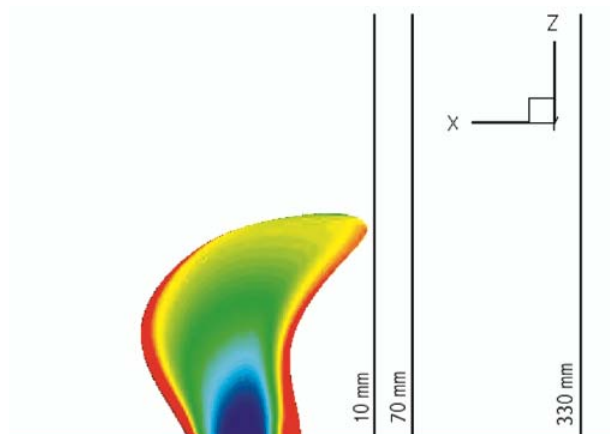
Fig. 4. *Location of the cross-sections of the tip vortex for computations and measurements*

The process of development of the optimum computational grid was conducted in three stages:
- the first, basic grid was constructed according to the general recommendations included in the manuals of the respective CFD codes (cf. Fig. 5). This was a block-structured grid, in which the O-type grid was employed around the hydrofoil and the H-type grid was used in the remaining part of the flow domain. The total number of finite volumes was around 1.250.000 and the size of the smallest volume close to the surface of the hydrofoil was about 0.02 mm.
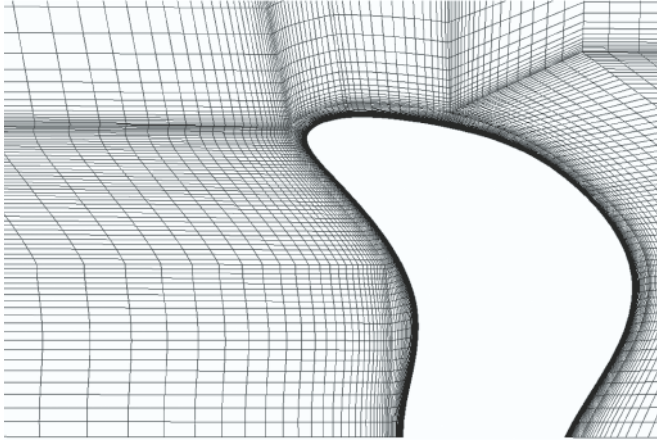
Fig. 5. Basic computational grid in the vicinity of the hydrofoil

- the second grid was refined inside the cylinder covering the anticipated location of the tip vortex (cf. Fig. 6). Inside this cylinder all initially defined finite volumes were divided into 8 smaller volumes, rising the total number of volumes to about 1.940.000.
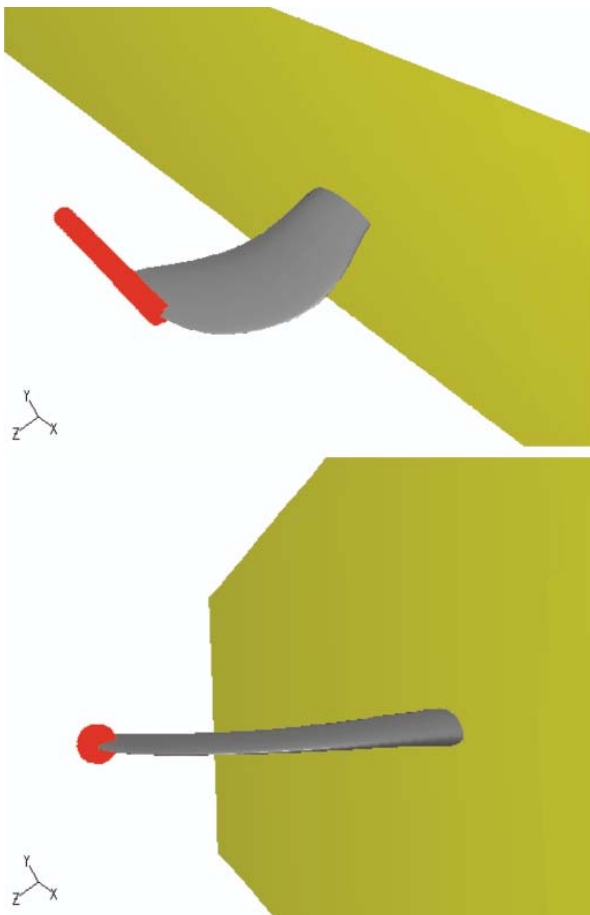
Fig. 6. Computational grid refined in an arbitrarily defined cylinder

- the third grid was refined in the semi-automatic way, using the criterion based on the local values of vorticity, as calculated using the basic grid (cf. Fig. 7). The values of vorticity were tested inside the blue region shown in Fig. 7 and the volumes inside the red region in which the vorticity exceeded the prescribed value were modified. Each finite volume in the modified region was divided into 16 smaller volumes, rising the total number of volumes to about 1.638.300. In order to have the refined grid in the tip vortex (core and vicinity), the streamwise voriticity has been selected as the criteria. The range of the streamwise vorticity for the grid adaptation is case dependent. In general, one can apply the maximum of the vorticity as the upper limit and 30% of the maximum with the opposite sign as the lower limit. The lower limit is also important, because the counter rotating vortices are generated downstream the trailing edge in some cases. They are much weaker than the main vortex, but their influence on the tip vortex development and the diffusion rate is important. In case of the Comet code, the streamwise velocity was applied as the criteria for the grid adaptation.
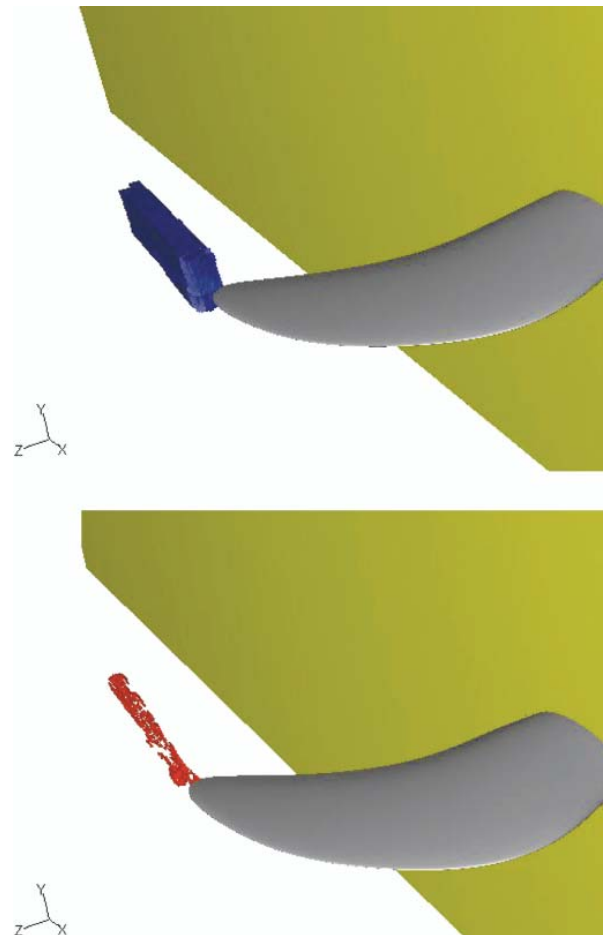
Fig. 7. Computational grid refined on the basis of the local values of vorticity

The distributions of the x-component of the resultant flow velocity and the x-component of the local vorticity calculated using the first grid, which were later used in the semi-automatic grid refinement, are shown in Fig. 8. In the same Figure the resulting grid structures in the consecutive stages: basic grid, adaptation 1 and adaptation 2 are shown.

It is easy noticeable that the basic grid is coarse. Such effect could be avoided if the tip vortex location could be foreseen during grid generation and the grid would be generated fine enough at the very beginning. It is difficult or even impossible
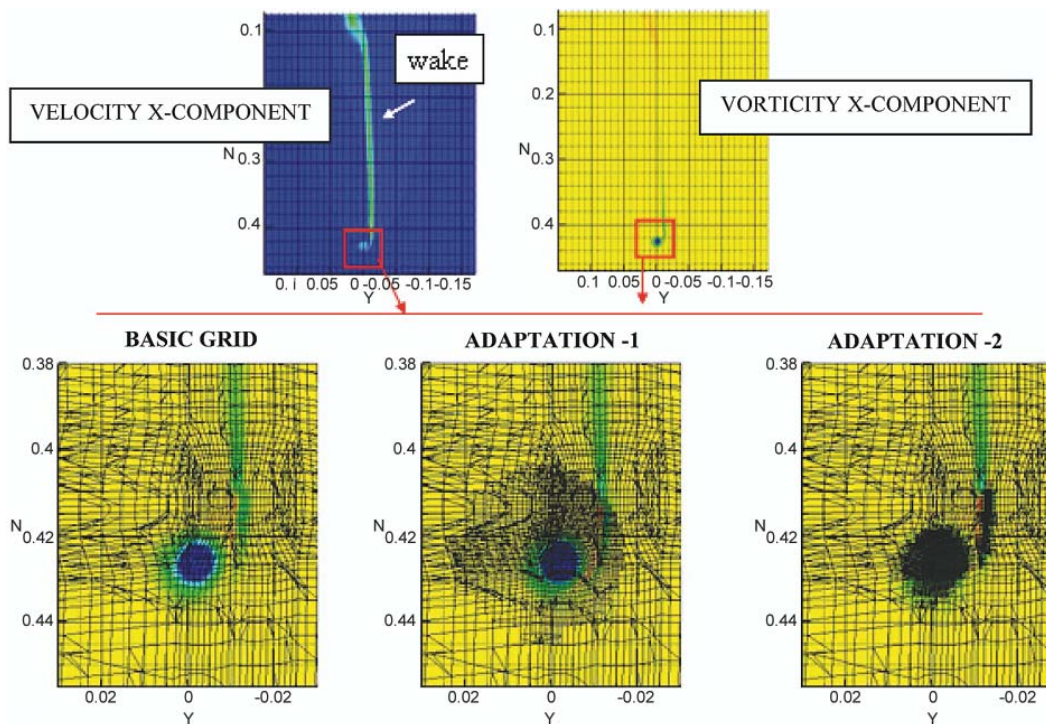
Fig. 8. *Process of grid refinement in the tip vortex area*

for the full 3D propeller analysis. In such a case, the coarse grid can be created and then it can be refined according to the local flow conditions. The local grid refinement (shown in Fig. 8) enables much better prediction of the local velocity and pressure gradients, which are very important for the cavitation prediction. It is shown that grid adaptation gives higher cells concentration in the tip vortex and such approach seems to be the most efficient.

ANALYSIS OF THE NUMERICAL AND EXPERIMENTAL RESULTS

The selected results of measurements and calculations included in this section are supposed to illustrate the agreement between them for the three consecutive stages of the grid refinement. Fig. 9 presents the axial velocity component in the cross-section 10 mm behind the hydrofoil, obtained
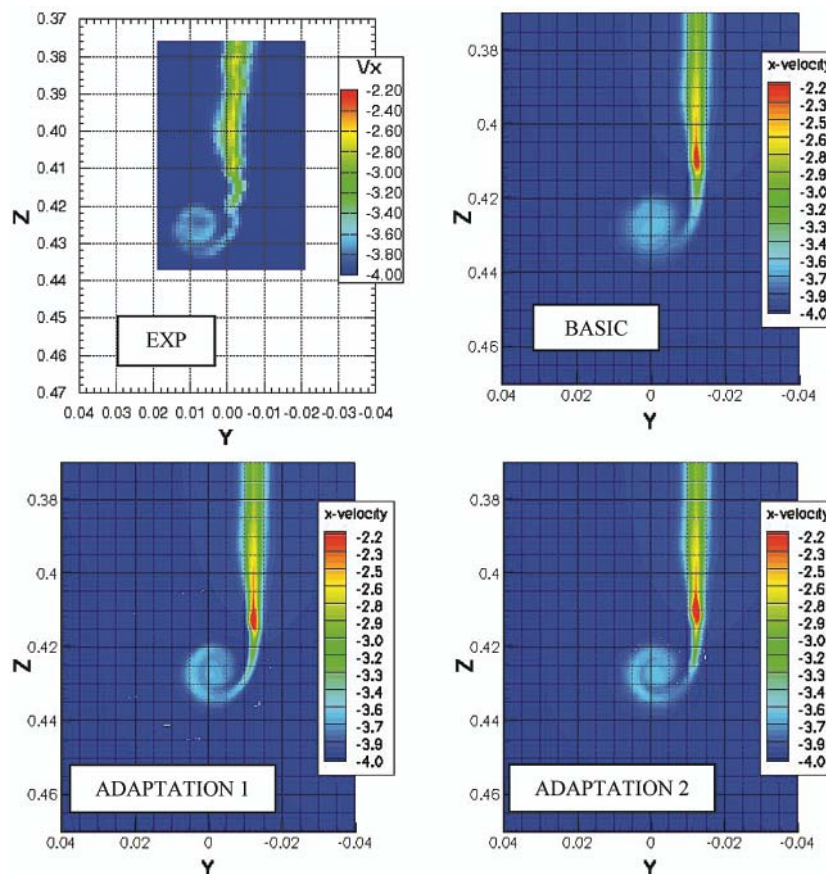
Fig. 9. *Axial component of the velocity - 10 mm – L+2.5 – Fluent (SST)*

experimentally and calculated using Fluent for the tip-loaded hydrofoil (L) at the angle of attack +2.5 degrees. This hydrofoil geometry in combination with the flow conditions should generate the most intensive vortex in the entire project. Fig. 10

shows the analogical results for the cross-section 70 mm behind the hydrofoil. Figs. 11 and 12 show similar results obtained by the program Comet. Figs 13 and 14 include the comparison of the experimental and computational results for the transverse
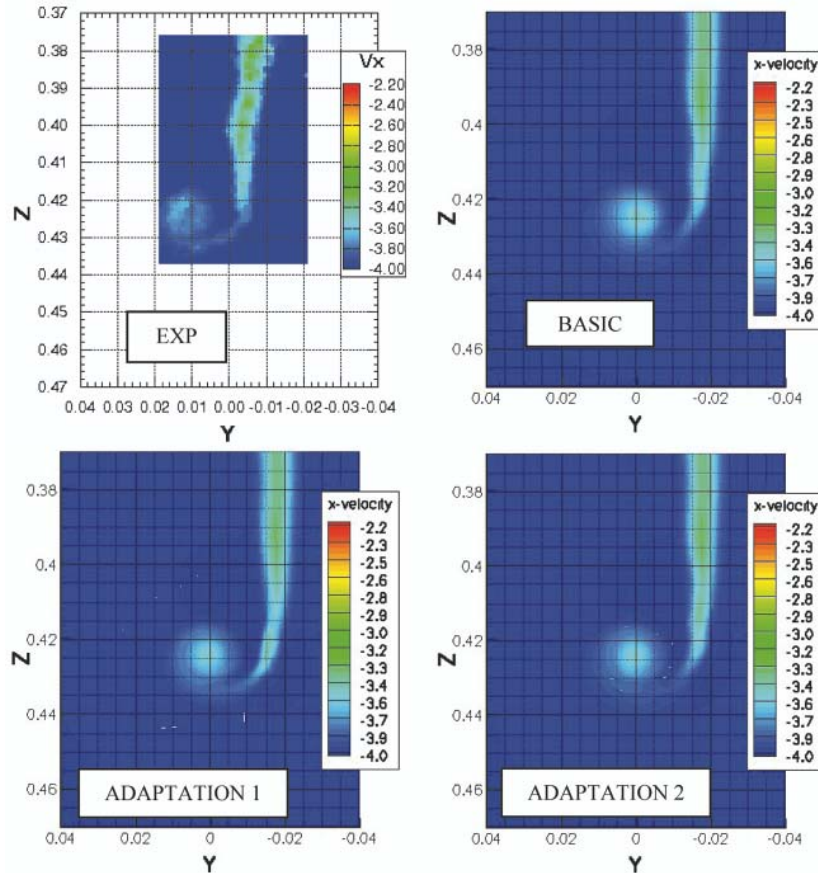
Fig. 10. Axial component of the velocity - 70 mm – L+2.5 – Fluent (SST)
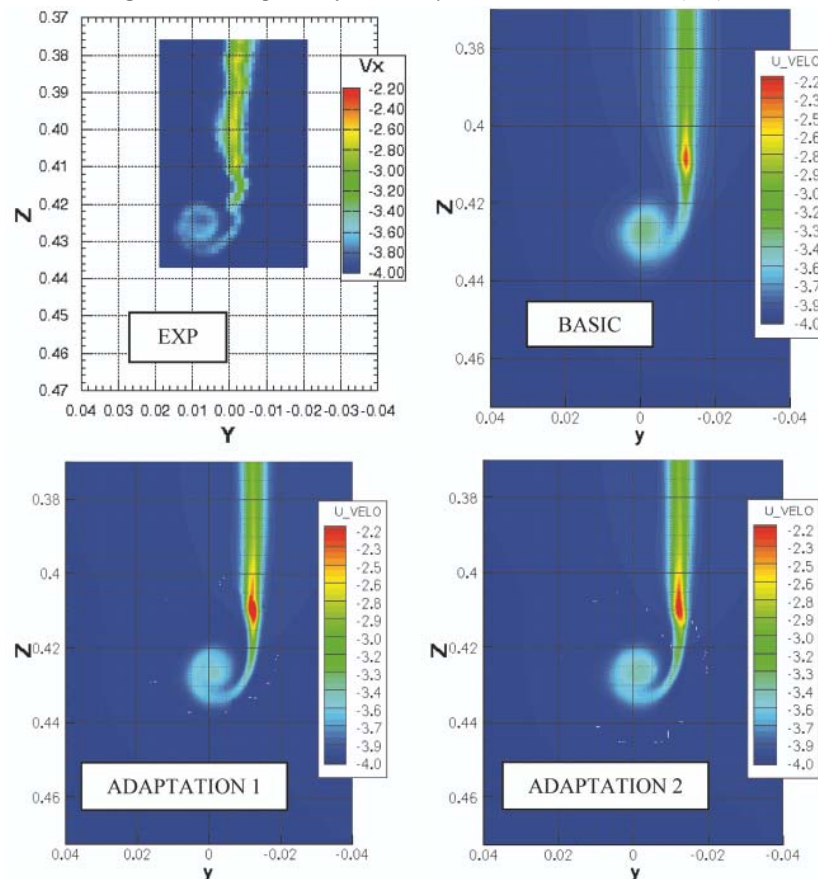
Fig. 11. Axial component of the velocity - 10 mm – L+2.5 – Comet (SST)

(vertical) velocity component at the cross-section 10 mm behind the tip-loaded hydrofoil at +2.5 angle of attack.

In all cases computed by Fluent, the best agreement with experimental data was obtained for the "adaptation-2". In the Comet code, because it was no possibility to set the vorticity as the grid refinement criterion, the longitudinal velocity was applied. For such a criterion, which is not so sensitive as the vorticity, the results obtained on the refined grids differ
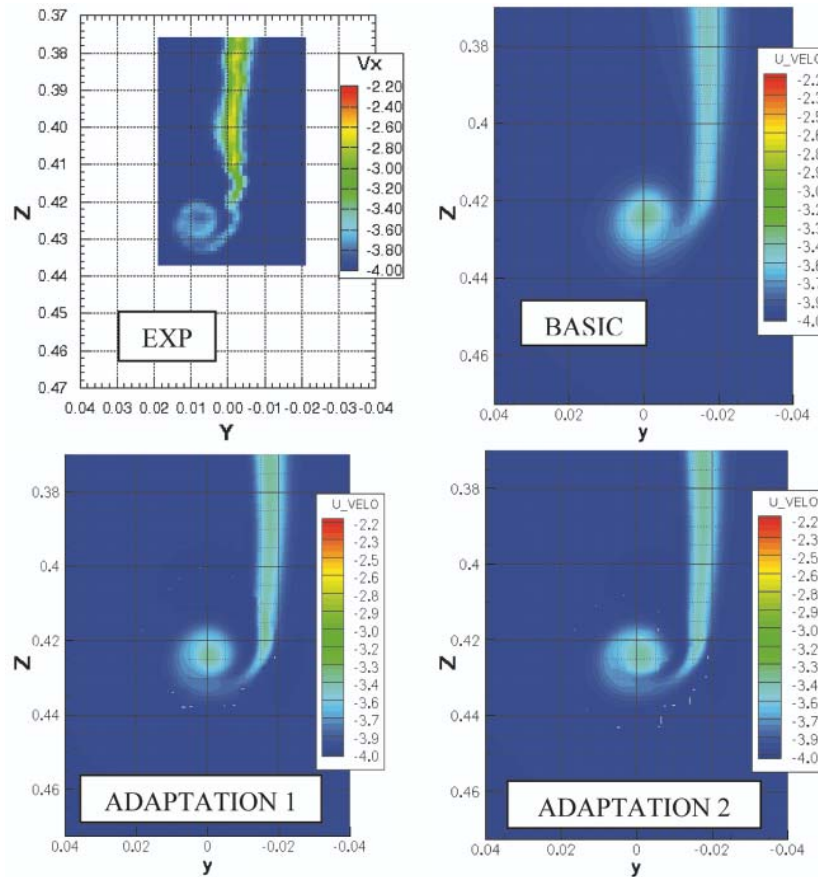
Fig. 12. Axial component of the velocity - 70 mm – L+2.5 – Comet (SST)
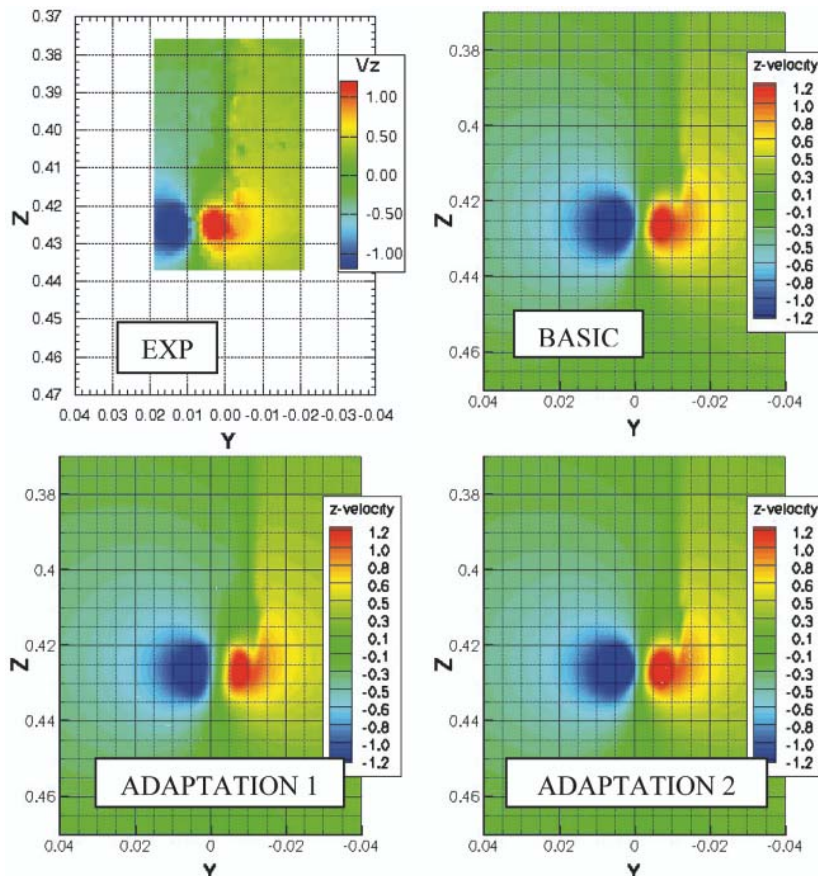
Fig. 13. Vertical component of the velocity - 10 mm – L+2.5 – Fluent (SST)
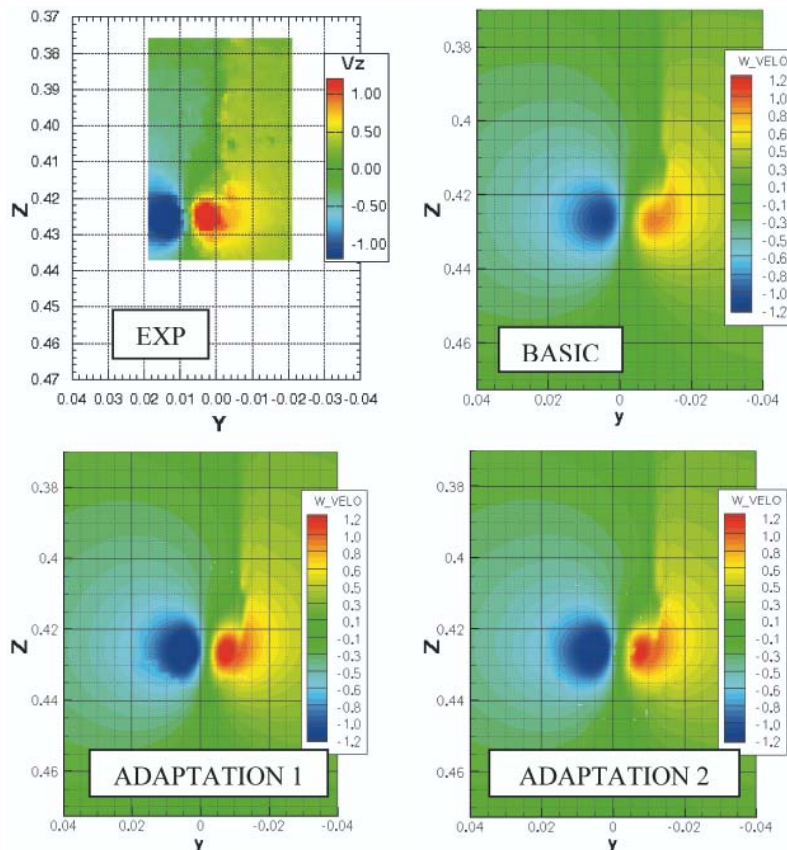
Fig. 14. *Vertical component of the velocity - 10 mm – L+2.5 – Comet (SST)*

from those obtained with Fluent. In some cases (Fig.11-12), the results obtained on the grid for the first adaptation (adaptation-1) are a bit closer to the measurements.

METHOD FOR NUMERICAL PREDICTION OF TIP VORTICES

The method developed and tested in the course of the described research project is in fact the method for effective and optimum use of the commercial CFD codes for the specific task of accurate prediction of the tip vortices generated by hydrofoils. This method is built on two basic recommendations:

- the computational grid may be initially constructed according to general rules applicable to the CFD code used. After performing the initial calculations using this grid, the region of the anticipated location of the tip vortex must be defined and the grid in this region should be modified (subdivided at least by a factor of 16), using the criterion based on the calculated x (streamwise) component of the local flow vorticity. Then the calculation should be repeated using the modified grid, producing the final results.
- in the RANS methods applied for the vortex-dominated flows the turbulence model k-ω SST should be used, because it is best suited for such flows and it gives the best results as far as the prediction of the detailed vortex structure is concerned.

These recommendations have been proven to be effective for two different commercial CFD codes used in the project. Therefore it may be safely assumed that they are valid also for other commercial codes. Calculations of the tip vortices generated by hydrofoils, which are conducted in accordance with the above recommendations, supply sufficiently accurate results for further analysis of the tip vortex cavitation.

CONCLUSIONS

The following final conclusions may be formulated on the basis of the research presented above and in [3]:

- contemporary Computational Fluid Dynamics methods are fully capable of predicting the vortex-dominated flows with accuracy sufficient for further analysis of the vortex cavitation inception and development

- the accuracy of numerical prediction of the vortex-dominated flows is significantly improved by the semi-automatic refinement of the computational grid in the region of the vortex, based on the pre-computed values of the local axial (streamwise) component of vorticity

- such a local refinement of the computational grid ensures acceptable accuracy of the results while keeping the calculation time to a reasonable minimum

- in the sufficiently dense grid (in both directions: crosswise and streamwise) the diagonal orientation of the resultant velocity vectors does not influence adversely the results of calculations of the vortex-dominated flow

- among the most popular turbulence models the k-ω SST model seems to be best suited for calculations of the vortex-dominated flows.

Acknowledgement

BIBLIOGRAPHY

1. Dymarski P., Szantyr J., Flaszyński P., Kraskowski M., Biernacki R.: *Modelling of Tip Vortex Behind a Blade Using Different Turbulence Models and Different RANSE Solvers. Comparison with LDA Measurements,* Proc. of the 11th Numerical Towing Tank Symposium, Brest, France, September 8-10 2008
2. Flaszyński P., Szantyr J., Dymarski P., Krasowski M*.: Numerical Prediction of Vortex Generated by a Hydrofoil,* Proc. of the International Symposium on Marine Propulsors, Trondheim, Norway, June 22-24, 2009
3. Flaszyński P., Szantyr J., Biernacki R., Dymarski P., Kraskowski M,: *An Experimental and Numerical Study of the Vortices Generated by Hydrofoils*, Polish Maritime Research Vol. 16, No. 4 (63), 2009
4. CTO S.A. Report No. RH-2008/T-133 *Results of measurements of the velocity field in the vortex path behind the hydrofoils* (in Polish)
5. CTO S.A. Report No. RH-2008/T-019 *Calculations for the first variant of the discrete mesh – program Fluent* (in Polish)
6. CTO S.A. Report No. RH-2008/T-020 *Calculations for the first variant of the discrete mesh – programs Comet and Solaga* (in Polish)
7. CTO S.A. Report No. RH-2008/T-110 *Calculations for the second variant of the discrete mesh – program Fluent* (in Polish)
8. CTO S.A. Report No. RH-2008/T-111 *Calculations for the second variant of the discrete mesh – program Comet* (in Polish)
9. CTO S.A. Report No. RH-2009/T-019 *Calculations for the third variant of the discrete mesh – program Comet* (in Polish)
10. CTO S.A. Report No. RH-2009/T-019 *Calculations for the third variant of the discrete mesh – program Comet* (in Polish)

CONTACT WITH THE AUTHORS

P. Flaszyński Ph. D. e-mail: pflaszyn@pg.gda.pl
J. A. Szantyr Prof. e-mail: jas@pg.gda.pl
R. Biernacki Ph. D., e-mail: rbiernac@pg.gda.pl

Faculty of Mechanical Engineering
Gdansk University of Technology
Narutowicza 11/12
80-231 Gdansk

P. Dymarski Ph. D., e-mail: padym@cto.gda.pl
M. Kraskowski M. Sc,
e-mail: Marek.Kraskowski@cto.gda.pl

Ship Design and Research Centre CTO S.A.
Wały Piastowskie 1
80-958 Gdansk

Numerical analysis of influence of streamline rudder on screw propeller efficiency

Tomasz Abramowski, Ph. D.
Jakub Handke, M. Sc.
Tadeusz Szelangiewicz, Prof.
West Pomeranian University of Technology, Szczecin

ABSTRACT

During designing the ship its designer tends to obtain as high as possible efficiency of ship propulsion system. To this end on certain ships additional elements such as: nozzles, half-nozzles or suitably profiled fins attached to underwater part of ship's hull before screw propeller, are applied (sometimes they are intended for the mitigating of vibration resulting from operation of screw propeller). Another device which affects operation of screw propeller is streamline rudder capable of improving its efficiency (most of the transport ships is fitted with single screw propeller and streamline rudder placed behind it). In this paper the influence of streamline rudder on screw propeller efficiency has been examined with the use of numerical methods of fluid dynamics (CFD).The obtained results indicate a very favourable influence of the rudder on screw propeller efficiency. Research in this area is continued and its results concerning impact of particular geometrical parameters of rudder on screw propeller efficiency, will be presented in the future.

Keywords: Streamline rudder, improvement of screw propeller efficiency,
computational fluid dynamics (CFD)

INTRODUCTION

During ship's design process one of the most important tasks is a design of its propulsion system which should ensure reaching the assumed service speed by the designed ship at its as high as possible propulsion efficiency. The crucial element of ship propulsion system is a screw propeller whose efficiency is decisive of overall propulsion efficiency. Geometry of screw propeller decides on its efficiency, hence it should be optimum one in assumed design conditions, i.e. screw propeller should develop demanded thrust at an assumed ship's service speed. Apart from the optimum design, screw propeller efficiency can be improved by using various additional devices such as: nozzles, half-nozzles, or suitably profiled fins attached to underwater part of ship's hull before screw propeller [5] (sometimes they are intended for the mitigating of hull plating vibration resulting from screw propeller operation). The additional devices are aimed at the improving of distribution (direction and velocity) of water stream flowing from around the hull towards the screw propeller. The devices produce a positive effect only in strictly defined conditions. As results from practice, they are applied very rarely.

Another device which influences screw propeller operation is a streamline rudder capable of improving its efficiency. Majority of transport ships is fitted with single screw propeller and streamline rudder placed behind it. Therefore it seems purposeful to examine which way and in which conditions streamline rudder affects screw propeller operation, and how much screw propeller efficiency can be increased.

SCREW PROPELLER – STREAMLINE RUDDER SYSTEM

The screw propeller – streamline rudder system is exemplified in Fig. 1.
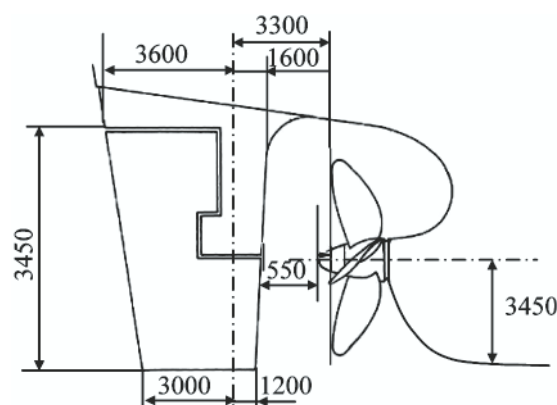
Fig. 1. The semi-spade rudder behind the screw propeller of B 573 ship [8]. (All the dimensions given in mm)

A few dozen years ago already it has been observed that a blade rudder of airfoil profile not only improves ship's manoeuvrability but also increases screw propeller efficiency and – in consequence – overall propulsion efficiency of ship [6]. The improvement of screw propeller efficiency results from the following reasons:

- part straightening the flow behind the propeller (which leads to lowering the induced circumferential velocity)
- a more favourable distribution of water pressure behind the propeller and reduction of vortices flowing downstream from the propeller, mainly from its boss.

However apart from knowledge of the facts there is a lack of results of systematic investigations, e.g. model tests, and in the subject-matter literature only a general information can be found, that does not provide any basis to state which way geometrical features of streamline rudder affect screw propeller efficiency and how large increase of the efficiency would be possible. Yet the application of numerical methods of computational fluid dynamics (CFD) to modelling water flow around propeller and rudder has made it possible to assess qantitively and qualitively influence of rudder on screw propeller efficiency. Most publications in which results obtained by means of CFD methods have been presented, deal mainly with influence of screw propeller on ruddder or with investigation of flow around the hull, propeller and rudder [1, 2, 3, 4 and 7]. In this paper preliminary results of numerical investigations concerning influence of rudder on screw propeller efficiency, are presented.

SCOPE OF THE INVESTIGATIONS

Within the frame of the conducted research project a numerical analysis of flow around screw propeller was performed by using Fluent system to determine the thrust coefficient K_t and torque coeffcient K_q as well as screw propeller efficiency η_o for:
- a free propeller
- a screw propeller accompanied with a rudder of HSVAMP73-20 profile in the position of no deflection
- for a screw propeller accompanied with a rudder of HSVAMP73-20 profile in the position of 15° deflection.

The investigations were performed for the hull of a B573 ship (built by Stocznia Szczecinska), its screw propeller and streamline rudder (Fig. 1).

As results of model tests on rudder / propeller interaction for the B 573 ship have been lacking, the obtained computational results were compared, only at the advance coefficient J = 0.70, with the values calculated on the basis of the propulsion prediction for free screw propeller [8].

Geometrical parameters of the screw propeller of B 573 ship (Fig. 1) [9]:

Diameter	D	5900 mm
Pitch ratio	P/D	0.739
Expanded area ratio	A_E/A_0	0.578
Number of blades	z	4

Geometrical parameters of the rudder of B 573 ship (Fig. 1) [8]:

The rudder was designed on the basis of HSVAMP73-20 profile. Its contour and size are in compliance with the rudder installed on B 573 ship.

The computational model of the rudder is shown in Fig. 2, and that of the screw propeller – in Fig. 3.

The computation domain consisted of three co-axial cylinders (Fig. 4). The screw propeller was placed inside the small cylinder put inside the fore large cylinder. Rear faces of both the cylinders were located in one common plane and adhered the fore face of the rear cylinder. Such arrangement makes it possible to apply the mesh for free-propeller calculations by using the sliding mesh method (the small cylinder is a rotating element and the large cylinders are motionless). For the free-propeller calculations no physical element is placed in the rear cylinder. For the calculations of propeller and rudder together in the rear cylinder is placed the rudder model either with or without deflection, respective of a modeled case.
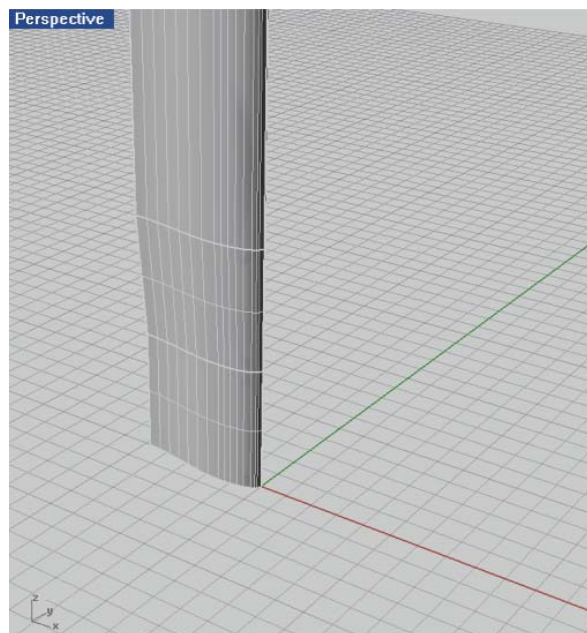
Fig. 2. Computational model of the rudder without any deflection
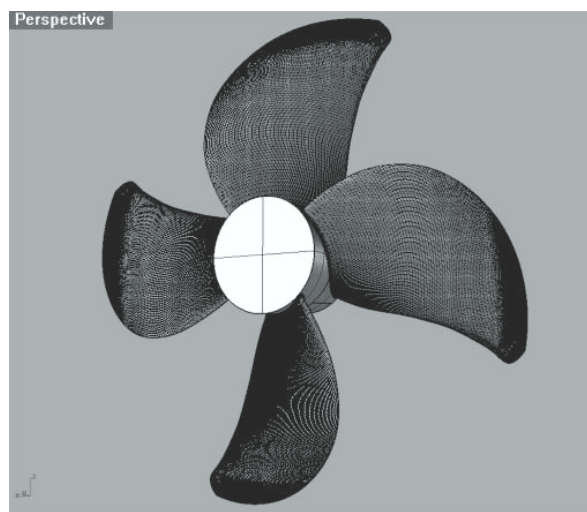
Fig. 3. Computational model of the screw propeller
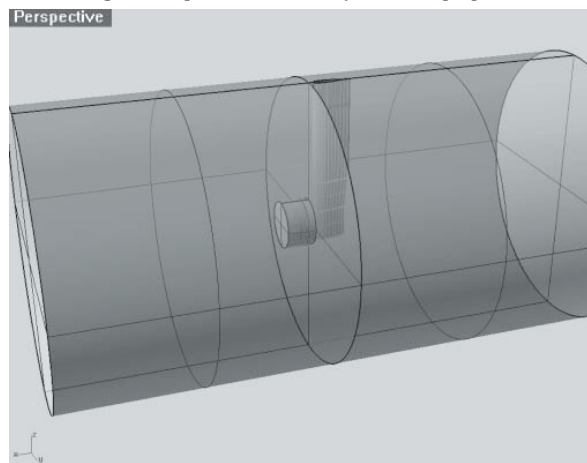
Fig. 4. Computation domain for the set of screw propeller and rudder

RESULTS OF THE NUMERICAL CALCULATIONS

In advance of the actual calculations of rudder influence on screw propeller efficiency, the following has been calculated:

- Hydrodynamic characteristics of the screw propeller model, which were compared with results of experimental model tests. The propeller model geometry acc. P 355 storage propeller and results of its model tests are contained in the report [8].

  Description of the numerical calculations of the hydrodynamic characteristics and their results are presented in [10].

- Hydrodynamic characteristics of the streamline rudder of B 573 ship, (Fig. 1). Results of numerical calculations of the characteristics are presented in [11].

The actual numerical calculations of screw propeller efficiency with accounting for impact of ruddder,were then performed. They were carried out for the real dimensions of the propeller and rudder installed on B 573 ship, Fig.1.

In Fig. 5 an example pressure distribution and streamlines for both the propeller and rudder without any deflection is presented, and in Fig. 6 – for both the propeller and the rudder deflected by 15º (The complete set of pressure and velocity distributions as well as streamlines is given in [12]).

Drag face of propeller

Driving face of propeller
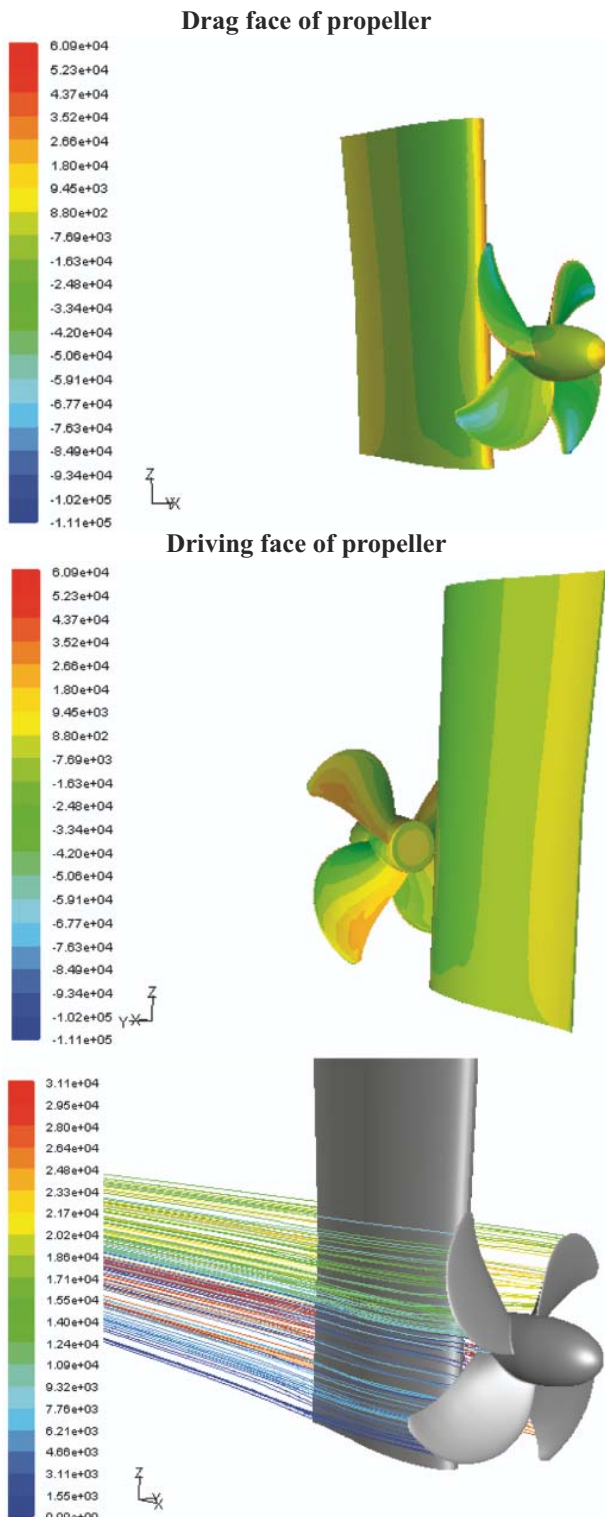
Fig. 5. *Pressure distribution and streamlines for the set of propeller and rudder without any deflection, the advance ratio J = 0.7*

Drag face of propeller

Driving face of propeller
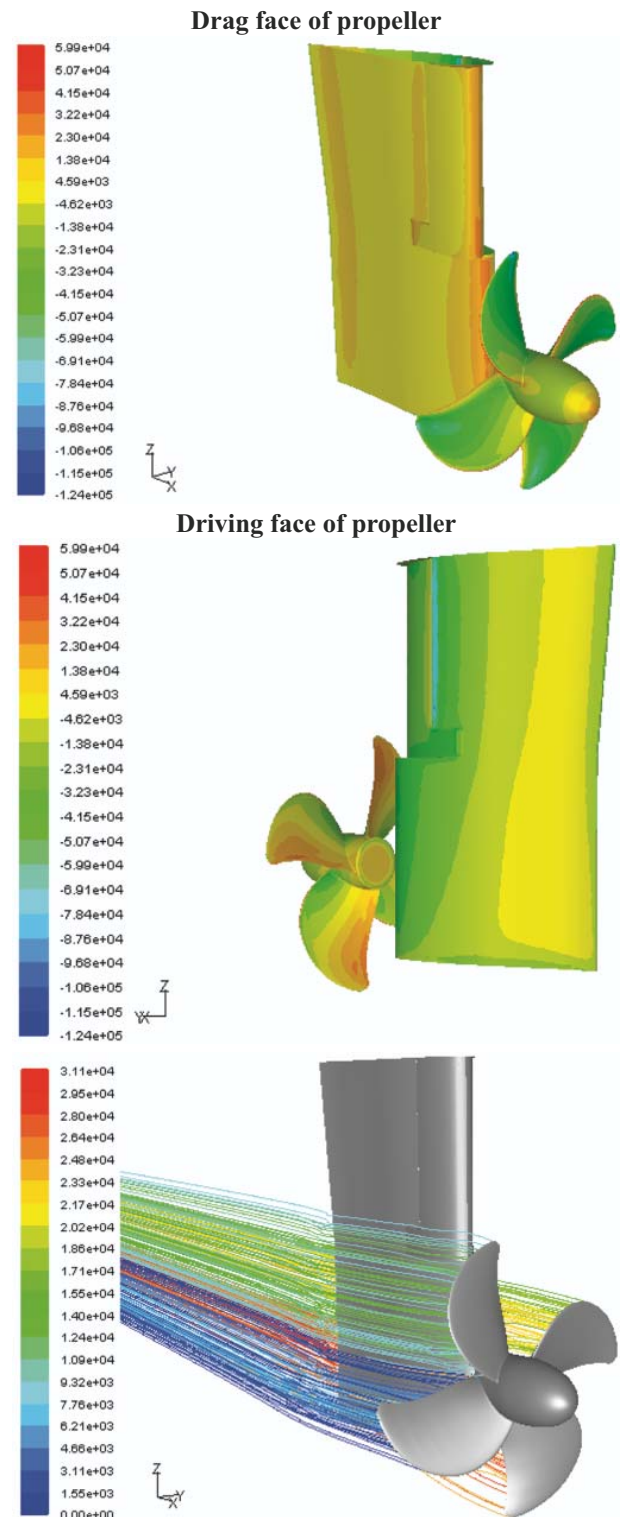
Fig. 6. *Pressure distribution and streamlines for the set of propeller and rudder deflected by 15°, the advance ratio J = 0.7*

Screw propeller without rudder									
No.	J [-]	D [m]	n [1/s]	V [m/s]	T [N]	Kt [-]	Q [Nm]	10Kq [-]	ρ [t/m³]	η₀ [-]
1	0.1	5.9	1.5	0.885	1624159	0.596514	948528.9	0.59046	998.66	0.160868
2	0.2	5.9	1.5	1.77	1365931	0.501673	839757.7	0.52275	998.66	0.305631
3	0.3	5.9	1.5	2.655	1122907	0.412416	722395.3	0.449691	998.66	0.438109
4	0.4	5.9	1.5	3.54	924202.1	0.339437	623854.7	0.38835	998.66	0.556719
5	0.5	5.9	1.5	4.425	720384.5	0.264579	518421.4	0.322718	998.66	0.652745
6	0.6	5.9	1.5	5.31	517910.9	0.190216	405355.8	0.252334	998.66	0.720215
7	0.7	5.9	1.5	6.195	281523.2	0.103397	281425.6	0.175188	998.66	0.657871
8	0.8	5.9	1.5	7.08	51307.51	0.018844	146254.1	0.091043	998.66	0.263667
Screw propeller + rudder without deflection									
No.	J [-]	D [m]	n [1/s]	V [m/s]	T [N]	Kt [-]	Q [Nm]	10Kq [-]	ρ [t/m³]	η₀ [-]
1	0.1	5.9	1.5	0.885	1529143	0.561616	930528	0.579254	998.66	0.154387
2	0.2	5.9	1.5	1.77	1295804	0.475917	802417.5	0.499505	998.66	0.303432
3	0.7	5.9	1.5	6.195	354941.1	0.130361	298832.2	0.186023	998.66	0.781123
Screw propeller + deflected rudder									
No.	J [-]	D [m]	n [1/s]	V [m/s]	T [N]	Kt [-]	Q [Nm]	10Kq [-]	ρ [t/m³]	η₀ [-]
1	0.1	5.9	1.5	0.885	1618327	0.594372	950265.5	0.591541	998.66	0.159998
2	0.2	5.9	1.5	1.77	1388741	0.51005	839860.6	0.522814	998.66	0.310697
3	0.7	5.9	1.5	6.195	380906.1	0.139897	315136.1	0.196172	998.66	0.794896

Results of the calculations of thrust, torque and efficiency of the propeller with accounting for the rudder, are presented in Tab. 1, and its hydrodynamic characteristics – in Fig. 7 through 10.
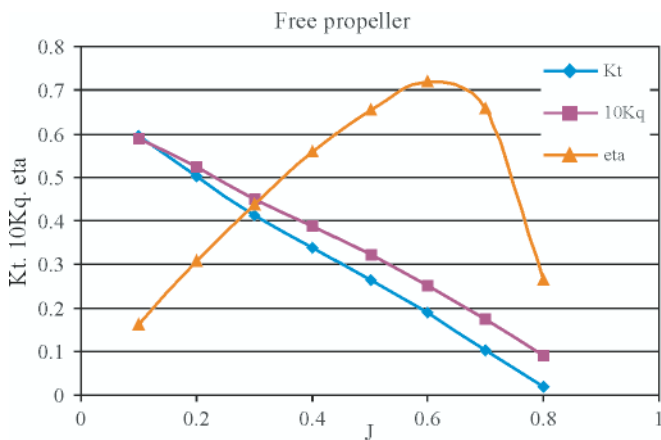
Fig. 7. *Hydrodynamic characteristics of the free propeller without rudder*
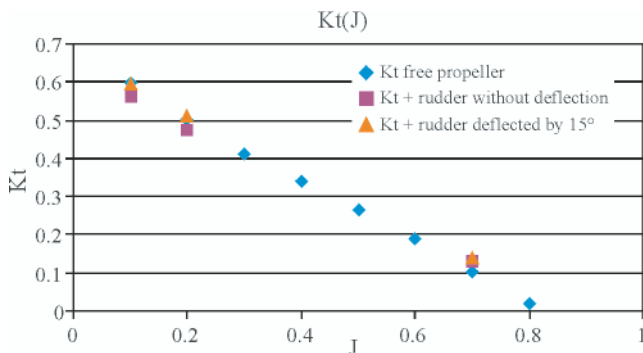
Fig. 8. *The thrust coefficient K_T for the free propeller, the set of the free propeller and rudder without deflection and that of the free propeller and rudder deflected by 15°*
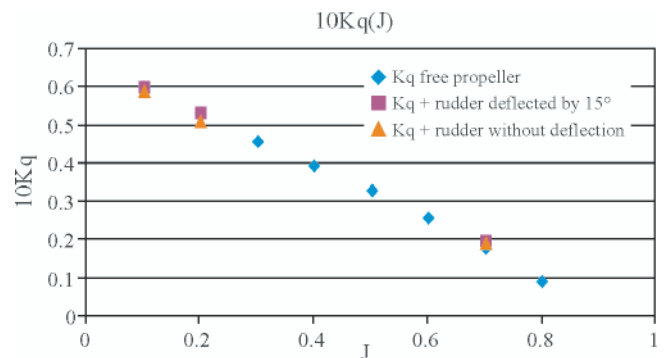
Fig. 9. *The torque coefficient Kq for the free propeller, the set of the free propeller and rudder without deflection and that of the free propeller and rudder deflected by 15°*
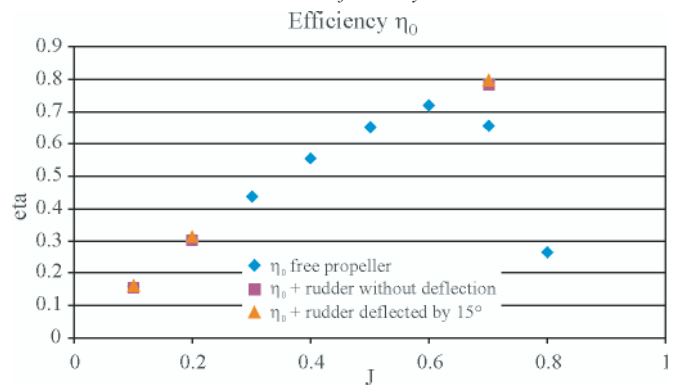
Fig. 10. *The efficiency η_0 for the free propeller, the set of the free propeller and rudder without deflection and that of the free propeller and rudder deflected by 15°*

CONCLUSIONS

As data concerning results of model tests are very scarce, to make comparison of the numerical analysis results with those of real model tests for free propeller is possible only for values corresponding with the advance ratio J = 0.70; relevant results of numerical calculations and model tests are compared in Tab. 2.

Tab. 2.

	model tests	numerical analysis	model / analysis
T	314800	281523.2	1.11820269
Q	228800	281425.59	0.81300354
η	0.564	0.65787141	0.8573104

The comparison of results for only one value of the advance ratio J does not allow to assess if the remaining results are correct or not, and does not provide information on correctness of run of the characteristics. However this is the only way of assessing the performed analysis in view of the lack of data.

Comparison of the efficiency, thrust and torque coefficients for free propeller, the set of propeller and rudder without deflection and that of propeller and rudder deflected by 15°, is performed in Tab. 3, 4 and 5.

Tab. 3.

Efficiency η_0				
No.	J	Free propeller	Propeller + rudder without deflection	Propeller + rudder deflected by 15°
1	0.1	0.160868285	0.154387068	0.159997698
2	0.2	0.305630894	0.303431839	0.310696571
3	0.7	0.65787141	0.781122746	0.794895671

Tab. 4.

Thrust coefficient K_T				
No.	J	Free propeller	Propeller + rudder without deflection	Propeller + rudder deflected by 15°
1	0.1	0.596513711	0.561616382	0.594371651
2	0.2	0.501672932	0.47591672	0.510050409
3	0.7	0.103396532	0.130361105	0.13989741

Tab.5.

Torque coefficient K_q				
No.	J	Free propeller	Propeller + rudder without deflection	Propeller + rudder deflected by 15°
1	0.1	0.059045983	0.057925422	0.05915408
2	0.2	0.052274967	0.049950537	0.052281374
3	0.7	0.01751876	0.018602322	0.019617241

In numerical calculations an applied computational model, type and size of mesh, and quality of geometrical model of analysed propeller play a very important role. The applied computational model could differ from the real propeller because of very scarce data on propeller geometry, hence to assess a degree of similarity between model and real propeller is not possible. The qualitative analysis performed by means of CFD methods demonstrated that the working screw propeller accompanied with streamline rudder located behind it, is capable of developing a greater efficiency than the free propeller without rudder.

As a result of presently conducted investigations an impact of geometrical parameters of rudder on propeller efficiency will be determined.

BIBLIOGRAPHY

1. Simonsen D. C.: *Rudder Propeller and Hull Interaction by RANS*. Doctoral thesis, Technical University of Denmark, Lyngby 2000
2. Bertram V., Heinemann B., House L.: *Practical Ship Hydrodynamics*. Jordan Hill Oxford OX2 8DP, 2000
3. El Moctar O.M. El., Bertram V.: *Selected Topics of CFD for Ship Manoeuvring*. INSEAN/Rome, 14-18 May 2001
4. Natarajan S.: *Computational Modeling of Rudder Cavitation and Propeller/Rudder Interaction*. The University of Texas at Austin, August 2003
5. Schneekluth H., Bertram V.: *Ship Design for Efficiency and Economy*. Butterworth Heinemann, Oxford 2004
6. Kobyliński L.: *Ship propellers* (in Polish). Wydawnictwo Komunikacyjne (Transportation publishers), Warsaw 1955
7. Koronowicz T., Waberska G., Krzemianowska Z.: *Influence of rudder on velocity field in waterstream behind the hull* (in Polish). Institute of Fluid Flow Machinery, Polish Academy of Sciences, Publ. No. 4493/4, Gdańsk 2004
8. Syrocki W.: *Ship B 573 - Results of the Model Tests* (in Polish). Ship Design and Research Centre, Technical Report No. RH–96/T–023A, Gdańsk 1995
9. Syrocki W.: *Ship B 573 - Final Design of Propeller* (in Polish). Ship Design and Research Centre, Technical Report No.RH-95/T-115A, Gdańsk 1995
10. Abramowski T., Żelazny K., Szelangiewicz T.: *Numerical analysis of influence of ship hull modification on resistance and propulsion characteristics, Part III: Influence of the modification on screw propeller efficiency*. To be published in PMR No 1/2010
11. Abramowski T., Szelangiewicz T.: *Numerical analysis of selected elements on effectiveness of streamline rudder*. To be published in PMR No 1/2010
12. Szelangiewicz T.: *Numerical investigations of rudder/propeller/ship stern interaction aimed at improving transport ship's propulsion and manoeuvrability qualities* (in Polish). Final report of the R&D project No. R 10 008 01, Szczecin 2009.

CONTACT WITH THE AUTHORS

Tomasz Abramowski, Ph. D.
Jakub Handke, M. Sc.
Tadeusz Szelangiewicz, Prof.
West Pomeranian University of Technology, Szczecin
Faculty of Marine Technology
Al. Piastów 41
71-065 Szczecin, POLAND
e-mail: tadeusz.szelangiewicz@ps.pl

Neural network-PID controller
for roll fin stabilizer

Hassan Ghassemi, Associate Prof.
Fatemeh Hoseini Dadmarzi, MSc Graduated
Parviz Ghadimi, Assistant Prof.
Faculty of Marine Technology, Amirkabir University of Technology, Tehran, Iran
Babak Ommani, MSc Graduated
Faculty of Mechanical Engineering, Sharif University of Technology, Tehran, Iran

ABSTRACT

Fin stabilizers are very effective devices for controlling the ship roll motion against external wave-generated moments. Lift forces due to flow around fin with an angle of attack produce anti - roll moment. Therefore control of attack angle plays important role in reducing roll of ships. This paper presents results of using a combined neural network and PID for roll control of ship with small draught. Numerical results are given of around-fin flow analysis with considering free surface effect modelled by neural network and imposed to controlling loop. Hydraulic machinery constraints are also considered in the modelling. The obtained results show good performance of the controller in reducing roll amplitude in random seas. The approach can be used for any irregular sea conditions.

Key words: Fin stabilizer; neural network; PID control; restoring force

INTRODUCTION

The aim of using roll stabilizing systems on ships depends on requirements of their mission such as the preventing against damage of cargo, increasing the effectiveness of crew or accuracy of positioning and handling weapons on naval vessels.

Roll motion is one of the most important ship motions. A large number of papers and publications are available on modelling the ship roll motion. There are many ship mission parameters influenced by rolling, such as safety of cargo, crew and passengers, fuel combustion, weapon positioning etc. Most of the roll stabilizers create a moment against roll exciting moment to decrease roll angle amplitude.

Fin stabilizer systems are found useful for roll damping. In this case, simulation of flow field around the fin and its performance has important role in research on decreasing the roll angle.

Lifting characteristics of the fins have been reasonably well predicted by semi-empirical formulae by Whicker and Fehlner [1] and Pitt et al. [2]. Sheldahl et al. [3] presented also experimental data of NACA0015 foil obtained in a wind tunnel test.

Hydrofoil lift characteristics are among thoroughly studied subjects and many papers and text books have been published in this regards (Newman. [4]).

Numerical results of foil analysis including cavitation and 2D and 3D free surface effects were published by Bal et al. [5]. They. presented also an improved numerical wave tank model for the hydrofoils by considering cavitations.

Effects of free surface and wave generated by a strut on fins attached to it were also studied numerically and experimentally by Lee et al. [6].

In this paper the results of flow field analysis around fin stabilizer including free surface, presented by the authors [7], are used for modelling the fin in the controlling loop. According to the results, hydrofoil lift characteristics are influenced by the presence of free surface in case of a considered small naval vessel.

There are many nonlinear and free-surface effects involved in modelling behaviour of fin stabilizer. The effects have been discussed in detail e.g. by Tristan Perez [8]. In dynamic modelling for controller design it is useful to include as much nonlinear and environmental effects as possible in order to achieve more accurate model without losing controllability of the system.

There are many controlling methods which could be used to achieve a good performance of fin stabilizers, for instance: PID, fuzzy logic, neural network. There are many papers on using traditional PID controller in fin stabilizers. The work by S. Surendrana et al. [9] can be referred to as an example of using PID in controlling the fin stabilizer. They used the CFD for calculating fin hydrodynamic behaviour by solving flow around a 3D horizontal fin attached to a wall.

In order to improve the performance of PID controller in fin stabilizing a combination of PID and modern controlling methods is sometimes used. For instance, the using of fuzzy-PID controller has been presented by Liang et al. [10].

In the present work the results of using NN-PID controllers in series arrangement are presented. The combined controller

in parallel arrangement was used for trajectory tracking of robotic manipulators by Wu et al. [11]. The performance of NN controlling algorithm was tested in four degrees-of-freedom by Zirilli et al. [12]. Moreover, Alarcin et al. [13] used neural network to control a rudder roll stabilizer.

In the present work the controlling loop consists of: ship dynamic model, neural network model of fin hydrodynamics, PID controller and inverse neural network model of ship heeling moment. In order to increase accuracy of the results, constraints of a hydraulic mechanism used for turning fins are also added to the fin model. According to the results presented by the authors [7] lifting force of fins with two opposite and equal attack angles, placed on two sides of sample ship should not be equal. In order to obtain a desirable restoring moment at large roll angles, two different angles of attack should be used instead of equal and opposite angles. Therefore in the present work, instead of using two equal angles with opposite signs for fins, equal portions of restoring moment from each fin is considered a desired situation. Neural network models are trained by using classical Error Back Propagation (EBP) technique. Combined NN-PID controllers are designed and optimized by using the MATLAB and Simulink environment. This combination shows good results in reducing ship roll motion resulting from external disturbances. It is worth to mention that instead of modelling the waves, exciting force is modelled as a disturbance in controlling loop.

GOVERNING EQUATION

There are many approaches to developing the ship roll governing equation, such as linear, nonlinear, coupled and uncoupled methods. In this paper the model presented by T. Perez [8] is used to derive a model for controlling loop design. The uncoupled ship roll motion equation is as follows:

$$I_{\phi\phi}\ddot{\phi} + B\dot{\phi} + C\phi = \tau_{control} + \tau_{exiting} \qquad (1)$$

In Eq. (1), $\tau_{control}$ is the restoring moment produced by fins, and $\tau_{exiting}$ is the roll exciting moment applied to the ship.

There are analytical equations for calculating the lift force of fins in function of angle of attack, but in the present work numerical results accounting for the free surface effects, were used.

It is important to note that the effective attack angle of fins may change because of roll motion and a new attack angle should be considered in finding the restoring moment. The formula for calculating the effective attack angle is given by Eq. (2) and (3):

$$\alpha_{fl} = \arctan\left(\frac{r_f\dot{\phi}}{U}\right) \approx \frac{r_f\dot{\phi}}{U} \qquad (2)$$

$$\alpha_{effective} = \alpha_{fl} + \alpha \qquad (3)$$

The force component which is directed perpendicularly to the flow velocity far ahead the foil constitutes the lifting force represented by the lift coefficient. Eq. (4) shows the relation between the restoring moment and lift coefficient used for calculating the moment:

$$M_{restoring} = \tfrac{1}{2}\rho A U^2 C_L r_f \qquad (4)$$

MODELING

The first step of controller design is modelling. There are two different elements which should be modelled in this problem: vessel and fin stabilizer.

Vessel modeling

In this work a naval vessel model prepared by Blanke and Christensen [14] is used. The model was also implemented by Perez [8] and MARINTEK at NTNU through open source MATLAB tool box, called MSS. The model contains all coefficients for nonlinear ship manoeuvring in surge, sway, yaw and roll. Tab. 1 shows the ship's main dimensions and properties.

Tab. 1. Main particulars of the ship

L	51.5 m
B	8.6 m
D	2.3 m
Δ	362000 Kg
I_{zz}	47934*10^6
I_{xx}	23763*10^6
U	8 m/s
KM	4.47 m
KB	1.53 m
GM	1.1 m
LCG	20.41 m
VCG	3.36 m

The model was modified in order to be combined with fin-stabilizer. The initial values are: surge, sway, roll and yaw velocities as well as roll and yaw angles. The inputs are: surge and sway forces as well as roll and yaw moments. For purpose of our task the sway and yaw moment is set to be zero and the surge force to be constant in order to simulate behaviour of the ship on straight course with the constant speed of about 8 m/s.

The roll moment is summation of the fin-stabilizing moment and an exciting moment due to environmental effects. The exciting roll moment is simply modelled by combining the sinusoidal moments with different amplitudes, frequencies and phase angles. It should be noted that it was not an intention of the authors of this work to calculate a real exciting roll moment in waves.

The model outputs are: surge, sway roll and yaw velocities as well as roll and yaw angles. Although the straight course at constant forward speed were only used for the simulation, the model is capable of being applied to simulating roll in turning or other manoeuvring scenarios.

Fin-stabilizer modeling

In the present work the fin-stabilizer consisted of two identical non-rectangular hydrofoils of a low aspect ratio, symmetrically placed on both sides of vessel. The geometrical properties of fins are specified in Tab. 2, and Fig. 1 shows schematically the shape of the fin.

Tab. 2. Fin parameters

Foil section	NACA0015
Tip chord [m]	0.9
Root chord [m]	1.8
Span [m]	1
Area [m²]	2.25

Hydrodynamic effects of the fin on vessel's behaviour are considered negligible. In other words it is assumed that, except of roll controlling moment, the fin does not have any other effect on vessel's manoeuvring model. Because of the small draught of the vessel, the free surface effects on hydrodynamic fin coefficient,

are important. Only the calm free surface effects are considered in modelling the fins hydrodynamic properties. Effects of waves could be later added to controlling loop as a disturbing noise.
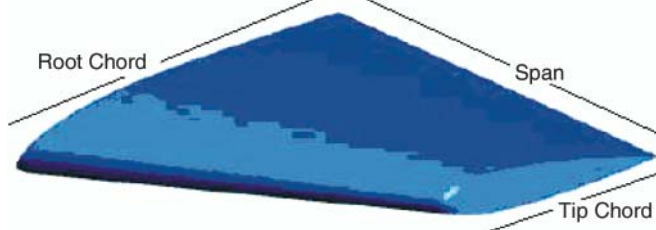
Fig. 1. Schematic shape of the fin

These authors investigated the flat free surface effects on hydrofoil's lift coefficients by using the CFD and RANS model presented elsewhere, [7]. A sample case of free surface shape around ship and fin is presented in Fig. 2. The results of hydrodynamic lift coefficient in function of attack angle of fin and roll angle of ship are presented in Fig. 3. For considering the fin's hydrodynamics in control loop, a simple neural network model is trained to follow this diagram. The trained neural network model inputs are: fin's attack angle and ship's roll angle, and the output is fin lift coefficient.
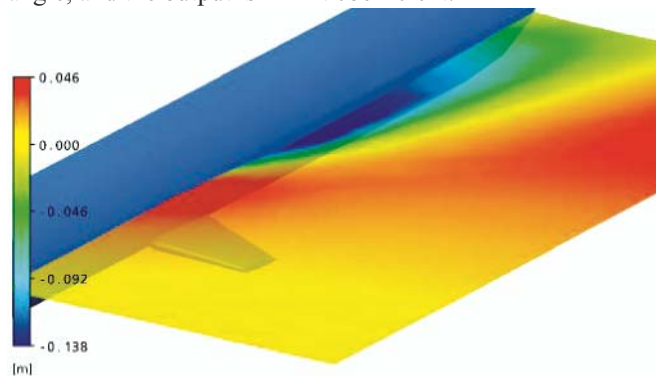
Fig. 2. Free surface profile around ship body and attached fin, at 8 m/s forward speed [7]

There are some constraints imposed by the hydraulic machinery such as: the maximum mechanical fin angle and speed of changing the fin angle. As Fig. 1 shows, after the stall angle the fin's lift coefficient falls down. Moreover, the presented NN model is not valid after stalling, therefore the stall angle is also added to the model as a constraint. Dynamic effects of the mechanical system used for fin angle changing are represented by a simple integration loop. The maximum mechanical fin angle and its maximum rate of change are assumed to be 25 degrees and 25 degrees per second, respectively, i.e. usual design values [8]. Fig. 4 shows the considered model.

To calculate a correct effective angle of attack is also important. As mentioned before, the effective angle of attack refers to the angle between net input velocity of foil and flow.

The net velocity will be here the summation of the inflow velocity due to ship forward speed and that due to ship rolling motion. Therefore another block added to the model to calculate the effective angle of attack is based on Eq. (3). Fig. 5 shows the complete model of the fin. The input to the fin's model is the desired fin angle, and the output is the fin lift coefficient accounting for the mechanical system dynamics and the flat free surface effects. Next, the fin's roll moment is calculated by multiplying the lift coefficient and a calibrating gain calculated from Eq. (4).

According to the results presented in Fig. 3, because of the free surface effects, two identical fins placed on two sides of the ship do not give the same roll moment even at equal angles of attack. Therefore to better model the fin stabilizer two fin models shown in Fig. 5, are used.
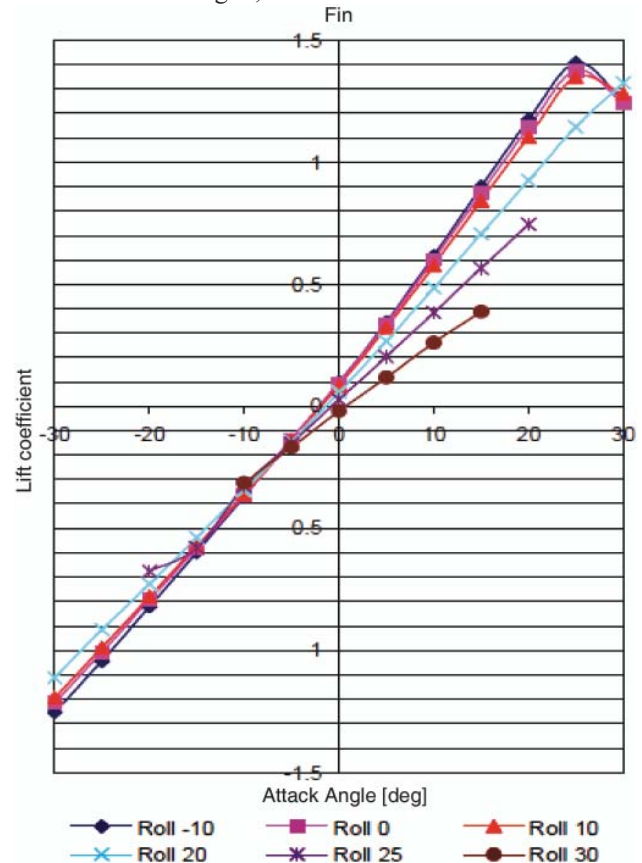
Fig. 3. Lift coefficient in function of angle of attack and various ship roll angles, U = 8 m/s [7]
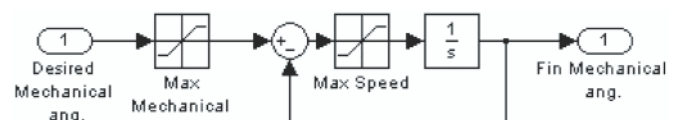
Fig. 4. Block diagram of fin mechanical system
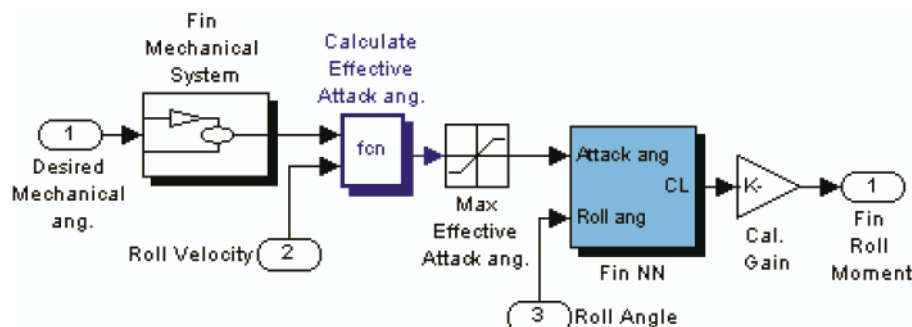
Fig. 5. Block diagram of fin model combined with mechanical system

CONTROL LOOP AND RESULTS

The next step is forming the controlling loop. To accomplish this and overcome complexities of models different controlling methods such as PID and neural network are combined. The PID controller is used as a main controlling tool. For considering complex behaviour of roll moment in function of roll angle in case of large angles and forward speed, an inverse neural network model is trained by using the Error Back Propagation technique (EBP) based on the results achieved from the introduced ship dynamic model. The input for the trained NN model is the heel angle and the output is the heeling moment caused by the input heel angle.

At the first step a simple controlling loop shown in Fig. 6, is used. The NN model of the ship heeling moment is placed in a closed control loop. Then the NN gains are optimized against positive and negative external pulses as disturbances, by using a genetic algorithm. By doing so, a more accurate and stable NN model for heeling moment is achieved.

In the next step the PID controller was added to the NN as shown in Fig. 7. Then the PID gains were optimized by using the genetic algorithm to achieve optimized controlling performance in response to the same disturbances as before. The gains were used as the first estimation for the complete controlling loop containing fin models.

The heel moment resulting from the NN model was considered as the desired roll moment which should be interacted by the fin stabilizer. The desired roll moment should be divided in two portions, translated into desired mechanical fin angle and then passed to the fin model. To achieve this, an inverse NN model of fin lift coefficient, was trained. Equal moments acting on two fins were used, which was equivalent to equal portions of heeling moment. Other portions could be also used to achieve equal angles of attack or maximum efficiency of fin stabilizer. The arrangement for one fin is shown in Fig. 8.

The output of the fin model will be an actual restoring moment produced by the fin stabilizer. In this step for this new arrangement the genetic algorithm is used to optimize PID gains against the same pulse disturbances. Therefore the steps of the complete controlling loop shown in Fig. 9, could be summarized as follows:

1. the PID controller receives vessel's roll angle and generates a suitable command;
2. the PID command is translated to a desired total restoring moment;
3. the desired total restoring moment is divided in two equal portions, one for each fin;
4. the desired moment for each fin is translated into a lift coefficient by dividing it by a calibrating gain;
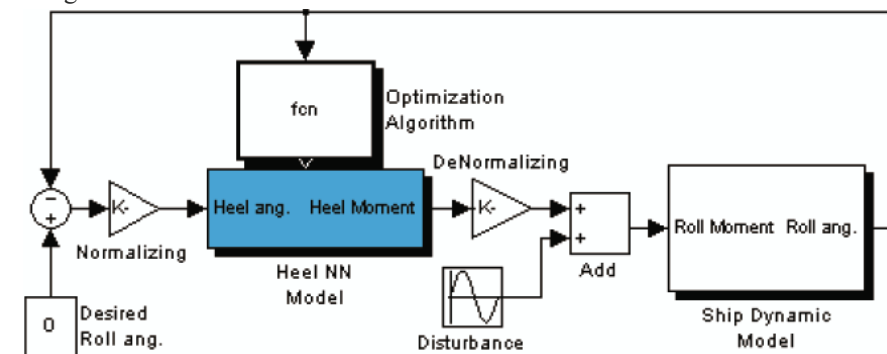
Fig. 6. Optimizing the NN gains in controlling the heel moment without application of fins, performed by means of a genetic algorithm
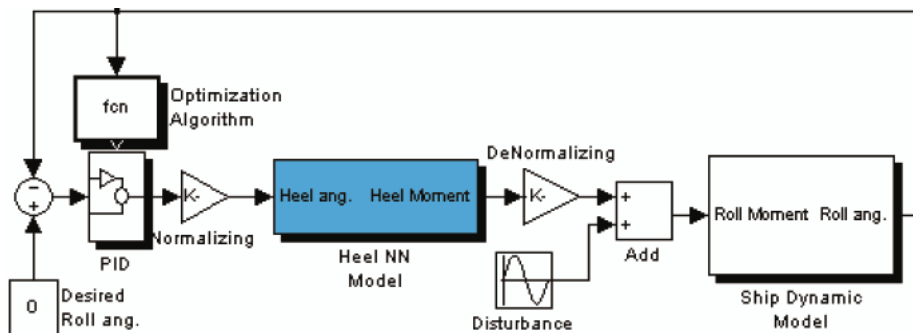
Fig. 7. Optimizing the PID gains in controlling roll moment of the vessel without fins, by using genetic algorithm
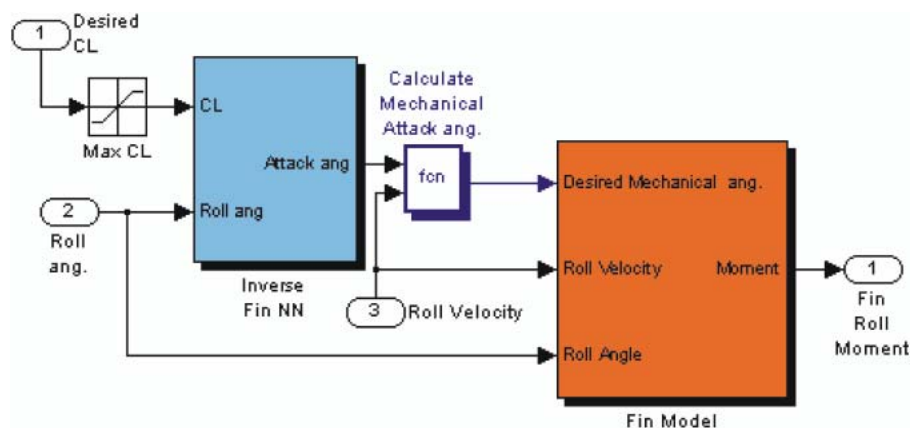
Fig. 8. The arrangement for translating the desired CL into the desired mechanical angle and actual fin moment
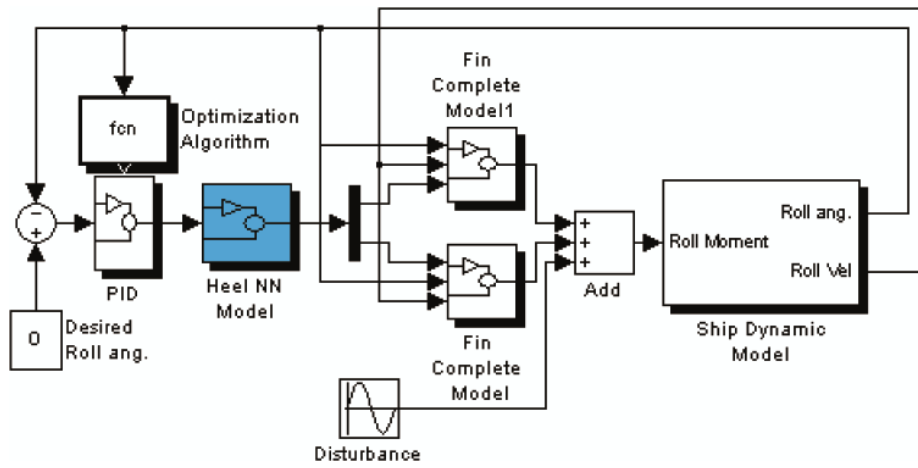
Fig. 9. *The complete controlling loop*

5. each resulted lift coefficient is checked and constrained by the maximum fin lift coefficient;
6. the lift coefficient is translated into a fin effective angle of attack by using the inverse NN model of fin lift coefficients;
7. by considering ship roll velocity, a desired mechanical attack angle is calculated and passed to the fin model;
8. the fin model gives an actual fin restoring moment by accounting for a fin mechanical system delay and free surface effect;
9. the fins' restoring moments are added to the environmental roll exciting moments and passed to the ship's dynamic model;
10. the ship dynamic model gives a new roll angle and roll velocity to be used in the next step.

The model responses to two roll exciting moments are simulated. Fig. 10 shows two sample time history of the exciting

moments. The upper figure is considered the case (a) and the lower figure - the case (b).

Fig. 11 shows ship's roll angle time history in case of the forward speed of 8 m/s in presence of the exciting roll moment (a), with and without fin stabilizers. As showed, the ship roll angle is reduced by using the active fin models. It is important to note that the fin angles are not necessarily the same on both sides of the ship and each fin angle is optimized by considering the free surface effects. Fig. 12 shows the same results for the case (b). Although the complex model including the free surface effects was used for fin stabilizers, the designed controller was capable to reduce roll angle amplitude effectively.

Fig. 10. *Two sample exciting moments: case (a) - the upper figure, case (b) - the lower figure*
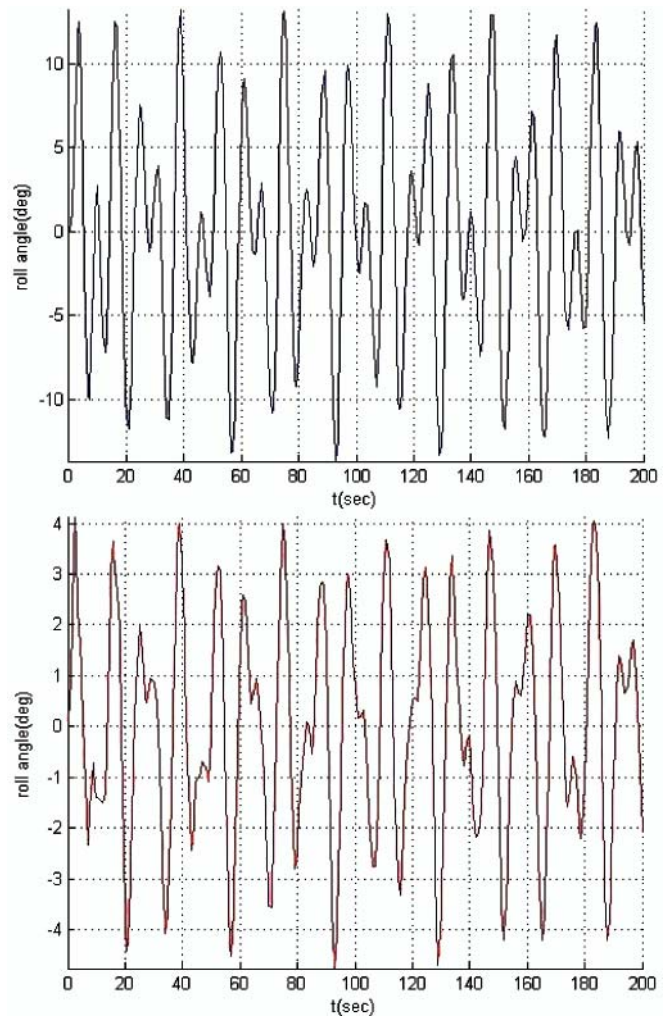
Fig. 11. *Time history of roll angles for the exciting moment (a): the upper figure - without action of the controller, the lower figure - with action of the controller*
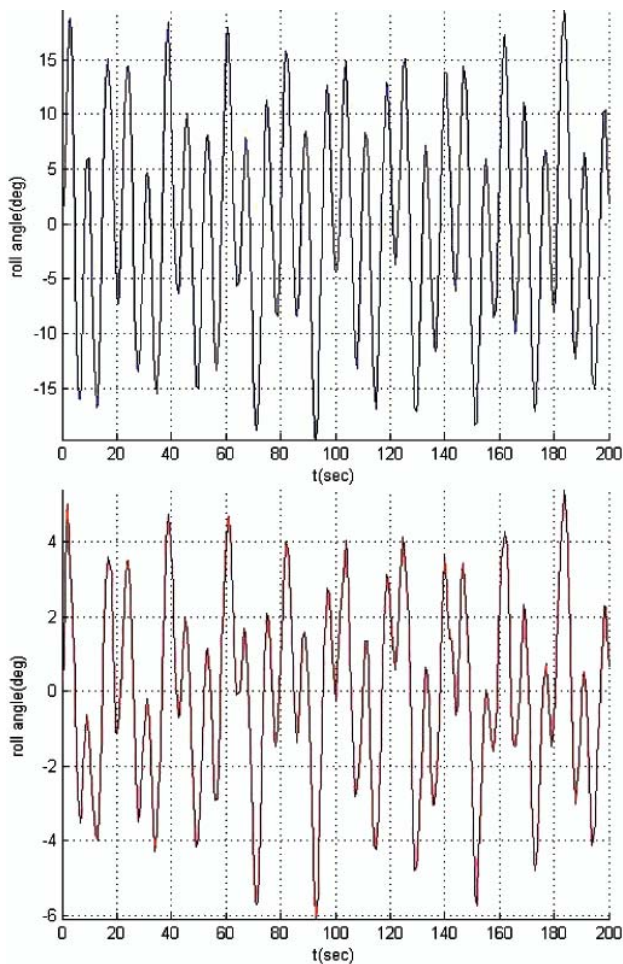
Fig. 12. *Time history of roll angles for the exciting moment (b): the upper figure - without action of the controller, the lower figure - with action of the controller*

CONCLUSION

New fin models accounting for free surface effects were developed to be used in dynamic modelling of ships with fin stabilizers. By using the new model the fin stabilizer dynamic model was improved. A neural network model was trained on the basis of CFD simulation of hydrodynamic behaviour of a fin close to free surface.

For the effective controlling of fin stabilizers combined PID - NN controllers were used. Two fins placed on both sides of the vessel were controlled in a different way to overcome unsymmetrical behaviour resulting from free surface effects. By doing so, more realistic and efficient behaviour of fins were achieved.

A genetic algorithm was used to optimize behaviour of NN and PID controlling system. Good performance and response of the controlling system was achieved by using the controlling approach even to more complex fin models.

NOMENCLATURE

ϕ	-	Roll angle
$\dot\phi$	-	Roll velocity
$\ddot\phi$	-	Roll acceleration
U	-	Ship service speed
h	-	Immersed depth
Fn_h	-	Submergence Froude number
C_L	-	Lift coefficient
r_f	-	Fin arm
C_P	-	Pressure coefficient
α	-	Fin attack angle
α_{eff}	-	Effective attack angle

L	-	Ship Length.
B	-	Ship Breath
D	-	Ship Draft
Δ	-	Ship Displacement
I_{zz}	-	Ship Moment of Inertia around Z axes
I_{xx}	-	Ship Moment of Inertia around X axes
KM	-	Ship meta-centric height from keel
KB	-	Ship center of buoyancy from keel
GM	-	Distance between ship's center of gravity and meta-center
LCG	-	Ship's longitudinal center of gravity
VCG	-	Ship's vertical center of gravity
PID	-	proportional-integral-derivative controller
NN	-	Neural Network
CFD	-	Computer Fluid Dynamics.

BIBLIOGRAPHY

1. Whicker L.F., Fehlner L.F.: *Free-stream characteristics of a family of low aspect-ratio, all-moveable control surface for application to ship design*. DTMB report, 1958
2. Pitt W.C., Nielsen J.N., Kaatari G.E.: *Lift and center pressure of wing–body–tail combinations at subsonic, transonic and supersonic speeds*. NACA report 1307, 1959
3. Sheldahl R. E. and Klimas P. C.: *Aerodynamic, Hydrofoil data*, Sandia National Laboratories, Albuquerque, New Mexico, March 1981
4. Newman J.N.: *Marine Hydrodynamics*, 1977
5. Bal S., Kinnas S. A., Lee H.: *Numerical analysis of 2-D and 3-D cavitating hydrofoils under a free surface*, J. Ship Res., 45, 1, 2001
6. Lee C.M., Park I.R., Chun H.H., Lee S.J.: *Effect of free surface and strut on fins attached to a strut*, Ocean Engineering 28, 2000
7. Hoseini Dadmarzi F., Ghassemi H., Ghadimi P., Ommani B.: *Flow field analysis around the ship fin stabilizer including free surface*, Proceedings of the OMAE2009, Hawaii, USA, 2009
8. Tristan Perez: *Ship motion control: course keeping and roll stabilization using rudder and fins*, Springer 2005
9. Surendran S., Lee S.K., Kim S.Y.: *Studies on an algorithm to control the roll motion using active fins*, Ocean Engineering 34, 2007
10. Lian Yan-hua, Jin Hong-zhang, Liang Li-hua: *Fuzzy-PID controlled lift feedback fin stabilizer*, J. Marine. Sci. Appl. (2008) 7
11. Wu C. and Huang C.: *A Neural Network Controller with PID Compensation for Trajectory Tracking of Robotic Manipulators*, J. Franklin Inst. Vol. 333(B), No. 4, 1996
12. Zirilli A., Roberts GN., Tiano A., Sutton R.: *Adaptive steering of a containership based on neural networks*, International Journal of Adaptive Control and Signal Proceedings of the Int. J. Adapt. Control Signal Process. 2000; 14
13. Alarcin F., Gulezb K.: *Rudder roll stabilization for fishing vessel using neural network approach*, Ocean Engineering 34, 2007
14. Blanke M. and Christensen A.: *Rudder-roll damping autopilot robustness to sway-yaw-roll couplings*. 10th Ship Control Systems Symposium, Ottawa, Canada (1993).

CONTACT WITH THE AUTHORS

Hassan Ghassemi, Associate Prof.
Fatemeh Hoseini Dadmarzi, MSc Graduated
Parviz Ghadimi, Assistant Prof.
Faculty of Marine Technology
Amirkabir University of Technology
Hafez Ave.,
Tehran, IRAN
e-mail: gasemi@cic.aut.ac.ir

Babak Ommani, MSc Graduated
Faculty of Mechanical Engineering,
Sharif University of Technology,
Tehran, IRAN

Entropy function application in the selection process of diagnostic parameters of marine diesel and gas turbine engines

Zbigniew Korczewski, Assoc. Prof.
Gdansk University of Technology

ABSTRACT

The article presents the method of analysing the diagnostic informativeness of the parameters characterizing gas dynamic processes observed inside the working spaces of marine diesel and gas turbine engines. The entropy function was used as the measure of indeterminacy of the identified set of engine unserviceability states. Based on numerical simulation experiments of the analysed gasodynamic processes, the amount of introduced diagnostic information was assessed and the most adequate parameters for the technical state of the engine were selected. These parameters compose the minimised set of diagnostic parameters which make it possible to assess unmistakably the technical state of the examined working spaces.

Keywords: marine diesel and gas turbine engines; diagnostics; diagnostic informativeness; entropy function

INTRODUCTION

Diagnostic investigation is a basic element of the diagnostic process of each technical device [1]. A diagnostician, expert in the given branch, collects so-called primary information on the examined object from organoleptic examination, or by measuring parameters of the signals generated by the object.

In the next step of the diagnostic activity the expert (diagnostician) performs a so-called measurement-based inference. He creates a set of symptoms, analyses it and formulates a preliminary diagnosis about the technical state of the machine based on his knowledge about past defects. Usually the created set of symptoms corresponds to a number of possible defects, therefore the diagnostician makes attempts to gain additional diagnostic information (symptoms), using more and more sophisticated (expensive and technically complicated) methods and means, to be able to eliminate less possible defects. An ideal situation is when only one possibility remains, being the final diagnosis characterised by a given probability [4].

The "bottleneck" of the diagnostic process organised in the above way, especially when it refers to technical objects of high complexity level, is the diagnostic knowledge resulting from the past experience of the diagnostician. This experience referring to the defect-symptom relations is gained from:
- experts' opinions,
- experimental investigations on a real object:
  - active experiments – with the introduction of real defects to the machine,
  - passive experiments – with many years' observation of a large number of examined machines of the same type, without interference into their technical state,

- simulation experiments on specially developed computer codes – with possible modelling of different types of machine defects.

Due to the dynamic development of the widely understood computer science and technology, in the next years to come the computer simulation methods can become very useful diagnostic tools. However, significant limitation in their practical application is the problem of experimental verification of the computer codes used for the simulation. The only way to confirm the credibility of the diagnostic simulation experiments is still the testing examination done on model rigs (or, if possible, on real objects), done with the aid of the traditional analogue technique.

DIAGNOSTIC PARAMETER TOLERANCE RANGE

Producers of marine internal combustion engines of both piston and turbine construction define a set of basic diagnostic parameters which can be determined by the user in sea conditions. They also give tolerance limits within which the values of these parameters should remain during engine operation. The parameters characterise the quality of engine operation and make it possible to assess its general technical state. When the value of any parameter goes beyond the given limits, it is a signal of inadmissible disturbance of the energy conversion processes taking place in the engine, and a threat of failure.

In this situation the user should begin to localise the defect by making attempt to collect detailed data on the technical state of

particular functional modules. He has to analyse a large number of diagnostic parameters whose values, nearing the limits of the operating tolerance ranges, can be the symptoms of small technical state changes, characteristic for the "approaching" state of unserviceability. All this leads to a conclusion that precise assessment of the diagnostic tolerances determines the depth and quality of the formulated diagnosis [1].

The problem with selecting a set of adequate diagnostic parameters and limits of their operating tolerance is particularly complicated when analysing dynamic characteristics of the engine. An effective tool which can be used in searching an analytical solution to this problem is the concept of the distance between functions, known from the classical mathematical analysis [8] – Fig.1.

The distance between two continuous functions $X(\tau)$ and $X'(\tau)$ is defined as:

$$J = \sqrt{\int_{\tau=0}^{\tau=t}[X(\tau) - X'(\tau)]^2 \, d\tau} \qquad (1)$$

where:
$X(\tau)$ – known form of the function which maps the time-history of changes of the diagnostic parameter of the fully serviceable engine;
$X'(\tau)$ – known form of the function which maps the time-history of changes of the diagnostic parameter of the technically unserviceable engine.

When the forms of the compared functions are not known, and the only information about them is given in the form of discrete values of the recorded dynamic time-histories, we can calculate the functional $J(x, x')$, bearing the name of metric, whose value for a given pair of elements $\{x, x'\}$ of the compared time-histories is the distance between points x and x'. The metric defined in the above way can be used in two ways:
• for quantitative assessment of the time-histories – as the averaged value [8]:

$$J(x, x') = \sqrt{\sum_{\tau=1}^{t}(x_\tau - x'_\tau)^2} \qquad (2)$$

• for qualitative assessment of the time-histories – ands the maximum value [8]:

$$J_{max}(x, x') = \max_{0 \le \tau \le t}|x_\tau - x'_\tau| \qquad (3)$$

where:
$x(\tau)$ – discrete value of the diagnostic parameter of the fully serviceable engine;
$x'(\tau)$ – discrete value of the diagnostic parameter of the technically unserviceable engine.

In both cases the value of the metric will be a number which expresses a certain dimension of the distance between the compared sets. The geometrical sense of the distance is explained in Fig. 1.

In order to perform a comparison analysis of a larger number of the recorded dynamic time-histories, given in different sets (units) of discrete function values, a concept of the referential metric is introduced, whose dimensionless value can be a general comparative factor for all analysed time-histories:

$$\delta J = \sqrt{\sum_{\tau=0}^{t}\left(\frac{x_\tau - x'_\tau}{x_\tau}\right)}\,100\% \qquad (4)$$

If X_τ is the set of discrete values of the time-history of changes of the (reference) control parameter recorded during the acceleration of the analysed machine system without defects and X'_τ is the time-history of changes of the same parameter for the system with a defect, then the value of the metric defined by formula (4) will be the value of the diagnostic parameter which characterises certain state of unserviceability, in a quantitative aspect. This value can be considered the measure of diagnostic sensitivity of the parameter.
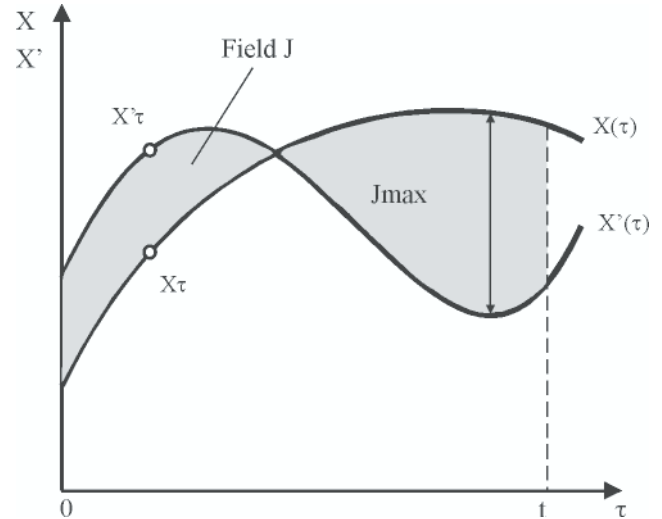
Fig. 1. Geometric interpretation of the distance between two functions recorded in the form of sets of discrete values

AMOUNT OF DIAGNOSTIC INFORMATION

The technical state of each module of the marine internal combustion engine is described by a relatively large set of diagnostic parameters (either directly measured or calculated), which could be initially determined after analysing its functional scheme. The analysis of all possible parameters in the diagnostic examination process is pointless and should be reduced to the optimal set of parameters which secures the control of the technical state of the engine and localisation of the identifiable (known and typical) engine defects. Therefore the hypothetical set of diagnostic parameters defined in the initial stage of the diagnostic process is to be minimised taking into account the following criteria:
• maximal amount of the introduced diagnostic information about the unserviceability states,
• diagnostic sensitivity of the examined engine type.

An attempt is to be made to reach a state in which the finally verified set of parameters provides opportunities for identification of each of operational unserviceability states of the analysed construction unit. The ideal situation is when one diagnostic parameter characterises unmistakably one certain fault. However, as results from the performed investigations [3, 7], in case of marine internal combustion engines one diagnostic parameter corresponds, as a rule, to a number of possible unserviceability states.

In order to perform a rational selection of diagnostic parameters, the degree of indeterminacy of the selected set of unserviceability states is analysed. According to Shannon, the amount of diagnostic information about the technical state of the engine which is carried by each analysed parameter can be assessed using:
• unconditional entropy – as the measure of indeterminacy of the set of unserviceability states:

$$E(S_n) = -\sum_{i=1}^{k} p_{bi} \log_2 p_{bi} \qquad (5)$$

where:

S_n – finite set of engine unserviceability states,

k – number of possible unserviceability states composing the set S_n,

p_{bi} – probability of appearance of one of possible unserviceability states.

- averaged conditional entropy – which makes it possible to calculate the decrease of the indeterminacy of the set of unserviceability states after one (successive) diagnostic parameter δx_j is determined:

$$E(S_n / \delta x_j) = p_{bj}(\delta x_j)E_{\delta x_j}(S_n) + p_{bj}(\overline{\delta x_j})E_{\overline{\delta x_j}}(S_n) \qquad (6)$$

where:

δx_j – diagnostic parameter value

$\overline{\delta x_j} = 1 - \delta x_j$ – value opposite to δx_j

$p_{bj}(\delta x_j), p_{bj}(\overline{\delta x_j})$ – probability with which the parameter δx_j reacts to engine unserviceability states, and the probability at which $\overline{\delta x_j}$ does not react,

$E_{\delta x_j}(S_n), E_{\overline{\delta x_j}}(S_n)$ – conditional entropies of the unserviceability set after determining the diagnostic parameter δx_j for the subset of states to which the parameter δx_j reacts and the subset of state to which $\overline{\delta x_j}$ does not react, respectively.

The amount of diagnostic information about the engine unserviceability states S_n which is carried by the parameter δx_j can be calculated using the formula:

$$I_{\delta x_j \rightarrow S_N} = E(S_n) - E(S_n / \delta x_j) \qquad (7)$$

SAMPLE RESULTS OF EMPIRICAL INVESTIGATIONS

The applicability of the proposed method to the process of selection of diagnostic parameters with the aid of the entropy function was verified using the results of past numerical experiments simulating gasodynamic processes realised in the working spaces of the selected marine engines: a medium speed diesel engine with pulsating turbo pressure charging system, and a three-shaft gas turbine engine with a separate power turbine [5, 6]. The mathematical models of processes, developed for this purpose, made it possible to simulate selected known and recognisable defects of the constructional structure of the examined engines, which are most frequently observed in the engine operation process.

The marine diesel engine

The states of engine unserviceability and the state of its full serviceability, which are used in the analysis, were obtained as a result of mathematical modelling of gasodynamic processes taking place in the working spaces of the marine engine. The analysed time-histories of gasodynamic parameters (temperature T, pressure p, and the speed v of the exhaust gas pressure peak amplitude displacement) were calculated for the selected control section of the exhaust gas outlet channel (the channel which connects engine cylinders with the turbo compressor turbine). Percent values of the referential metrics (diagnostic parameters) δx_j which are given in Tab. 1, were assessed by comparing the standard time-histories of gasodynamic parameters recorded during the simulation of engine processes in full serviceability conditions, and corresponding curves recorded for the engine with the modelled operational unserviceability states S_{n1}, S_{n2}, S_{n3}, S_{n4}, S_{n5}, S_{n6}, S_{n7}, S_{n8}, S_{n9}, S_{n10}, S_{n11}, S_{n12}, S_{n13} and S_{n14}.

Mutual relations between the finite set of engine working space unserviceability states S_{ni} and diagnostic parameters δx_j, identifying those states can be clearly presented using so called diagnostic matrices – Tab. 2. It was assumed that if the diagnostic parameter value δx_j exceeds the tolerance range limits by 10 percent or more ($\delta x_j \geq 10\%$) while reacting to the unserviceability state S_{ni}, then "1" is placed in the diagnostic matrix entry situated at the crossing of the j-th row and the i-th column. If the parameter does not react to the unserviceability state – "0" is placed. The last matrix column contains the amounts of diagnostic information calculated using formula (7).

Tab. 1. *Metric values δx_j for the modelled operational unserviceability states of the working spaces of SULZER engine 6AL20/24 type*

		Operational unserviceability states														
		S_{n1}	S_{n2}	S_{n3}	S_{n4}	S_{n5}	S_{n6}	S_{n7}	S_{n8}	S_{n9}	S_{n10}	S_{n11}	S_{n12}	S_{n13}	S_{n14}	S_{n15}
		[%]	[%]	[%]	[%]	[%]	[%]	[%]	[%]	[%]	[%]	[%]	[%]	[%]	[%]	[%]
Diagnostic parameter	δT	6.28	12.7	15.7	6.1	12.4	15.4	20.5	20.5	13.5	14	6.96	9.57	5.31	7.75	0
	δp	6.81	13.9	17.2	6.35	13	16.1	20.7	20.7	13.9	14.5	6.96	10	5.6	8.22	0
	δv	20.3	50.6	49.8	15.2	30.4	37.4	31.9	31.9	22	25	14.4	20	10.8	15.3	0

S_{n1} – decreasing outlet valve active cross-section areas in cylinders 1, 2 and 3 by 5 %,

S_{n2} – decreasing outlet valve active cross-section areas in cylinders 1, 2 and 3 by 20 %,

S_{n3} – decreasing outlet valve active cross-section areas in cylinders 1, 2 and 3 by 30 %,

S_{n4} – decreasing outlet valve active cross-section areas in cylinder 1 by 5 %,

S_{n5} – decreasing outlet valve active cross-section areas in cylinder 1 by 20 %,

S_{n6} – decreasing outlet valve active cross-section areas in cylinder 1 by 30 %,

S_{n7} – changing outlet valve opening and closing angles in cylinders 1, 2 and 3 by +5° OWK,

S_{n8} – changing outlet valve opening and closing angles in cylinders 1, 2 and 3 by -5° OWK,

S_{n9} – changing outlet valve opening and closing angles in cylinder 1 by +5° OWK,

S_{n10} – changing outlet valve opening and closing angles in cylinder 1 by -5° OWK,

S_{n11} – decreasing combustion chamber volumes in cylinder sections 1, 2 and 3 by 25%,

S_{n12} – decreasing combustion chamber volumes in cylinder sections 1, 2 and 3 by 50%,

S_{n13} – decreasing combustion chamber volumes in cylinder section 1 by 25%,

S_{n14} – decreasing combustion chamber volumes in cylinder section 1 by 50%,

S_{n15} – state of full operational serviceability of engine working spaces.

		Operational unserviceability states													
		S_{n1}	S_{n2}	S_{n3}	S_{n4}	S_{n5}	S_{n6}	S_{n7}	S_{n8}	S_{n9}	S_{n10}	S_{n11}	S_{n12}	S_{n13}	S_{n14}	S_{n15}	**I**
Diagnostic parameter	δT	0	1	1	0	1	1	1	1	1	1	0	0	0	0	0	1.000
	δp	0	1	1	0	1	1	1	1	1	1	0	1	0	0	0	0.970
	δv	1	1	1	1	1	1	1	1	1	1	1	1	1	1	0	0.355

As results from the numerical data collected in the diagnostic matrix (Tab. 2), the diagnostic information maximum criterion, I = max, leads to the selection of the exhaust gas temperature as the best diagnostic parameter ($I_{\delta T}$ = 1.0). This makes it possible to reduce the diagnostic inference analysis to eight states, to which this parameter reacts, or seven remaining states, depending on the value which it reaches in the control process.

The diagnostic parameter of similar applicability is the exhaust gas pressure in the outlet channel, for which the amount of the introduced diagnostic information about the analysed technical states of the engine working spaces is equal to $I_{\delta p}$ = 0.970.

At the same time we can neglect the exhaust gas velocity which introduces the smallest amount of diagnostic information, $I_{\delta v}$ = 0.355. This parameter reacts to all analysed unserviceability states by exceeding the assumed operating tolerance limits.

In this case the selection of the adequate diagnostic parameters should be done using the criterion of control sensitivity of the examined engine type and ability to perform necessary measurements. Since the measurements of the working medium temperature reveal remarkable inertia, which forces the use of thermo-elements of an order of several tens of micrometers in diameter [9], it is the exhaust gas pressure in the outlet channel which should be selected for further analysis, as the measurement of this parameter seem to be most reasonable taking into account the marine engine diagnosing technology.

Based on the results of the diagnostic investigations of the diesel engines used in the RP Navy, it was assumed that "k" engine working space unserviceability states S_{ni}, where i = 1, ... k, compose a finite set of equally probable events p_{bi} = 1/k [3, 7]. Therefore the formula which defines the unconditional entropy takes the form:

$$E(S_n) = -\sum_{i=1}^{k} \log_2 \frac{1}{k} = \log_2 k \qquad (8)$$

For the analysed system k = 15, hence the unconditional entropy:

$$E(S_n) = \log_2 15 = 3.908 \qquad (9)$$

The selected diagnostic parameters δT, δp and δv, collected in the diagnostic matrix 2, include only part of the diagnostic information about the technical state of the engine working spaces. Despite the fact that the condition which unmistakably determines the initial measure of indeterminacy of the analysed states is not met:

$$E(S_n) = I(\delta T) + I(\delta p) + I(\delta v) \qquad (10)$$

We can name four groups of equally probable unserviceability states. For instance, when we analyse a set of diagnostic parameters (tab. 2) we can conclude that if the result: {δT, δp, δv} = {0, 0, 1}, appears in the diagnostic examination process, this may testify to the appearance of the following

unserviceability states: S_{n1}, S_{n4}, S_{n11}, S_{n13} and S_{n14}, respectively. Any identical configuration of the results of the examination does not appear anywhere except these five cases.

At the same time, equally probable appearance of the unserviceability states S_{n2}, S_{n3}, S_{n5}, S_{n6}, S_{n7}, S_{n8}, S_{n9} and S_{n10} is fully defined by the result: {δT, δp, δv} = {1, 1, 1}. In a similar way the unserviceability state S_{n12} – {δT, δp, δv} = {0, 0, 1} can be identified. When the result {δT, δp, δv} = {0, 0, 0} is obtained in the diagnostic examination process, this may signal full serviceability of the engine working spaces, provided that relation (10) is met. But this is not true, as the sum of the amounts of diagnostic information on the technical state of the engine working spaces introduced by parameters δT, δp, δv is equal to 2.325, and the unconditional entropy is equal to 3.908. To reduce the level of indeterminacy of the analysed unserviceability states (missing 1.583 of the amount of diagnostic information) we have to complete the set of diagnostic parameters in such a way that the condition (10) of the ability to make unmistakable distinction between these states is met.

The missing amount of the diagnostic information about the technical state of the engine working spaces (additional diagnostic parameters) can be obtained from the harmonic analysis of the time-histories of pressure pulsations in the exhaust gas channel recorded experimentally on real objects (with real introduction of defects to laboratory engines) and systematic observations of the thermal and flow processes on a large number of examined objects of the same type, without interference into their technical state (such observations of the engines in operation on RP Navy vessels have been conducted for three years now).

Marine gas turbine engine

Operational conditions and small control sensitivity of a gas turbine engine installed in the marine power plant impose certain limits on the possible measurements of engine operation parameters. In numerous cases, complicated and extremely expensive measuring methods, only applicable in the engine test bed, are to be used. The sea conditions do not provide opportunities for introducing defects and changes in control procedures to confirm experimentally their impact on the quality of engine functioning and lifetime, and to assess diagnostic tolerances for indirect control parameters, which define a permissible course of the realised dynamic processes. The diagnostic tolerances should take into account uniqueness of engine production, i.e. individual characteristics of each engine unit, as well as different operating conditions and times of operation which result in different rates of aging and wear of elements.

Determining the nature of mutual relations between the set of unserviceability states of functional engine modules and the set of diagnostic parameters which unmistakably identify those states is a basic goal of the diagnostic activity. A promising method of collecting so-called defect-symptom relations to be used in marine diagnostics of the gas turbine engines is

modelling unserviceability states of turbine subunits with the aid of computer simulation [2, 5]. This method is extremely useful at the stage of designing the diagnostic system for engines used in marine conditions, as it makes it possible, in a relatively simple way, to:

- determine initial static and dynamic characteristics of the engine, taking into account the deformation of their time-histories resulting from the action of external conditions, production differences, and irreversible aging and wear processes,
- determine the set of possible unserviceability states for selected functional modules,
- determine a minimal set of diagnostic parameters which unmistakably identify the modelled defects.

When analysing the quality of functioning of the selected gas turbine engines, used on RP Navy vessels [4], the following unserviceability states were modelled based on the information about the defects recorded during their operation:

S_{m1} – pollution of compressor passages in SNC – assuming 10% decrease in the efficiency and mass flow rate of the working medium compressed in the compressor and 2% compression decrease,

S_{m2} – simultaneous pollution of the compressor passages in SNC and SWC – assuming 10% decrease in efficiency and mass flow rate of the working medium compressed in the compressors, along with 2% compression decrease for SNC and 7% compression decrease for SWC,

S_{m3} – leakage in the compressor passages – assuming that the mass flow rate of the "lost" working medium is equal to: $\dot{m}_{nieszczel.} = 0.05 \dot{m}_{SWCzr}$,

S_{m4} – leakage in one of two air release valves behind SWC – assuming 10% decrease in SWC compression, 2.2% decrease in SNC compression, 4.9% increase of the mass flow rate of the working medium compressed in SWC and 2,8% increase of the mass flow rate of the working medium compressed in SNC,

S_{m5} – defect of the automatic engine fuel supply system which results in forcing the engine acceleration process – the time of the working medium pressure increase, set at the same range behind SWC, was assumed to be reduced from 15 to 10 seconds.

The object of simulation investigations was the process of acceleration of a three-shaft engine after introducing the modelled defects. The simulation aimed at determining the effect of changes of parameters that characterise the constructional structure of the analysed machine system on its dynamic characteristics.

Tab. 3 collects per cent values of the metrics (diagnostic parameters), which were assessed by comparing the referential time-histories of the gasodynamic parameters recorded during the simulation of the process of acceleration of the fully serviceable engine, with corresponding time-histories for the engine with the modelled unserviceability states S_{n1}, S_{n2}, S_{n3}, S_{n4} and S_{n5}. These values were calculated using the referential metric (4) in the same way as for the diesel engine, as was described in Section 4.1.

This way a set of nineteen diagnostic parameters was obtained. This set is to be minimised using the entropy function:

δT_{IP}, δp_{IP}, δm_{IP} – temperature, pressure and mass of the air accumulated in the inter-compressor space, respectively

δT_M – averaged temperature of the flow passage constructional material,

$\delta \tau_p$ – time of the air flow in the compressor space,

δn_{HPCzr} – rotational speed of the high pressure rotor (reduced to the normal atmospheric conditions at SWC inlet),

$\delta \pi^*_{LPC}$, $\delta \pi^*_{HPC}$ – compression of the low and high pressure compressor, respectively

$\delta \dot{m}_{LPC}$, $\delta \dot{m}_{HPC}$, $\delta \dot{m}_{HPCo}$ – is the mass flow rate through SNC and SWC, respectively

$\delta \eta^*_{LPC}$, $\delta \eta^*_{HPC}$ – is the SNC and SWC efficiency, respectively

δT^*_{21}, δp^*_{21} – is, respectively, the air temperature and pressure behind SNC,

δT^*_{12}, δp^*_{12} – is, respectively, the air temperature and pressure at SWC inlet,

δT^*_{22}, δp^*_{22} – is, respectively, the air temperature and pressure behind SWC.

Tab. 3. Metric values δx_j for the modelled unserviceability states of the three shaft ZORYA marine gas turbine engine UGT3000 type

		Operational unserviceability states				
		S_{n1}	S_{n2}	S_{n3}	S_{n4}	S_{n5}
Diagnostic parameter δx_j	δT_{IP}	38.3	41.7	2.1	6.9	9.2
	δT_M	2.1	2.3	2.3	1.1	0.4
	δp_{IP}	38.9	38.3	5.4	8.7	9.2
	δm_{IP}	3.2	6.4	4.1	10.2	16.6
	$\delta \tau_p$	16.3	22.8	7.8	17.0	24.9
	δn_{HPCzr}	20.5	22.4	1.0	3.4	4.8
	$\delta \pi^*_{LPC}$	38.7	38.1	5.1	8.0	8.3
	$\delta \pi^*_{HPC}$	70.6	14.7	9.1	32.7	34.6
	$\delta \dot{m}_{LPC}$	17.5	18.5	6.1	8.0	8.5
	$\delta \dot{m}_{HPC}$	10.7	11.5	6.8	16.4	19.1
	$\delta \dot{m}_{HPCo}$	17.5	18.4	2.9	8.0	8.5
	$\delta \eta^*_{LPC}$	66.9	66.9	5.2	10.9	8.4
	$\delta \eta^*_{HPC}$	44.6	45.1	3.7	7.7	62.9
	δp^*_{21}	38.7	38.1	5.0	8.0	8.3
	δp^*_{12}	38.3	37.7	5.1	7.9	8.3
	δp^*_{22}	26.8	29.3	13.5	38.6	42.3
	δT^*_{21}	38.2	41.7	2.1	6.9	9.3
	δT^*_{12}	38.1	41.6	2.1	6.8	9.3
	δT^*_{22}	9.1	24.3	4.1	7.1	31.0

Firstly, the diagnostic matrix was created, at the same assumptions as for the earlier analysed diesel engine – matrix 1 in Fig. 2. The last column in matrix 1 contains the amounts of diagnostic information carried by particular parameters and calculated using formula (7). Applying the criterion I_1 = max we can select fourteen diagnostic parameters which carry identical amount of information $I_1 = 0.971$. But as the first step, a parameter is to be selected whose measurement is the simplest from the constructional point of view. In this case the selected parameter was the pressure of the working medium accumulated in the compressor space, δp_{PM}. It is noteworthy that the diagnostic parameter which reacts (or not) to all unserviceability states carries no diagnostic information - for δT_M and δp^*_{22} we get, respectively: $I_1(\delta T_M) = 0$ and $I_1(\delta p^*_{22}) = 0$.

In the next selection steps, by proper restructuring of the diagnostic matrices and using available generalised calculation procedures [8], we can relatively easily select next parameters which carry the maximal amount of diagnostic information, provided that the first, second and next diagnostic parameter

Matrix 1

	Diagnostic Parameter δx_j	Unserviceable states					I_1
		S_{n1}	S_{n2}	S_{n3}	S_{n4}	S_{n5}	
1	δT_{PM}	1	1	0	0	0	0.971
2	δT_{M}	0	0	0	0	0	0
3	δp_{PM}	1	1	0	0	0	0.971
4	δm_{PM}	0	0	0	1	1	0.971
5	$\delta \tau_{p}$	1	1	0	1	1	0.722
6	δn_{SWCzr}	1	1	0	0	0	0.971
7	$\delta \pi^*_{SNC}$	1	1	0	0	0	0.971
8	$\delta \pi^*_{SWC}$	1	1	0	1	1	0.722
9	$\delta \dot{n}_{SNC}$	1	1	0	0	0	0.971
10	$\delta \dot{n}_{SWC}$	1	1	0	1	1	0.722
11	$\delta \dot{n}_{SWCo}$	1	1	0	0	0	0.971
12	$\delta \eta^*_{SNC}$	1	1	0	1	0	0.971
13	$\delta \eta^*_{SWC}$	1	1	0	0	1	0.971
14	δp_{21}	1	1	0	0	0	0.971
15	δp^*_{12}	1	1	0	0	0	0.971
16	δp^*_{22}	1	1	1	1	1	0
17	δT^*_{21}	1	1	0	0	0	0.971
18	δT^*_{12}	1	1	0	0	0	0.971
19	δT^*_{22}	0	1	0	0	1	0.971

Matrix 2

	Diagnostic Parameter δx_j	d1			d2		I_2
		S_{n1}	S_{n2}	S_{n3}	S_{n4}	S_{n5}	
3	δp_{PM}	1	1	0	0	0	0
1	δT_{PM}	1	1	0	0	0	0
4	δm_{PM}	0	0	0	1	1	0.551
5	$\delta \tau_{p}$	1	1	0	1	1	0.551
6	δn_{SWCzr}	1	1	0	0	0	0
7	$\delta \pi^*_{SNC}$	1	1	0	0	0	0
8	$\delta \pi^*_{SWC}$	1	1	0	1	1	0.551
9	$\delta \dot{n}_{SNC}$	1	1	0	0	0	0
10	$\delta \dot{n}_{SWC}$	1	1	0	1	1	0.551
11	$\delta \dot{n}_{SWCo}$	1	1	0	0	0	0
12	$\delta \eta^*_{SNC}$	1	1	0	1	0	0.551
13	$\delta \eta^*_{SWC}$	1	1	0	0	1	0.551
14	δp_{21}	1	1	0	0	0	0
15	δp^*_{12}	1	1	0	0	0	0
17	δT^*_{21}	1	1	0	0	0	0
18	δT^*_{12}	1	1	0	0	0	0
19	δT^*_{22}	0	1	0	0	1	0.951

Matrix 3

	Diagnostic Parameter δx_j	d1 S_{n2}	d2 S_{n1}	d3 S_{n5}	S_{n3}	d4 S_{n4}	I_3
19	δT^*_{22}	1	0	1	0	0	0
4	δm_{PM}	0	0	1	0	1	0.4
5	$\delta \tau_{p}$	1	1	1	0	1	0.4
8	$\delta \pi^*_{SWC}$	1	1	1	0	1	0.4
10	$\delta \dot{n}_{SWC}$	1	1	0	0	1	0.4
12	$\delta \eta^*_{SNC}$	1	1	1	0	1	0.4
13	$\delta \eta^*_{SWC}$	1	1	0	0	0	0

Matrix 4

	Diagnostic Parameter δx_j	Unserviceable states				
		S_{n1}	S_{n2}	S_{n3}	S_{n4}	S_{n5}
3	δp_{PM}	1	1	0	0	0
19	δT^*_{22}	0	1	0	0	1
4	δm_{PM}	0	0	0	1	1

Fig. 2. Scheme for determining the minimum number of diagnostic parameters

were selected - matrices 2 and 3. In each case the diagnostic sensitivity is also analysed.

The selection is continued until full diagnostic information about the technical state of the examined engine is obtained.

Assuming that "k" engine compressor system unserviceability states, S_{ni}, i = 1, ... k, compose a finite set of equally probable events $p_{bi} = 1/k$, which in cases of gas turbine engines is confirmed in practice [3,4], we get k = 5 for the analysed system, hence the unconditional entropy is:

$$E(S_n) = \log_2 5 = 2.322 \qquad (11)$$

The selected diagnostic parameters δp_{PM}, δT^*_{22} and δm_{PM}, collected in matrix 4, carry, in total, full diagnostic information on the technical state of the compressor system. Then the condition is met which unmistakably defines the initial measure of indeterminacy of the analysed states:

$$E(S_n) = I_1(\delta p_{PM}) + I_2(\delta T^*_{22}) + I_3(\delta m_{PM}) \quad (12)$$

Analysing the minimised set of diagnostic parameters we can conclude that if the result: $\{\delta p_{PM}, \delta T^*_{22}, \delta m_{PM}\} = \{1, 0, 0\}$, appears in the diagnostic investigation process, then we can conclude about intensive pollution of blade passages in SNC (S_{n1}). Any identical arrangement of the results of investigations does not exist anywhere except this only case.

Simultaneous intensive pollution of blade passages in the two cooperating compressors (S_{n2}) is completely defined by the result: $\{\delta p_{PM}, \delta T^*_{22}, \delta m_{PM}\} = \{1, 1, 0\}$. In a similar way we can identify the leakage in the air release valve (S_{n4}) – (δp_{PM}, δT^*_{22}, δm_{PM}) = $\{0, 0, 1\}$, and the defect of the engine fuel supply system (S_{n5}) – $\{\delta p_{PM}, \delta T^*_{22}, \delta m_{PM}\} = \{0, 1, 1\}$. When the result $\{\delta p_{PM}, \delta T^*_{22}, \delta m_{PM}\} = \{0, 0, 0\}$ is obtained in the diagnostic investigation process, it signals full serviceability of the engine. The modelled defect consisting in the leakage in the compressor passage (S_{n3}) did not bring any substantial disturbance to engine operation which would result in exceeding tolerance range limits for the selected set of diagnostic parameters.

CONCLUSIONS

The method presented in the article consists in assessing the diagnostic informativeness of the measureable gasodynamic parameters of marine engines of both piston and turbine constructions. This assessment makes it possible to select a set of diagnostic parameters which precisely defines the technical state of constructional elements of the marine engine working spaces. The method provides opportunities for calculating the amount of diagnostic information of the selected parameters with the aid of the entropy function. As a consequence, it eliminates those diagnostic parameters which do not introduce valuable information on the technical state of the engine working spaces.

BIBLIOGRAPHY

1. Będkowski L.: *Elements of technical diagnostics*, (in Polish) WAT, Warsaw, Poland, 1992
2. Cohen H., Rogers G.F.C., Saravanamuttor H.I.H.: *Gas turbine theory*, Longman Scientific & Technical, New York, USA, 1987
3. Charchalis A., Dyson P.K., Korczewski Z.: *Evaluation of operating conditions of the passages of naval gas turbines by gas path analysis*, The Institute of Marine Engineers, London, UK, 1996
4. Girtler J.: *Statistic and probabilistic measures of diagnosis likelihood on the state of self-ignition combustion engines.* Journal of POLISH CIMAC, Vo. 2, No 2, 2007
5. Korczewski Z.: *Method of diagnostic parameters determination applicable to dynamic processes of a naval gas turbine*, Polish Maritime Research, Vol. 4, No 2, 1997
6. Korczewski Z., Zacharewicz M.:, *The research of turbocharging system of marine diesel engines by means of simulation changes of technical state.* Diagnostyka, No1(45), 2008
7. Korczewski Z.: *Endoscopy of marine engines* (in Polish), AMW, Gdynia, Poland, 2008
8. Kudrewicz J.: *Functional analysis for automatic and electronic engineers*, (in Polish) PWN Warszawa, Poland, 1976
9. Wajand J.A., Wajand J.T.: *Medium- and high-speed piston internal-combustion engines* (in Polish), WNT, Warszawa, Poland, 2005.

CONTACT WITH THE AUTHOR

Zbigniew Korczewski, Assoc. Prof.
Faculty of Ocean Engineering
and Ship Technology
Gdansk University of Technology
Narutowicza 11/12
80-233 Gdansk, POLAND
fax: (058) 347-21-81,
e-mail: zbigniew korczewski@pg.gda.pl

Operational problems of large power diesel engines combusting biofuels, considered together with assessment of their operation

Jerzy Girtler, Prof.
Zbigniew Korczewski, Assoc. prof.
Gdansk University of Technology
Jacek Mańczak, M. Sc.
H. CEGIELSKI – Poznan S. A.

ABSTRACT

In this paper the problem is discussed of supplying high power diesel engines with biofuels in the aspect of consequences which occurr during their operation. Attention was paid to advantages and difficulties associated with application of biofuels to self-ignition engines. A relevant research problem was characterized and research targets were proposed to make it possible to most favourably shape energy merits of the engines. Special attention was given to wear process of such engines and their failures resulting from application of biofuels. The following problems were also considered: calcium carbonate sedimentation, closing graphite platelets in structure of cylider bearing surface and surface defects of piston rings made of aluminium bronze. It was demonstrated that to assess operation of the engines is possible under the assumption that in a valuating approach their operation can be compared to a physical quantity represented numerically and measured with the use of the joule*sec unit. Conclusions resulting from the domestic and foreign investigations on power and reliability of such engines were also presented.

Keywords: biofuel; operation; engine about automatic ignition; expendable

INTRODUCTION

In 21st century world economy has been dominated from its beginning by two problems: warfare against global warming-up and energy shortage, mainly electric one, and threat of running- low natural energy raw material resources, closely associated with the first. The themes are very closely connected to each other. Limitations associated with the global climate warming-up, consisting a. o. in reduction of emission limits of noxious gases such as NOx, SOx and first of all CO_2, have resulted in searching for alternative, pure and renewable energy sources [12]. However in applying renewable energy sources the today demand on electric power was to be taken into account.

Until now in lower developed countries (e. g.Poland) electric power demand has been mainly covered by conventional coal-fired power plants operating on the basis of steam-turbine-driven electric generators. Unfortunately, the electric power stations appear to be the largest emitters of carbon dioxide, and their efficiency is rather not high.

An alternative to the conventional electric power stations, as far as large power blocks are concerned, seems to be nuclear power industry, however after the Czarnobyl disaster its development has been effectively slowed down, at least in Eastern Europe.

Development of nuclear power industry is associated with a high initial cost of electric power plants. The highest outlays should be incurred during the building of nuclear reactor and before its putting into operation. Its investment cycle is also relatively long. Therefore it should be stated that power industry of the kind is rather intended for reach countries and its impact could be really felt at the end of the second decade.

Pure energy sources are represented obviously by water - power plants as well as wind - power plants flourishing now in Europe. Experience gained at the run of century has showed that the wind-driven generator itself does not solve the problem in question as lack of wind is capable of leading to „black-out" and consequently paralysing life of the entire country as it was the case of Denmark and Holland. Presently we know that the wind electric power plants are to be bufferred at least in 50% by another power source being in a hot stand-by state. To this end, electric generators driven either by four-stroke self-ignition engines or medium- or large- power gas turbines, are commonly used.

The self-ignition engine since its very beginning has been used for driving the electric generating sets, however it has practically been auxiliary, emergency, small power generators installed on objects requiring continuous supply or located far from electric networks, as well as generators on board of ships. Their output does not generally exceed 1 MW.

Contemporary power industry surely expects solutions of electric generating sets of a much greater output – up to 20 MW and more - and available from one unit. The most modern diesel engines both

four-stroke and two-stroke ones, designed on the basis of main engines intended for propelling large ships, are capable of coping with such tasks. Morover, a high efficiency of electric generating set driven by diesel engine supports attractivity of such solution.

The large-power, two-stroke crosshead engine has an advantage which cannot be overestimated: it is relatively insensitive to fuel of a low quality, because of its specific design solution and adjustment to combusting heavy oils, of a rather not high quality, usually. This is especially important today in the situation of runing-low resources of natural liquid fuels and searching for alternative ones. For this reason research investigations on application of alternative fuels of vegetable origin, so called biofuels to self-ignition engines have been conducted for many years by domestic and foreign scientific research institutions[1].

GENERAL ASSESSMENT OF RESULTS OF THE INVESTIGATIONS HAVE BEEN CONDUCTED SO FAR

Research work on applicability of biofuels to supplying self-ignition engines, of small power in particular, has been carried out by various scientific and scientific-industrial research centres. The activity has been triggered off due to growing awareness that [1, 2,3,8]:
- crude oil resources are lower and lower,
- it is urgently necessary to limit emission of noxious compounds contained in exhaust gases,
- bio-fuels are bio-degradeable.

It resulted in that biofuels which are methyl esters (sometimes ethyls) of fatty acids (FAME – Fatty Acid Metyl Esters) have achieved greater and greater importance in worldwide power industry. In Poland the methyl esters of fatty acids of rape oil (EMKOR) are mainly used. In this case their biodegradeability due to which they may be considered pro-ecological fuels, is of a special importance. The feature of biofuels has really directed interest of leading diesel engine producers to the fuels; it may be hence expected that investigations on consequences of application of such fuels will be continued.

The conducted research [1, 13, 15, 16] deals mainly with: the methyl ester of fatty acids of rape oil, soybean oil, sunflower oil, their mixtures with diesel oil, and the methyl ester of fatty acids of palm oil, just recently. Investigations on application of animal fat waste as an alternative fuel are also carried out. It brings an additional advantage due to reduction of waste utilization cost.

The vegetable fuels and their mixtures with diesel oil are characterized by a higher viscosity as compared with that of diesel oil, that makes engine starting-up process much more difficult. However engine starting-up features can be improved by providing heaters for biofuels characterized by high viscosity. The heating-up of such fuels can reduce their viscosity down to a level comparable to that of diesel oil. As results also from the invstigations, there are still important problems concerning the following items: excessively long combustion, reduced ignition lag, long injection process, slowed down evaporation of fuel droplets and worser fuel spraying quality. Moreover the fuels show high aggressiveness (chemical activity of highly acid reaction) against fuel piping and apparatus, that makes it necessary to apply special materials (stainless steel, sealings etc). Also, they do not have good lubricating features for

precision pairs of injection pumps and injectors, moreover they should have a low impact on change of physical and chemical features of lubricating oils in case of a leakage of the fuels to the oils resulting from loss of tightness of injection apparatus. For the above mentioned reasons further resrach is necessary to reach the following aims [8]:
- improvement of starting-up features of engines from cold state, especially at low ambient temperatures,
- determination of impact of vegetable fuels and their derivatives on: fuel piping corrosion, wear of injection pumps, injectors and the tribological system consisted of piston, rings and cylinder liner (resulting from friction and corrosion wear, sedimentation of lakes and calcium carbonate, cracks in piston heads and cylinder liners etc) as well as wear of crankshaft bearings,
- determination of impact of vegetable fuels and their derivatives, in case of their leaking to lubricating oils during operation of engines, on physical and chemical features of the oils.

The investigations have been performed so far, on applicability of the vegetable oils and their esters in question as alternative fuels for diesel engines, have yielded promising results.

As a matter of fact from results of investigations on combustion of biofuels in engines the following was concluded: a decrease of their output, increase of specific fuel consumption (especially at higher engine speeds) and a decrease of efficiency, but simultaneously – decrease of exhaust smokiness, as compared with the case of diesel oil combustion in the engines. Exhaust gas temperature of biofuel-fed engine is lower as compared with that produced during diesel oil combustion.

As stated from the performed investigations, the supplying of diesel engines with biofuels results in:
- greater sedimentation of contaminations on surfaces of combustion chamber elements as well as on surfaces of spraying nozzles of injectors,
- worsened operational parameters of the engines in question (lower output, higher specific fuel oil consumption, lower efficiency), sometimes higher smokiness of exhaust gas at lower rotational speeds of the engines,
- increased emisssion of noxiuos exhaust-gas components such as: CO and C_nH_m, resulting in a lower content of CO_2, but also lower content of NO_x in exhaust gas at higher engine loads.

The higher content of hydrocarbons (C_nH_m) in exhaust gas of the engines combusting biofuels results mainly from that the flame ionization detectors of C_nH_m analyzer do not seperate, from the hydrocarbons, aldehydes which are in a much greater amount in biofuels than in diesel oils.

Along with growing engine wear the differentiation of emission of the above mentioned compounds increases. When analyzing the presented research results it should be observed that they are promising as compared with the results obtained from investigations of gas and steam turbines used in electric power stations. The quantative data given in Fig. 1 and 2 and in Tab. 1 support the statement.

As illustrated by the presented data, in spite of the very promising prospects of the application of self-ignition engines to driving the electric generating sets it should be however

---

[1] Already in 1900 Rudolf Diesel anticipating that in the future crude oil and coal tar may be in shortage, presented, during Paris exhibition, an engine combusting arachis oil. For many years such fuels have not been used as the fuel obtained from crude oil was (and is still) less expensive

stated that the results obtained during the investigations have been performed so far on combustion processes in biofuel-fed engines, could not fully reveal their operational merits, as they have dealt only with energy aspects. No complex investigations concerning durability of main tribological units of the engines have been conducted with accounting for technical diagnostics, endoscopy based in particular. Proposals of such investigations are presented in this paper.

Fig. 1. *Specific emission of CO₂ contained in exhaust gases for various types of electric power stations and mineral fuels [14]*

Fig. 2. *Comparison of efficiency of typical driving units used in electric power stations [14]*

Summing up, further development of drives based on self-ignition engines should be expected in power industry, and the crucial aspect deciding on reaching the success will be their reliability and reliability of electric power station as a whole.

PROBLEM OF WEAR OF BIOFUEL-FED ENGINES AND THEIR TESTS

Initial remarks

The promising results of the investigations associated with determination of energy merits of biofuels proposed for self-ignition engines, have made that also research on intensity of degradation process of structures of such engines have been undertaken in order to determine a guaranteed time to failure of their particular constructional units. The results of diagnostic tests performed by MAN Diesel Co, have been obtained so far, showed that the energy parameters of „bio-engine" are kept in the range of contractual values, but values of the structural parameters of its working space change significantly due to calcium carbonate contamination – Fig. 3 [15, 16]. From the performed microscopic tests of a cylinder liner it was additionally concluded that the closing of graphite platelets in its cristallic structure took place. (Fig. 4), that may within a short time result in growing rate of wear of cylinder bearing surface - and consequently - worsening engine performance and efficiency of realized heat-and-fluid-flow processes [15, 16]. Many defects of sliding coating (aluminium bronze) of piston sealing rings of cylinder systems (Fig. 5) confirm the observation.

Formation of calcium carbonate sediments on surfaces of combustion chamber elements

During a routine overhaul of internal spaces of one of MAN Diesel biofuel – fed engines a large amount of light-beige contaminations („chalk-like" hard sediments) were found on piston head surface as well as cylinder head from the side of combustion chamber, in all cylinder systems of the engine. Similar sediments were also found in internal spaces of the waste-heat boiler [15]. As preliminarily stated the cause of its occurence was an accumulated excess of non-used (non-combusted) additions to lubricating oil, a.o. detergent, in the form of acid calcium carbonate $Ca(HCO_3)_2$ which, in high

Tab. 1. *Comparison of features of selected technological methods for electric power production [14]*

Technology	Size of units	Investment period	Initial cost/kW	Operational cost	Fuel price	CO₂ emission	Regulation risk
Piston engines	small	very short	low	low	high	low	low
Coal	large	long	high	medium	medium	high	high
Gas turbine - combined cycle	medium	short	low	low	high	medium	low
Nuclear	very large	long	high	medium	low	null	high
Hydro	large	long	very high	very low	null	null	high
Wind	small	short	high	very low	null	null	medium
Fuel cell	small	very short	very high	medium	high	medium	low
Photovoltaic	very large	very short	very high	very low	null	null	low

Fig. 3. *View of cylinder space of the engine working on a biofuel produced on the basis of crude (not processed) palm oil.*
a) *Calcium carbonate (CaCO₃) layer sedimented on piston head.*
b) *Contamination layer sedimented on the head from the side of combustion chamber in the vicinity of outlet valve and fuel injector*
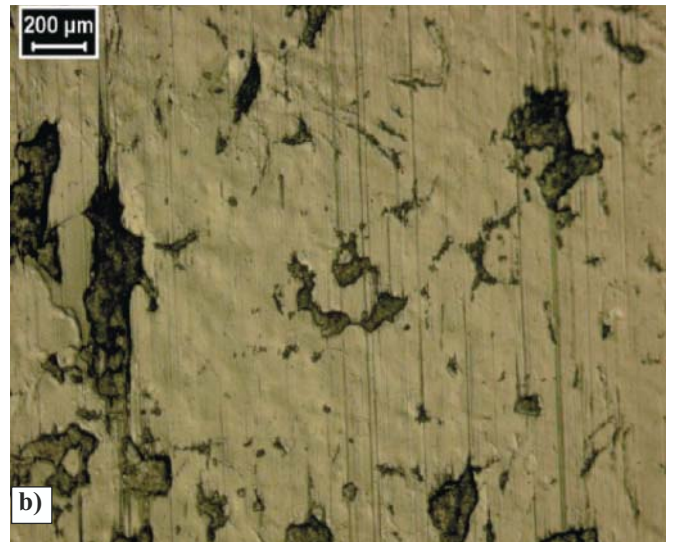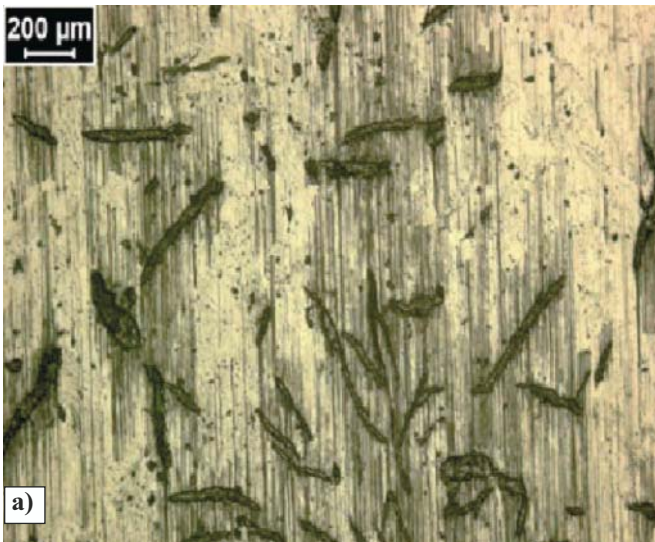
Fig. 4. *Enlarged view of cylinder bearing surface of the engine working on a biofuel produced on the basis of crude (not processed) palm oil.*
a) *Cylinder bearing surface – opened graphite platelets of good tribological qualities.*
b) *Cylinder bearing surface – partly closed graphite platelets of worser tribological qualities*

Fig. 5. *Ring part of piston – the engine working on a biofuel produced on the basis of crude (not processed) palm oil.*
a) *Sliding surface of piston sealing ring – defects of aluminium bronze layer in the vicinity of piston-ring joint.*
b) *Sliding surface of piston sealing ring – defects of aluminium bronze layer*

temperatures, releases calcium carbonate $CaCO_3$, water vapour H_2O w and carbon dioxide CO_2:

$$Ca(HCO_3)_2 \rightarrow CaCO_3 + H_2O + CO_2 \qquad (1)$$
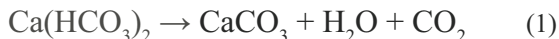
As deemed, it was caused by mutual interaction (an inappropriate combination) of base number of lubricating oil (TBN40) and a supplied fuel not containing sulfur. On the other side there is no commercial production of a lubricating oil of a base number smaller than TBN40. As separated hard particles of calcium carbonate sediments disturbe oil film as well as stable work of piston rings, they contribute in accelerated friction and errosion wear process of the cylinder bearing surface. Knowing that an inceased charge of cylinder oil could not improve the situation, but on the contrary it could accelerate rate of $CaCO_3$ sedimentation, one decided to limit the charge of lubricating oil (supplied to cylinder bearing surface through two lubricators) to the value of 1.05 g/kWh. According to MAN Diesel Co statement, such value should be generally determined on the basis of the relation of $F \times S\%$, where the empirical coefficient F takes values from 0.26 to 0.34 (and S% - percentage content of sulfur in fuel oil). Positive results of the lubrication at the lower coefficient have been demonstrated by tests and such values are recommended today. Generally, it can be concluded that the cylinder oil charge should not be taken lower than 0.8 g/kWh. From the producer's experience have been gained so far it results that CL-DX405 oil of a reduced base number TBN40, reduced acid calcium carbonate content, at maintained high washing capacity, is the best adjusted cylinder oil for biofuel -fed engines (as well as for engines fed with fuel oil having sulfur content smaller than 1.5%).

One may expect very soon that producers of lubricating means for low-speed engines will undertake intensive research on a new composition of lubricating oil of a TBN value close to 20 mgKOH/g. It results not only from demands put by biofuels but first of all from new legal regulations dealing with sea environment protection (Anex VI to Marpol 73/78 Convention) in which some navigation regions were specified (a.o. the Baltic Sea, selected regions of the North Sea, region of La Manche Channel etc) where only use of fuel oils of sulfur content smaller than 1.5 %, with its target value lowered to 0.5%, is permitted.

Because of the so small amount of lubricating oil applied to cylinder liner, it must be very precisely spread over the entire cylinder bearing surface in order to ensure a high quality of all realized functions of lubricating oil, namely:
- limitation of adhesive wear by eliminating direct metal-to-metal contact of faying surfaces of piston rings and cylinder bearing surface,
- limitation of corrosion wear by neutralizing acid combusion products, first of all sulfuric acid, in the form of calcium carbonate,
- ensurance of stable (durable) oil film between piston ring and cylinder bearing surface,
- limitation of sedimenting rate of contaminations in engine working spaces (combustion chambers),
- ensurance of proper sealing the rings in piston grooves.

Therefore a perspective, effective way to further control of oil consumption for lubrication of cylinder liners is the supplying of oil in an amount proportional to engine load (i.e. fuel oil charge delivered to cylinders) and proportional to percentage content of sulfur in fuel oil. In older solutions the functions have been realized by using a mechanical system connected with engine load indicator, today – by specialty electronic systems, e.g. the Alfa–lubrication system for MAN Diesel engines – Fig. 6, intended for controlling value of cylinder oil charge.

However two basic conditions must be fulfilled:
1. the cylinder oil charge cannot be smaller than a value which limits tribological wear of friction surfaces to a minimum,
2. amounts of alkalic anticorrosive additions and detergents should be limited to a minimum necessary to neutralize formed acids and keep piston rings clean (ensurance of a sufficient washing capacity).

In the case of the engine fed with sulfur - free biofuel the cylinder oil charge should be proportional to engine's load with taking into account measurement results of contamination of the lubrication oil by Fe-particles. This makes it possible to estimate rate of wear of cylinder bearing surface and on this basis to correct an optimum charge from lubricator. As determined from service measurements of wear of cylinder
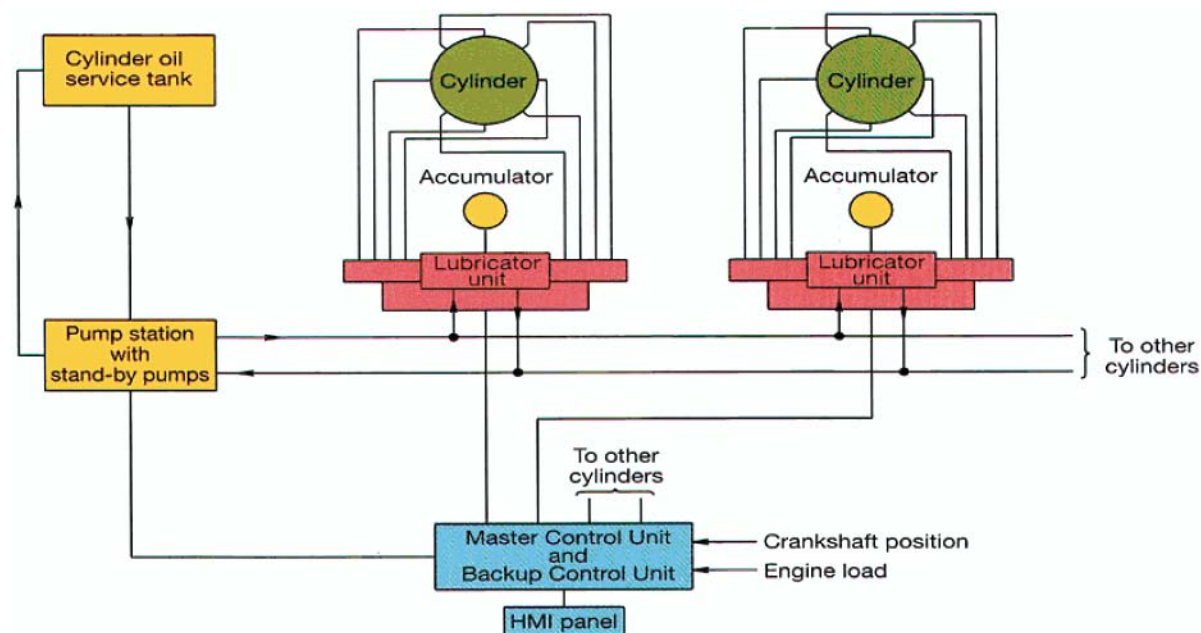
Fig. 6. Schematic diagram of the Alfa–lubrication system for controlling cylinder oil charge in MAN Diesel engines [14]

liners of MAN Diesel two-stroke engines, the mean rate of wear of cylinder liner was not greater than 0,1 mm/1000 h [15,16] (the data concerned the heavy-oil-fed engines).

Closing graphite platelets in outer layer of cylinder bearing surface

As concluded from results of diagnostic tests have been conducted so far on large power diesel engines, lubrication conditions can be improved to a certain extent by allowing controlled corrosion process of cylinder bearing surface to happen [15]. Local corrosion cells occurring in the form of microscopic „pocketlets" filled with lubricating oil support hydrodynamical lubrication process. Complete elimination of erosion and corrosion processes may lead to a loss of honing structure and polishing effect of cylinder bearing surface (Fig. 7).

It usually results in closing the graphite platelets within cristallic structure of outer layer of cylinder bearing surface, that disturbes the building process of essential oil film. Consequently, it leads to increasing consumption of lubricating oil, scuffing piston rings in cylinder liner, and even seizing effects in PRC (Piston-Rings-Cylinder) system.
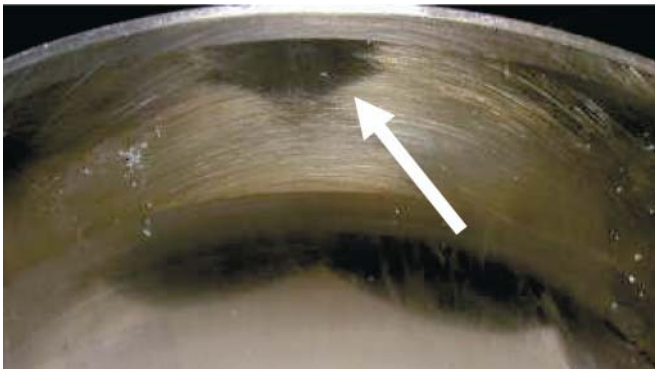
Fig. 7. Polished (mirror) cylinder bearing surface

4. Wear-affected operation of engines

Operation of diesel engines consists in the transforming and transferring of supplied energy [4, 5]. It becomes worser and worser along with growing wear of the engines. To assess their operation is hence deemed necessary.

Doing so, one should take into account that the transformation of energy in the form of heat or work, which occurs in working spaces of every diesel engine, should be such as to make the work to be done within a given time, as large as possible, or to do the work as fast as possible. In practice it is also important to release, during combustion process, as much heat as possible, and to reduce waste heat to a possible minimum. If due to wear of the engine to obtain such most favourable energy transformation is not possible, then the operation of the engine is considered incorrect and it is assumed that the engine is then in the state of partial serviceability [4, 5].

As the operation of such engines consists in the transformation of the energy E into the form of the work L and heat Q it can be hence generally interpreted as follows:

$$D = \int_0^t E(\tau)d\tau \qquad (2)$$

where:
D − engine operation
E − transformed (obtained) energy which makes realization of the task Z possible,
t − duration time of transforming (using) the energy E

In the most general case, $E(\tau)$ may be considered the internal combustion gas energy which makes it possible to do the useful work $L_e(\tau)$ by the engine. The energy is obviously obtained from the chemical energy contained in air-fuel mixture during fuel combustion in working spaces of every engine. Transformation of the chemical energy during operation of the engine results in the thermal and mechanical loading of the engine, that consequently results in growing wear of the engine and energy losses associated with the wear [4, 10, 11]. To conclude about serviceability of a particular engine is possible after calculating value of its operation from Eq. (2), which, in the proposed interpretation, is equated to a physical quantity having the measure unit called joule-second. In order to determine the area of operation (D) it is obviously necessary to know a functional relation of energy and time, i.e. E = f(t). The so-understood operation determined by Eq. (2), can be presented in the coordinate frame „E−t", hence also in the form of a diagram called diagram of operation [4, 5]. In view of that D = f(E, t) the operation of devices can be presented in the coordinate frame „D−E−t" [4, 5].

In the case of an arbitrary self-ignition engine, the transformation of the chemical energy (contained in air-fuel mixture produced in combustion chambers) into thermal one and then mechanical one, makes it possible to generate the crankshaft torque (M_o) at a given rotational speed (n) [5]. Therefore the engine operation described by Eq. (2) may be interpreted as the energy transformation into the form of the useful work L_e and expressed by the formula:

$$D_{L_e} = \int_0^t L_e(\tau)d\tau = 2\pi \int_0^t n(\tau)M_o(\tau)\tau d\tau \qquad (3)$$

As results from the presented considerations, it is reasonable to analyze not only the work L_e but also the operation (D) of such engines, in this case understood as the energy transformation in the engine, which leads to achieving a necessary amount of the useful work (L_e) within a definite time (t). It makes it possible to determine if the possible engine operation (D_M) in given conditions is at least equal to the demanded operation (D_W) necessary for realization of a given task Z.

The task (Z) to realization of which the combustion engine is adjusted in the phase of its designing and manufacturing, can be realized only when the following inequality is satisfied:

$$D_M \geq D_W \qquad (4)$$

i.e. when:

$$t_M \geq t_W, \text{ and simultaneously } E_M \geq E_W$$

where:
t_M − possible operational time of engine
t_W − demanded operational time of engine
E_M − energy which can be transformed by engine
E_W − energy demanded (necessary) to realize the task Z (energy which must be transformed to realize the task Z).

It means that by analyzing energy merits of combustion engines in a general sense with the use of Eq. (2), one can consider serviceability of the engines in the following variants, acounting for their wearing:

$$t_M = t_W, \text{ and simultaneously } E_M = E_W$$
$$t_M = t_W, \text{ and simultaneously } E_M > E_W$$
$$t_M > t_W, \text{ and simultaneously } E_M = E_W$$
$$t_M > t_W, \text{ and simultaneously } E_M > E_W \qquad (5)$$

In the particular case when in assessing the engine operation it is important the definite work L_e to be done by the engine, then the relation (5) should be presented in the following form:

$$\left.\begin{array}{l} t_M = t_W,\ \text{and simultaneously}\ L_{eM} = L_{eW} \\ t_M = t_W,\ \text{and simultaneously}\ L_{eM} > L_{eW} \\ t_M > t_W,\ \text{and simultaneously}\ L_{eM} = L_{eW} \\ t_M > t_W,\ \text{and simultaneously}\ L_{eM} > L_{eW} \end{array}\right\} \quad (6)$$

where:
t_M – possible operational time of engine
t_W – demanded operational time of engine
L_{eM} – useful work which can be done by engine
L_{eW} – useful work which is demanded (necessary) to realize the task Z (useful work which must be done to realize the task Z).

As a rule it is important to do the useful work L_e within a definite time. Then to assess the engine operation it is necessary to know how fast the work can be done. A physical quantity which contains such information is the effective power N_e as it determines, in case of any machine, how fast a given work will be (or can be) done within a given time. Hence in the case of assessing the engine operation when it is important the engine to develop a definite power (N_e), the relation (6) can be presented as follows:

$$\left.\begin{array}{l} t_M = t_W,\ \text{and simultaneously}\ N_{eM} = N_{eW} \\ t_M = t_W,\ \text{and simultaneously}\ N_{eM} > N_{eW} \\ t_M > t_W,\ \text{and simultaneously}\ N_{eM} = N_{eW} \\ t_M > t_W,\ \text{and simultaneously}\ N_{eM} > N_{eW} \end{array}\right\} \quad (7)$$

where:
t_M – possible operational time of engine
t_W – demanded operational time of engine
N_{eM} – effective power which can be developed by engine
N_{eW} – effective power demanded (necessary) to realize the task Z (effective power which must be generated to realize the task Z).

In the case when the inequality is satisfied:

$$D_M < DW \quad (8)$$

then it should be concluded that the engine in question is damaged and not capable of realizing the assumed task Z.

In the case of considering the situations (6) and (7) the inequality (8) should be expressed as follows:

$$L_{eM} < L_{eW}\ \text{or}\ N_{eM} < N_{eW} \quad (9)$$

Therefore in order to determine if a given engine is serviceable to realize a given task, its operation should be identified [10, 11]. As the operation depends on a degree of engine's wear, its identification must be connected with identification of engine's wear, e.g. in a way presented above in this paper.

RECAPITULATION. FINAL REMARKS AND CONCLUSIONS

Features of diesel oil and considered alternative fuels are very different. Therefore it should be expected that self-ignition engines must be subjected to a special adjustment, or even modification, depending on a kind of fuel delivered to them. To adjust the engine fuel system to features of vegetable fuel oils of and their mixtures with diesel oil is necessary because of their high viscosity as compared with that of diesel oil. One of the possible ways of decreasing the viscosity of biofuels and improving their spraying quality is to apply a heating-up system to the fuel oils, that makes it necessary to supplement the fuel system, not only with the fuel - oil heater but also a viscometer for measuring fuel oil viscosity as well as a viscostat - for controlling flow of heating medium through the heater and maintaining this way fuel oil viscosity on a required level.

Biodegradability of the vegetable fuel oils is a very positive quality. However to be capable of serving as fully useful fuel oils they should:
• ensure similar energy qualities as compared with diesel oil,
• do not cause an excessive wear of engine and consequently reduce life time of engine,
• be a source of only low quantities of environmentally noxious substances (CO_2),
• ensure a low specific fuel oil consumption by engine,
• facilitate recycling of raw and packing materials associated with their production.

Choice of an alternative fuel oil obtained from fatty acid esters of vegetable oils and being their mixture with diesel oil should be based on research results dealing not only with energy and ecology aspects but also with durability and reliability of crucial structural units of the engines, namely: injection, crankshaft and piston-cylinder systems.

In order to be able to select a kind of biofuel, out of those have been tested so far, additional tests on durability of biofuel-fed self-ignition engines should be performed.

For application of biofuels it is necessary to achieve credible information concerning not only the energy aspects and potential pollution hazard to the environment by noxious substances, but also the developing of wear processes within the engine, i.e. its reliability and durability. In order to achieve a comprehensive knowledge dealing with the problems technical diagnostics should be used [6, 9].

Features of diesel oil and the considered alternative fuel oils influence in a different way not only energy merits of self-ignition engines but also their wear and operation.

The operation of engines may be understood in different ways. In this paper it is understood as the process of generating, by the engines, the energy E within a definite time t. It has been equated to a physical quantity expressed by a numerical value measured by the unit called joule-second [J · sec]. The so-understood operation becomes worser and worser along with progressing wear of such engines. It means that value of the operation within a given time decreases as a result of lowering amount of energy generated by the engine. The so-interpreted operation depends on a technical state of the engine characterized simultaneously by the energy transformed by it and the energy generating time.

The engine operation presented in this version is of such virtue that it can be investigated by performing measurements of quantities which characterize energy and can be expressed numerically as a value measured by the joule-second unit [J · sec] (Eq. 2 and 3), as well as presented in a graphical form as an area of operation.

Depending on practical needs and possibile assessment of operation of the engines, their operation can be valuated as a result of consideration of the useful work (6) which can be done by the engine, or the effective power (7) which can be developed by the engine. As engine's power contains information on how fast the work can be done, hence the effective engine power can be considered an energy rate of its operation (engine operation rate).

The so-interpreted operation, in spite of that it was formulated with a view of self-ignition engines, may deal also with spark-iginition ones. Similar interpretation of operation can be applied also to gas turbines and other power devices.

BIBLIOGRAPHY

1. Adamczyk A., Lotko W.: *Application of mixtures composed of alternative fuels and diesel oil to direct-injection engines* (in Polish). AUTO-Technika Motoryzacyjna (CAR - Motorization Engineering), No. 11, 1990
2. Heywood J.B.: *Internal Combustion Engine Fundamentals*. McGraw-Hill Book Company, Series in Mechanical Engineering, New York 1988
3. Höglund P.G., Ydstedt A.: *Reduced Air Pollution and Fuel Consumption with Preheated Car Engines*. Urban Transport and the Environment for the 21st Century, International Conference, Lisbon 1998
4. Girtler J.: *Possibility of valuation of operation of marine diesel engines*. Journal of Polish CIMAC, Vol. 4, No. 1, 2009
5. Girtler J.: *Energetic aspect of diesel engine operation*. Silniki Spalinowe (Combustion Engines), No. 2, (2009).
6. Korczewski Z. *Endoscopy of ship engines* (in Polish). Polish Naval Academy, Gdynia 2008
7. Lindl B., Schmotz H.G.: *Cold Start Equipment for Diesel Direct Injection Engines*. SAE Technical Paper 1999-01-1244.
8. Lotko W.: *Supplying combustion engines with alternative fuels* (in Polish). ITE, Radom 1995
9. Polanowski S.: *Assessing diagnostic applicability of heat release characteristics determined on the basis of ship engine indicator diagram*. Polish Maritime Research. No. 3(61) Vol. 16, 2009
10. Rudnicki J.: *On making operational decisions with taking into account value of operation applied to ship main propulsion engine as an example*. Journal of Polish CIMAC, Vol. 4, No.1, 2009
11. Rudnicki J.: *Assessment of operation of energy system of serial reliability structure on the example of ship main propulsion system*. Journal of Polish CIMAC, Vol. 3, No. 2, 2008
12. Svensson B.: *IMO's MARPOL Annex VI will affect engine lubrication*. Diesel & Gas Turbine Worldwide, May 2006
13. Szlachta Z.: *Supplying high-pressure engines with rape oil fuels* (in Polish). WKiŁ (Transport and Communication Publishers), Warsaw 2002
14. Wędzik A.: *Combined electric power generating systems* (in Polish). Elektroenergetyka (Electric power engineering), No.06/05/02
15. Woodyard D.: *Cylinder oil challenges and choices*. Marine Propulsion & Auxiliary Machinery. 12/2009,01/2010
16. Woodyard D.: *Marine diesel engines and gas turbines*. 8th Edition, Elsevier Ltd, 2004

CONTACT WITH THE AUTHORS

Jerzy Girtler, Prof.
Zbigniew Korczewski, Assoc. Prof.
Faculty of Ocean Engineering
and Ship Technology
Gdansk University of Technology
Narutowicza 11/12
80-952 Gdansk, POLAND
tel.: (+48 58) 347-24-30; fax: (+48 58) 347-19-81
e-mail: jgirtl@pg.gda.pl
e-mail: zbigniew korczewski@pg.gda.pl

Jacek Mańczak, M. Sc.
H. CEGIELSKI – Poznan S. A.

Energy losses in the hydraulic rotational motor definitions and relations for evaluation of the efficiency of motor and hydrostatic drive

Zygmunt Paszota, Prof.
Gdansk University of Technology

Abstract

The evaluation methods of energy losses and efficiency of the hydraulic rotational motors for the hydrostatic drives, used so far in the scientific research and in the industrial practice, give wrong results because the parameters that the losses and efficiencies are a function of are themselves dependent on those losses.
The aim of the paper is to define the motor operating parameters, developed powers, energy losses and efficiencies and also to show the respective relations. Conclusions are drawn, based on the analyses of presented definitions and relations, on the motor energy investigations.

Keywords: hydrostatic drive; hydraulic motor; energy efficiency

INTRODUCTION

Evaluation of the energy behaviour of a hydraulic motor is an evaluation of its overall efficiency $\eta_M = f(n_M, M_M, \nu)$, i.e. evaluation of the overall efficiency η_M as a function of motor shaft speed n_M and load M_M and of the working fluid viscosity ν. This is also assessment of the value and proportions of the motor mechanical, volumetric and pressure losses deciding of the motor mechanical η_{Mm}, volumetric η_{Mv} and pressure η_{Mp} efficiency, where the product $\eta_M = \eta_{Mm} \eta_{Mv} \eta_{Mp}$ determines the motor overall efficiency η_M. The energy losses and the corresponding efficiencies η_{Mm}, η_{Mv} and η_{Mp} should be determined as a function of parameters having a direct impact on the particular losses and efficiencies.

Designers and makers of rotational hydraulic motors and hydrostatic systems have not had so far a tool to determine their energy behaviour in the $(0 \leq \overline{\omega}_M \langle \overline{\omega}_{Mmax}, \ 0 \leq \overline{M}_M \langle \overline{M}_{Mmax})$ field of change of the hydraulic motor shaft speed and load coefficients and in the $\nu_{min} \leq \nu \leq \nu_{max}$ field of change of the working fluid viscosity.

The rotational motor producers make erroneous routine evaluations of the following energy efficiencies and work parameters:
– the motor overall efficiency η_M as a function of the shaft speed n_M and motor pressure decrease Δp_M (e.g. [11÷14])
– the motor overall efficiency η_M as a product of the volumetric efficiency η_{Mv} and the so called „mechanical – hydraulic efficiency" η_{Mmh}, determined all the three as a function of the same parameters (e.g. [11, 12])
– motor shaft speed n_M as a function of the motor capacity Q_M and volumetric efficiency η_{Mv}, determined in turn as a function of the motor pressure decrease Δp_M (e.g. [11, 13])

– motor shaft torque M_M as a function of pressure decrease Δp_M and the so called „mechanical – hydraulic efficiency" η_{Mmh} of the motor (e.g. [11÷14])
– motor capacity Q_M as a function of the shaft speed n_M and volumetric efficiency η_{Mv}, determined in turn as a function of the motor pressure decrease Δp_M (e.g. [11÷13])
– motor shaft usefull power P_{Mu} as a function of the motor capacity Q_M and pressure decrease Δp_M and as a function of the motor overall efficiency η_M determined in turn as a function of the motor shaft speed n_M and pressure decrease Δp_M (e.g. [11÷13]).

The hydraulic motor researchers evaluate in a wrong way the losses arising in the motor:
– the motor torque M_{Mm} of mechanical losses as a function of the motor pressure decrease Δp_M and shaft speed n_M
– a sum of torque M_{Mm} of mechanical losses and the so called „torque of pressure losses" (resulting from the pressure losses Δp_M in the motor) – as a function of motor pressure decrease Δp_M and the shaft speed n_M
– the intensity Q_{Mv} of volumetric losses in the motor as a function of the motor pressure decrease Δp_M (or as a function of the motor shaft torque M_M) and as a function of the motor shaft speed n_M.

The evaluation methods of the energy losses and efficiency of the rotational hydraulic motors, used so far in the scientific research and in the industrial practice give wrong results because the parameters that the losses and efficiencies are a function of are themselves dependent of those losses.

There are very few informations of the motor makers presenting properly the motor overall efficiency $\eta_M = f(n_M,$

M_M) as a function of the motor shaft speed n_M and torque M_M at a specified fluid viscosity ν and presenting the impact of viscosity ν on the overall efficiency η_M (e.g. [10]).

It is a common deficiency that no information is given about the dependence of the motor mechanical, volumetric and pressure losses on the kinematic viscosity ν of the working fluid used in the hydrostatic drive system.

The fundamental reason of the erroneous evaluations are commonly accepted views on the research methodology and on the method of determining the energy losses in pumps and in hydraulic motors . That method is based, among others, on the traditional reading of the energy balance of a hydrostatic drive system from the Sankey diagram [1÷9]. The present unsatisfactory state is also effect of using simplified evaluations of the relations of particular losses to the motor or pump working parameters and to the working fluid viscosity.

Therefore, the aim of this paper is to define the work parameters, developed powers, losses and energy efficiency of a rotational hydraulic motor and also demonstrating their complex interdependence. The analysis of those definitions and relations will be a basis of conclusions regarding the investigations of motor energy characteristics.

ROTATIONAL HYDRAULIC MOTOR – WORK PARAMETERS, POWERS, ENERGY LOSSES, ENERGY EFFICIENCY – DEFINITIONS AND RELATIONS

– Motor shaft rotational (angular) speed n_M (ω_M) varies in the ($0 \leq \overline{\omega}_M \langle \overline{\omega}_{Mmax}$, $0 \leq \overline{M}_M \langle \overline{M}_{Mmax}$) field of the hydrostatic drive system operation. The instantaneous n_M (ω_M) value is required by the machine (device) driven by the motor. The instantaneous value of the n_M (ω_M) speed is independent of the instantaneous value of the M_M torque loading the motor shaft and also independent of the energy losses in the hydraulic motor and in the hydrostatic drive system.
– M_M torque loading the motor shaft varies in the ($0 \leq \overline{\omega}_M \langle \overline{\omega}_{Mmax}$, $0 \leq \overline{M}_M \langle \overline{M}_{Mmax}$) field of the hydrostatic drive system operation. The instantaneous value of M_M torque is required by the motor driven machine (device). The instantaneous value of M_M torque is independent of the instantaneous value of the required motor shaft speed n_M (ω_M) and also of the energy losses in a hydraulic motor and in the hydrostatic drive system.
– Working fluid (hydraulic oil, oil-water emulsion) kinematic viscosity ν changes in the $\nu_{min} \leq \nu \leq \nu_{max}$ range. The instantaneous value ν of the viscosity of fluid flux reaching the hydraulic motor is independent of the motor and of the energy losses in the motor.
– Motor useful power P_{Mu}, required on the motor shaft by the driven machine (device), is a product of the required M_M torque loading the motor shaft and the required shaft angular speed ω_M:

$$P_{Mu} = M_M \, \omega_M = 2\Pi \, M_M \, n_M \qquad (1)$$

The motor useful power P_{Mu} is independent of the energy losses in the hydraulic motor and the hydrostatic drive system.
– M_{Mm} torque of mechanical losses in the motor, occurring in the „shaft – working chambers" assembly, is a function of the required M_M torque loading the motor shaft and of the required shaft rotational speed n_M. The n_M speed influences the inertia forces of „shaft – working chambers" assembly elements and in effect the friction losses in the piston, satellite and vane motors. The M_{Mm} torque of losses is to a some extent also a function of the working fluid viscosity ν.

The impact of fluid viscosity on the mechanical losses in the „shaft – working chambers" assembly occurs mainly in the piston motors with fluid in the motor casing:

$$M_{Mm} = f\,(M_M, n_M, \nu) \qquad (2)$$

– Power ΔP_{Mm} of mechanical losses in the motor, occuring in the „shaft – working chambers" assembly, is a product of the M_{Mm} torque of mechanical losses and shaft angular speed ω_M:

$$\Delta P_{Mm} = M_{Mm} \, \omega_M = 2\Pi \, M_{Mm} \, n_M \qquad (3)$$

– M_{Mi} indicated torque in the motor working chambers (at the point of conversion of the working fluid pressure energy into mechanical energy of the „shaft – working chambers" assembly), required by the motor from the driving working fluid, must be greater than the M_M torque loading the motor shaft [required by the driven machine (device)] because of the necessity of balancing also the M_{Mm} torque of mechanical losses in the „shaft – working chambers" assembly. The M_{Mi} torque is equal to the sum of shaft torque M_M and M_{Mm} torque of mechanical losses. The indicated torque M_{Mi} requires a value of the product of decrease Δp_{Mi} of the indicated pressure in working chambers and the theoretical motor capacity q_{Mt} per one shaft revolution (theoretical motor working volume V_{Mt}) in accordance with the expression:

$$\frac{\Delta p_{Mi} \; q_{Mt}}{2\Pi} = M_{Mi} = M_M + M_{Mm} \qquad (4)$$

The M_{Mi} torque indicated in the motor working chambers is not a function of the decrease Δp_{Mi} and of theoretical motor capacity q_{Mt} per one shaft revolution.
For evaluation of the M_{Mi} torque indicated in the motor working chambers a formula can be used relating the M_M torque loading the motor shaft with the known motor mechanical efficiency η_{Mm} [formula (11)]:

$$\frac{\Delta p_{Mi} \; q_{Mt}}{2\Pi} = M_{Mi} = \frac{M_M}{\eta_{Mm}} \qquad (5)$$

with: $\eta_{Mm} = f\,(M_{Mm}, M_M) = f\,(M_M, n_M, \nu)$

i.e. a formula where mechanical efficiency η_{Mm} is defined as a function of parameters influencing the M_{Mm} torque of mechanical losses in the „shaft – working chambers" assembly and as a function of the M_M torque loading the motor shaft.
– Pressure decrease Δp_{Mi} indicated in the motor working chambers is a function of the required M_{Mi} torque indicated in the chambers and theoretical capacity q_{Mt} per one shaft revolution:

$$\Delta p_{Mi} = \frac{2\Pi \, M_{Mi}}{q_{Mt}} = \frac{2\Pi(M_M + M_{Mm})}{q_{Mt}} \qquad (6)$$

Therefore, the pressure decrease Δp_{Mi} indicated in the motor working chambers (with determined theoretical capacity q_{Mt} per one shaft revolution) is a function of the required M_M torque loading the motor shaft and the M_{Mm} torque of mechanical losses in the „shaft – working chambers" assembly. The pressure decrease Δp_{Mi} is indirectly a function of the shaft rotational speed n_M and a function of the working fluid viscosity ν, which have an impact (apart from M_M) on the M_{Mm} torque of mechanical losses:

$$\Delta p_{Mi} = f\,(M_M, M_{Mm}) = f\,(M_M, n_M, \nu) \qquad (7)$$

For evaluation of the decrease Δp_{Mi} of pressure indicated in the motor working chambers (with determined theoretical

capacity q_{Mt} per one shaft revolution) a formula can be used relating the M_M torque loading the motor shaft with the known motor mechanical efficiency η_{Mm} [formula (11)]:

$$\Delta p_{Mi} = \frac{2\Pi M_M}{q_{Mt}\,\eta_{Mm}} \qquad (8)$$

with: $\eta_{Mm} = f(M_{Mm}, M_M) = f(M_M, n_M, \nu)$

i.e. a formula where mechanical efficiency η_{Mm} is defined as a function of parameters influencing the M_{Mm} torque of mechanical losses in the „shaft – working chambers" assembly and as a function of the M_M torque loading the motor shaft.

- P_{Mi} indicated power in the motor working chambers is required by the motor from the driving working fluid at the point of conversion of the working fluid pressure energy into mechanical energy of the „shaft – working chambers" assembly. The P_{Mi} is equal to the product of the M_{Mi} torque indicated in the chambers and the shaft angular speed ω_M. The power P_{Mi} indicated in the working chamber is a sum of useful power P_{Mu} [required on the motor shaft by the driven machine (device)] and the power ΔP_{Mm} of mechanical losses in the „shaft – working chambers" assembly:

$$\frac{\Delta p_{Mi}\,q_{Mt}}{2\Pi}\,\omega_M = \Delta p_{Mi}\,q_{Mt}\,n_M = P_{Mi} =$$
$$= M_{Mi}\,\omega_M = (M_M + M_{Mm})\,\omega_M = P_{Mu} + \Delta P_{Mm} \qquad (9)$$

The P_{Mi} power indicated in the motor working chambers is not a function of the decrease Δp_{Mi} of pressure indicated in the chambers and of theoretical motor capacity q_{Mt} per one shaft revolution.

For evaluation of the P_{Mi} power indicated in the motor working chambers a formula can be used relating the motor shaft useful power P_{Mu} with the known motor mechanical efficiency η_{Mm} [formula (11)]:

$$P_{Mi} = \frac{P_{Mu}}{\eta_{Mm}} \qquad (10)$$

with: $\eta_{Mm} = f(M_{Mm}, M_M) = f(M_M, n_M, \nu)$

i.e. a formula, where mechanical efficiency η_{Mm} is defined as a function of parameters influencing the M_{Mm} torque of mechanical losses in the „shaft – working chambers" assembly and as a function of the M_M torque loading the motor shaft.

- The motor mechanical efficiency η_{Mm} is a ratio of useful power P_{Mu} on the shaft [required by the motor driven machine (device)] to the power P_{Mi} indicated in the motor working chambers (required by the motor of the driving fluid at the point of conversion (change) of the working fluid pressure energy into the mechanical energy of the „shaft – working chambers" assembly). The η_{Mm} efficiency can be also determined by the ratio of motor shaft torque M_M to the torque M_{Mi} indicated in the working chambers:

$$\eta_{Mm} = \frac{P_{Mu}}{P_{Mi}} = \frac{P_{Mu}}{P_{Mu} + \Delta P_{Mm}} =$$
$$= \frac{M_M\,\omega_M}{(M_M + M_{Mm})\,\omega_M} = \frac{M_M}{M_M + M_{Mm}} = \frac{M_M}{M_{Mi}} \qquad (11)$$

The motor mechanical efficiency η_{Mm} is a function of torque M_{Mm} of mechanical losses in the „shaft – working chambers" assembly and the shaft loading torque M_M. Therefore, the η_{Mm} efficiency is a function of torque M_M and shaft rotational speed n_M and a function of working fluid viscosity ν, which influences (apart from M_M) the torque M_{Mm} of mechanical losses in the „shaft – working chambers" assembly:

$$\eta_{Mm} = f(M_{Mm}, M_M) = f(M_M, n_M, \nu) \qquad (12)$$

because: $M_{Mm} = f(M_M, n_M, \nu)$.

The motor mechanical efficiency η_{Mm} can be also evaluated from the formula:

$$\eta_{Mm} = \frac{2\Pi M_M}{\Delta p_{Mi}\,q_{Mt}} \qquad (13)$$

However, mechanical efficiency η_{Mm} is not a function of the decrease Δp_{Mi} of pressure indicated in the motor working chambers and of the motor theoretical capacity q_{Mt} per one shaft revolution.

- Intensity Q_{Mv} of the motor volumetric losses in the working chambers takes into account internal volumetric losses (between the chamber inlet channel and chamber outlet channel) and external volumetric losses (between chambers and casing and then led out of the casing). The intensity Q_{Mv} of motor volumetric losses (with determined theoretical capacity q_{Mt} per one shaft revolution) is a function of the decrease Δp_{Mi} of pressure indicated in the chambers and, to some extent, of the shaft rotational speed n_M as well as working fluid viscosity ν:

$$Q_{Mv} = f(\Delta p_{Mi}, n_M, \nu) \qquad (14)$$

The intensity Q_{Mv} of volumetric losses in the motor working chambers is a complex function of torque M_M and motor shaft speed n_M and also working fluid viscosity ν, i.e. of parameters independent of the motor and motor losses. The decrease Δp_{Mi} of pressure indicated in the chambers, influencing directly Q_{Mv} [formula (14)], is a function [formula (6)] of the shaft torque M_M and of torque M_{Mm} of mechanical losses in the „shaft – working chambers" assembly and, in turn, torque M_{Mm} of the losses [formula (2)] is a function of torque M_M and of motor shaft speed n_M and also of the working fluid viscosity ν. At the same time, the impact of shaft speed n_M and working fluid viscosity ν on the intensity Q_{Mv} of the volumetric losses in working chambers differs from the impact of n_M and ν on the torque M_{Mm} of mechanical losses in the „shaft – working chambers" assembly. A direct evaluation of the relation of intensity Q_{Mv} of volumetric losses in the motor working chambers to the motor shaft torque M_M and speed n_M and also to the working fluid viscosity ν would be unjustified and wrong because it would be under a complex impact of the torque M_{Mm} of mechanical losses.

- Power ΔP_{Mv} of the motor volumetric losses, in the working chambers, is a product of decrease Δp_{Mi} of pressure indicated in the chambers and intensity Q_{Mv} of volumetric losses in the chambers (on the assumption that the external volumetric losses are small and negligible from the energy point of view):

$$\Delta P_{Mv} = \Delta p_{Mi}\,Q_{Mv} \qquad (15)$$

- Motor capacity Q_M required by the motor from the driving fluid must be greater than the product $q_{Mt}\,n_M$ [theoretical capacity q_{Mt} per one shaft resolution and motor shaft rotational speed n_M required by the motor driven machine (device)] because of the necessity of balancing also the intensity Q_{Mv} of volumetric losses in the motor working chambers. Capacity Q_M is equal to the sum of intensity $q_{Mt}\,n_M$ and intensity Q_{Mv}:

$$Q_M = q_{Mt}\,n_M + Q_{Mv} \qquad (16)$$

Evaluation of the motor capacity Q_M (with determined theoretical capacity q_{Mt} per one shaft revolution) can be performed with a formula including the motor shaft rotational speed n_M required by the motor driven machine and known motor volumetric efficiency η_{Mv} [formula (23)]:

$$Q_M = \frac{q_{Mt} \, n_M}{\eta_{Mv}} \qquad (17)$$

with: $\eta_{Mv} = f(Q_{Mv}, n_M) = f(\Delta p_{Mi}, n_M, v)$

i.e. a formula, where the volumetric efficiency η_{Mv} is determined as a function of parameters influencing the intensity Q_{Mv} of volumetric losses in the working chambers and as a function of the motor rotational speed n_M.

– Power P_{Mci} of the working fluid absorbed by the motor in working chambers is required by the motor from the driving fluid as a difference between power $p_{M1i} Q_M$ of the fluid inflowing in the working chambers from the inlet channel and power $p_{M2i} Q_M$ of the fluid outflowing from the chambers to the outlet channel. Assuming that the external volumetric losses are small and negligible from the energy point of view, it may be accepted that the intensity of the outflowing flux is equal to the intensity Q_M of the inflowing flux. Therefore, power P_{Mci} may be determined as a product of the decrease Δp_{Mi} of pressure indicated in working chambers and the motor capacity Q_M. Power P_{Mci} must be greater than power P_{Mi} indicated in the chambers (required by the motor from the driving fluid at the point of conversion (change) of pressure energy of working fluid into the mechanical energy of the „shaft – working chambers" assembly) because of the necessity of balancing also the power ΔP_{Mv} of volumetric losses in the chambers. Power P_{Mci} is equal to the sum of power P_{Mi} and power ΔP_{Mv}:

$$P_{Mci} = p_{M1i} Q_M - p_{M2i} Q_M =$$
$$= \Delta p_{Mi} Q_M = \Delta p_{Mi} (q_{Mt} n_M + Q_{Mv}) = \qquad (18)$$
$$= \Delta p_{Mi} q_{Mt} n_M + \Delta p_{Mi} Q_{Mv} = P_{Mi} + \Delta P_{Mv}$$

Power P_{Mci} of the working fluid consumed by the motor in working chambers is a sum of useful power P_{Mu} [required on the motor shaft by driven machine (device)], power ΔP_{Mm} of mechanical losses in the „shaft – working chambers" assembly and power ΔP_{Mv} of volumetric losses in the motor working chambers:

$$P_{Mci} = P_{Mu} + \Delta P_{Mm} + \Delta P_{Mv} \qquad (19)$$

After replacing in the equation (19) the useful power P_{Mu}, power ΔP_{Mm} of mechanical losses and power ΔP_{Mv} of volumetric losses by the expressions relating those powers to the parameters and losses deciding of their values, a picture can be obtained of the impact of those parameters and losses on power P_{Mci} consumed in the working chambers:

$$P_{Mci} = M_M \omega_M + M_{Mm} \omega_M + \Delta p_{Mi} Q_{Mv} =$$
$$= M_M \omega_M + M_{Mm} \omega_M + \frac{2\Pi (M_M + M_{Mm})}{q_{Mt}} Q_{Mv} = \quad (20)$$
$$= 2\Pi (M_M + M_{Mm}) \left(n_M + \frac{Q_{Mv}}{q_{Mt}} \right)$$

Power P_{Mci} of working fluid consumed by the motor in working chambers can be evaluated by means of a formula expressing the ratio of power P_{Mi} indicated in the working chambers to a known volumetric efficiency η_{Mv} of the motor [formula (23)]:

$$P_{Mci} = \frac{P_{Mi}}{\eta_{Mv}} \qquad (21)$$

with: $\eta_{Mv} = f(Q_{Mv}, n_M) = f(\Delta p_{Mi}, n_M, v)$

i.e. a formula where volumetric efficiency η_{Mv} is determined as a function of parameters influencing the intensity Q_{Mv} of volumetric losses in the working chambers and as a function of the motor rotational speed n_M.
Power P_{Mci} of the working fluid consumed by motor in the working chambers can be evaluated also from the known useful power P_{Mu} on the motor shaft, known mechanical efficiency η_{Mm} [formula (11)] and known volumetric efficiency η_{Mv} of the motor [formula (23)]:

$$P_{Mci} = \frac{P_{Mu}}{\eta_{Mm} \, \eta_{Mv}} \qquad (22)$$

with: $\eta_{Mm} = f(M_{Mm}, M_M) = f(M_M, n_M, v)$
and: $\eta_{Mv} = f(Q_{Mv}, n_M) = f(\Delta p_{Mi}, n_M, v)$

i.e. a formula where mechanical efficiency η_{Mm} is determined as a function of parameters influencing the torque M_{Mm} of mechanical losses in the „shaft – working chambers" assembly and as a function of torque M_M loading the motor shaft, and the volumetric efficiency η_{Mv} is determined as a function of parameters influencing the intensity Q_{Mv} of volumetric losses in the working chambers and of the motor rotational speed n_M.

– Volumetric efficiency η_{Mv} of the motor is a ratio of power P_{Mi} indicated in the motor working chambers to power P_{Mci} of working fluid consumed by the motor in the chambers:

$$\eta_{Mv} = \frac{P_{Mi}}{P_{Mci}} = \frac{P_{Mi}}{P_{Mi} + \Delta P_{Mv}} =$$
$$= \frac{\Delta p_{Mi} q_{Mt} n_M}{\Delta p_{Mi} q_{Mt} n_M + \Delta p_{Mi} Q_{Mv}} = \qquad (23)$$
$$= \frac{q_{Mt} n_M}{q_{Mt} n_M + Q_{Mv}} = \frac{q_{Mt} n_M}{Q_M}$$

The motor volumetric efficiency η_{Mv} (with determined theoretical capacity q_{Mt} per one shaft revolution) is a function of intensity Q_{Mv} of volumetric losses in the motor and of the motor shaft rotational speed n_M. Therefore, efficiency η_{Mv} is a function of the decrease Δp_{Mi} of pressure indicated in working chambers and a function of the rotational speed n_M as well as a function of the working fluid viscosity v (which have an impact on the intensity Q_{Mv} of volumetric losses) and also directly a function of rotational speed n_M:

$$\eta_{Mv} = f(Q_{Mv}, n_M) = f(\Delta p_{Mi}, n_M, v) \qquad (24)$$

because: $Q_{Mv} = f(\Delta p_{Mi}, n_M, v)$.

– Losses Δp_{Mp} of working fluid pressure in the motor channels are a sum of two pressure losses i.e. loss Δp_{Mp1} of pressure in the inlet channel (between the motor inlet point and working chambers) and loss Δp_{Mp2} of pressure in the outlet channel (between the working chambers and the motor outlet point). Losses Δp_{Mp} are a function of motor capacity Q_M and of working fluid viscosity v:

$$\Delta p_{Mp} = \Delta p_{Mp1} + \Delta p_{Mp2} = f(Q_M, v) \qquad (25)$$

Losses Δp_{Mp} of working fluid pressure in the motor channels

are a complex function of the motor shaft speed n_M and torque M_M and the working fluid viscosity ν, i.e. parameters independent of the motor and of losses in it. The motor capacity Q_M, having a direct impact on Δp_{Mp} [formula (14)], is a function [formula (16)] of the shaft rotational speed n_M and of intensity of volumetric losses Q_{Mv} in the working chambers. The decrease Δp_{Mi} of pressure indicated in the working chambers, having a direct impact on Q_{Mv} [formula (14)], is a function [formula (6)] of the shaft torque M_M and of torque M_{Mm} of mechanical losses in the „shaft – working chambers" assembly, and the torque M_{Mm} of mechanical losses [formula (2)] is in turn a function of the motor shaft torque M_M and speed n_M and of the viscosity ν of working fluid. At the same time, the impact of working fluid viscosity ν on the losses Δp_{Mp} of fluid pressure in the channels differs from the impact of viscosity ν on the intensity Q_{Mv} of volumetric losses in the working chambers and from the impact of ν on the torque M_{Mm} of mechanical losses in the „shaft – working chambers" assembly. Also the impact of shaft speed n_M on the intensity Q_{Mv} of volumetric losses in the working chambers differs from the impact of n_M on the torque M_{Mm} of mechanical losses in the „shaft – working chambers" assembly. Direct evaluation of the dependence of pressure losses Δp_{Mp} of the working fluid in the motor channels on the motor shaft speed n_M and torque M_M and on the viscosity ν of working fluid would be unjustified and wrong, because it would be under a complex impact of the intensity Q_{Mv} of volumetric losses in working chambers and of torque M_{Mm} of mechanical losses in the „shaft – working chambers" assembly.

– Power ΔP_{Mp} of pressure losses in the motor, in the motor channels, with the assumption that external volumetric losses are small and negligible from the energy point of view, is a product of the pressure losses Δp_{Mp} in the channels and the motor capacity Q_M:

$$\Delta P_{Mp} = \Delta p_{Mp} \, Q_M \qquad (26)$$

– Decrease Δp_M of pressure in the motor (with determined theoretical capacity q_{Mt} per one shaft revolution), required by the motor from the driving working fluid, must be greater than decrease Δp_{Mi} of pressure indicated in the working chambers (required by the torque M_{Mi} indicated in the chambers) because of the necessity of balancing also the losses Δp_{Mp} of pressure in the motor channels. Decrease Δp_M is equal to the sum of the indicated decrease Δp_{Mi} and losses Δp_{Mp}:

$$\Delta p_M = \Delta p_{Mi} + \Delta p_{Mp} \qquad (27)$$

Replacing in the equation (27) the decrease Δp_{Mi} of pressure indicated in the working chambers with expression (6), we obtain the dependence of decrease Δp_M of pressure in the motor on the required torque M_M loading the motor shaft and on the torque M_{Mm} of mechanical losses in the „shaft – working chambers" assembly and also on the pressure losses Δp_{Mp} in the motor channels:

$$\Delta p_M = \frac{2\Pi \, (M_M + M_{Mm})}{q_{Mt}} + \Delta p_{Mp} \qquad (28)$$

The decrease Δp_M of pressure in the motor can be evaluated by means of a formula expressing the ratio of decrease Δp_{Mi} of pressure indicated in the working chambers to the known pressure efficiency η_{Mp} of the motor [formula (37)]:

$$\Delta p_M = \frac{\Delta p_{Mi}}{\eta_{Mp}} \qquad (29)$$

with: $\eta_{Mp} = f(\Delta p_{Mp}, \Delta p_{Mi}) = f(Q_M, \Delta p_{Mi}, \nu)$

i.e. formula where the motor pressure efficiency η_{Mp} is defined as a function of parameters influencing the losses Δp_{Mp} of working fluid pressure in the channels and as a function of the decrease Δp_{Mi} of pressure indicated in the working chambers.

Decrease Δp_M of pressure in the motor can be evaluated also from a known torque M_M loading the motor shaft, from a known mechanical efficiency η_{Mm} [formula (11)] and a known motor pressure efficiency η_{Mp} [formula (37)]:

$$\Delta p_M = \frac{2\Pi \, M_M}{q_{Mt} \, \eta_{Mm} \, \eta_{Mp}} \qquad (30)$$

with: $\eta_{Mm} = f(M_{Mm}, M_M) = f(M_M, n_M, \nu)$
and: $\eta_{Mp} = f(\Delta p_{Mp}, \Delta p_{Mi}) = f(Q_M, \Delta p_{Mi}, \nu)$

i.e. formula, where the mechanical efficiency η_{Mm} is defined as a function of parameters influencing the torque M_{Mm} of mechanical losses in the „shaft – working chambers" assembly and a function of torque M_M loading the motor shaft and the pressure efficiency η_{Mp} is defined as a function of parameters influencing the losses Δp_{Mp} of pressure in the channels and as a function of decrease Δp_{Mi} of pressure indicated in the motor working chambers.

– Working fluid power P_{Mc} consumed by the motor must be greater than power P_{Mci} (consumed by the motor in the working chambers) because of the necessity of balancing also the power ΔP_{Mp} of pressure losses in the motor channels. Power P_{Mc} is equal to the sum of power P_{Mci} and power ΔP_{Mp} of the losses. Power P_{Mc} is a product of the decrease Δp_M of pressure in the motor and motor capacity Q_M:

$$\begin{aligned} P_{Mc} &= \Delta p_M \, Q_M = (\Delta p_{Mi} + \Delta p_{Mp}) \, Q_M = \\ &= \Delta p_{Mi} \, Q_M + \Delta p_{Mp} \, Q_M = P_{Mci} + \Delta P_{Mp} \end{aligned} \qquad (31)$$

The working fluid power P_{Mc} consumed by the motor is a sum of useful power P_{Mu} (required on the motor shaft by the driven machine (device)], power ΔP_{Mm} of mechanical losses in the „shaft – working chambers" assembly, power ΔP_{Mv} of volumetric losses in the working chambers and power ΔP_{Mp} of pressure losses in the motor channels:

$$P_{Mc} = P_{Mu} + \Delta P_{Mm} + \Delta P_{Mv} + \Delta P_{Mp} \qquad (32)$$

After replacing in equation (32) the useful power P_{Mu} and power ΔP_{Mm} of mechanical losses, power ΔP_{Mv} of volumetric losses and power ΔP_{Mp} of pressure losses with formulae expressing dependence on parameters and losses deciding of the values of those powers, we can obtain a picture of the impact of parameters and losses on the consumed power P_{Mc}:

$$\begin{aligned} P_{Mc} &= M_M \, \omega_M + M_{Mm} \, \omega_M + \Delta p_{Mi} \, Q_{Mv} + \Delta p_{Mp} \, Q_M = \\ &= M_M \, \omega_M + M_{Mm} \, \omega_M + \frac{2\Pi (M_M + M_{Mm})}{q_{Mt}} Q_{Mv} + \\ &\quad + \Delta p_{Mp} (q_{Mt} n_M + Q_{Mv}) = \\ &= 2\Pi (M_M + M_{Mm}) \left(n_M + \frac{Q_{Mv}}{q_{Mt}} \right) + \\ &\quad + \Delta p_{Mp} (q_{Mt} n_M + Q_{Mv}) \end{aligned} \qquad (33)$$

The expression describing the working fluid power P_{Mc} consumed by the motor can be also obtained from the

product of decrease Δp_M of pressure in the motor [formula (28)] and motor capacity Q_M [formula (16)]:

$$P_{Mc} = \Delta p_M Q_M =$$

$$= \left[\frac{2\Pi (M_M + M_{Mm})}{q_{Mt}} + \Delta p_{Mp} \right] (q_{Mt} n_M + Q_{Mv}) \quad (34)$$

Expressions (33) and (34) are equivalent.
Evaluation of the working fluid power P_{Mc} consumed by the motor can be performed with a formula expressing the ratio of working fluid power P_{Mci} consumed by the motor in the working chambers to the motor pressure efficiency η_{Mp} [formula (37)]:

$$P_{Mc} = \frac{P_{Mci}}{\eta_{Mp}} \quad (35)$$

with: $\eta_{Mp} = f (\Delta p_{Mp}, \Delta p_{Mi}) = f (Q_M, \Delta p_{Mi}, \nu)$

i.e. a formula where the pressure efficiency η_{Mp} is defined as a function of parameters influencing the losses Δp_{Mp} of working fluid pressure in the channels and as a function of decrease Δp_{Mi} of pressure indicated in the motor working chambers.

The working fluid power P_{Mc} consumed by the motor can be evaluated from the known useful power P_{Mu} on the motor shaft, a known mechanical efficiency η_{Mm} [formula (11)], known volumetric efficiency η_{Mv} [formula (23)] and known pressure efficiency η_{Mp} [formula (37)] of the motor:

$$P_{Mc} = \frac{P_{Mu}}{\eta_{Mm} \eta_{Mv} \eta_{Mp}} \quad (36)$$

with: $\eta_{Mm} = f (M_{Mm}, M_M) = f (M_M, n_M, \nu)$
$\eta_{Mv} = f (Q_{Mv}, n_M) = f (\Delta p_{Mi}, n_M, \nu)$
and: $\eta_{Mp} = f (\Delta p_{Mp}, \Delta p_{Mi}), = f (Q_M, \Delta p_{Mi}, \nu)$.

In formula (36), the mechanical efficiency η_{Mm} is defined as a function of parameters influencing the torque M_{Mm} of mechanical losses in the „shaft – working chambers" assembly and as a function of torque M_M loading the motor shaft. The volumetric efficiency η_{Mv} is defined as a function of parameters influencing the intensity Q_{Mv} of volumetric losses in the working chambers and as a function of the motor shaft rotational speed n_M. The pressure efficiency η_{Mp} is defined as a function of parameters influencing the pressure losses Δp_{Mp} of working fluid in the channels and as a function of the decrease Δp_{Mi} of pressure indicated in the motor working chambers.

– The motor pressure efficiency η_{Mp} is a ratio of the working fluid power P_{Mci} consumed by the motor in the working chambers to the power P_{Mc} consumed by the motor:

$$\eta_{Mp} = \frac{P_{Mci}}{P_{Mc}} = \frac{P_{Mci}}{P_{Mci} + \Delta P_{Mp}} =$$

$$= \frac{\Delta p_{Mi} Q_M}{(\Delta p_{Mi} + \Delta p_{Mp}) Q_M} = \frac{\Delta p_{Mi}}{\Delta p_{Mi} + \Delta p_{Mp}} = \frac{\Delta p_{Mi}}{\Delta p_M} \quad (37)$$

Therefore, the pressure efficiency can by presented as a ratio of the decrease Δp_{Mi} of pressure indicated in the working chambers to the decrease Δp_M of pressure in the motor. The motor pressure efficiency η_{Mp} is a function of losses Δp_{Mp} of the working fluid pressure in motor channel and decrease Δp_{Mi} of pressure indicated in the motor working chambers. Therefore, efficiency η_{Mp} is a function of the motor capacity Q_M and a function of the working fluid viscosity ν (which influence the losses Δp_{Mp} of working fluid pressure in the

channels) as well as a function of the decrease Δp_{Mi} of pressure in the motor working chambers:

$$\eta_{Mp} = f (\Delta p_{Mp}, \Delta p_{Mi}) = f (Q_M, \Delta p_{Mi}, \nu) \quad (38)$$

because: $\Delta p_{Mp} = f (Q_M, \nu)$.
– The motor overall efficiency η_M is a ratio of the useful power P_{Mu} on the motor shaft required by the driven machine (device) to the power P_{Mc} consumed by the motor:

$$\eta_M = \frac{P_{Mu}}{P_{Mc}} = \frac{M_M \omega_M}{\Delta p_M Q_M} = \frac{2\Pi M_M n_M}{\Delta p_M Q_M} \quad (39)$$

Replacing in formula (39) the power P_{Mc} consumed by the motor with equations describing its dependence on the useful power P_{Mu} and on the powers ΔP_{Mm}, ΔP_{Mv} and ΔP_{Mp} of the energy losses in the motor (with a determined theoretical capacity q_{Mt} per one shaft revolution), we obtain the expressions describing the motor overall efficiency η_M as a function of the losses:

with reference to equation (32):

$$\eta_M = \frac{P_{Mu}}{P_{Mc}} = \frac{P_{Mu}}{P_{Mu} + \Delta P_{Mm} + \Delta P_{Mv} + \Delta P_{Mp}} \quad (40)$$

with reference to equation (33):

$$\eta_M = \frac{2\Pi M_M n_M}{2\Pi (M_M + M_{Mm}) \left(n_M + \dfrac{Q_{Mv}}{q_{Mt}} \right) + \Delta p_{Mp} (q_{Mt} n_M + Q_{Mv})} \quad (41)$$

with reference to equation (34):

$$\eta_M = \frac{2\Pi M_M n_M}{\left[\dfrac{2\Pi (M_M + M_{Mm})}{q_{Mt}} + \Delta p_{Mp} \right] (q_{Mt} n_M + Q_{Mv})} \quad (42)$$

Expressions (41) and (42) are equivalent.

The motor overall efficiency η_M is therefore a function of torque M_{Mm} of mechanical losses in the „shaft – working chambers" assembly, intensity Q_{Mv} of volumetric losses in the working chambers and losses Δp_{Mp} of pressure in the motor channels. The η_M efficiency is also a function of the motor shaft torque M_M and speed n_M required by the driven machine (device):

$$\eta_M = f (M_{Mm}, Q_{Mv}, \Delta p_{Mp}, M_M, n_M) \quad (43)$$

Torque $M_{Mm} = f (M_M, n_M, \nu)$ of mechanical losses from friction of elements in the motor „shaft – working chambers" assembly is a function of the required torque M_M loading the motor shaft. In the piston, satellite and vane motors, torque M_{Mm} of the losses is also a function of the required speed n_M influencing the inertia forces in the „shaft – working chambers" assembly and in effect the forces of friction between those elements. In the piston motors in particular, with working fluid in the casing, the torque M_{Mm} of the losses is also a function of the fluid viscosity ν, which influences the friction between the „shaft – working chambers" assembly elements and the fluid.

Intensity $Q_{Mv} = f (\Delta p_{Mi}, n_M, \nu)$ of volumetric losses in the motor working chambers is a function of the decrease Δp_{Mi} of pressure indicated in the chambers and, to some extent, a function of motor shaft rotational speed n_M and also a function of working fluid viscosity ν.

Losses $\Delta p_{Mp} = f (Q_M, \nu)$ of the working fluid pressure in the motor channels are a function of the motor capacity Q_M and of the working fluid viscosity ν.

In order to evaluate the dependence of overall efficiency η_M of the motor (with determined theoretical capacity q_{Mt} per one shaft revolution) on parameters independent of the losses in the motor, i.e. evaluate η_M as a function of the required motor shaft torque M_M and speed n_M and also as a function of the working fluid viscosity ν, a product of the motor mechanical efficiency η_{Mm}, volumetric efficiency η_{Mv} and pressure efficiency η_{Mp} must be used:

$$\eta_M = f(M_M, n_M, \nu) = \eta_{Mm}\,\eta_{Mv}\,\eta_{Mp} \qquad (44)$$

with: $\quad \eta_{Mm} = f(M_{Mm}, M_M) = f(M_M, n_M, \nu)$
because: $\quad M_{Mm} = f(M_M, n_M, \nu)$ [equation (12)]
$\qquad\qquad \eta_{Mv} = f(Q_{Mv}, n_M) = f(\Delta p_{Mi}, n_M, \nu)$
because: $\quad Q_{Mv} = f(\Delta p_{Mi}, n_M, \nu)$ [equation (24)]
and: $\qquad \eta_{Mp} = f(\Delta p_{Mp}, \Delta p_{Mi}) = f(Q_M, \Delta p_{Mi}, \nu)$
because $\quad \Delta p_{Mp} = f(Q_M, \nu)$ [equation (38)].

In the above equation describing the overall efficiency η_M, mechanical efficiency η_{Mm} is defined as a function of parameters influencing the torque M_{Mm} of mechanical losses in the „shaft – working chambers" assembly and as a function of torque M_M loading the motor shaft. Volumetric efficiency η_{Mv} is defined as a function of parameters influencing the intensity Q_{Mv} of volumetric losses in the working chambers and also as a function of the motor shaft rotational speed n_M. Pressure efficiency η_{Mp} is defined as a function of parameters influencing the losses Δp_{Mp} of working fluid pressure in the channels and a function of decrease Δp_{Mi} of pressure indicated in the motor working chambers.

After replacing in equation (44) η_{Mm} with expression (13), η_{Mv} with expression (23) and η_{Mp} with expression (37), we obtain a formula describing the motor efficiency η_M as a ratio of useful power P_{Mu} to power P_{Mc} consumed by the motor, i.e. a formula confirming correctness of the expressions describing η_{Mm}, η_{Mv} and η_{Mp}:

$$\eta_M = f(M_M, n_M, \nu) = \eta_{Mm}\eta_{Mv}\eta_{Mp} =$$
$$= \frac{2\Pi M_M}{\Delta p_{Mi} q_{Mt}}\,\frac{q_{Mt} n_M}{Q_M}\,\frac{\Delta p_{Mi}}{\Delta p_M} = \frac{2\Pi M_M n_M}{Q_M \Delta p_M} = \frac{P_{Mu}}{P_{Mc}} \qquad (45)$$

In equation (45), the required motor capacity Q_M [equation (17)] is a function:

$$Q_M = \frac{q_{Mt} n_M}{\eta_{Mv}}$$

with: $\quad \eta_{Mv} = f(Q_{Mv}, n_M) = f(\Delta p_{Mi}, n_M, \nu)$
because: $\quad Q_{Mv} = f(\Delta p_{Mi}, n_M, \nu)$

and the required pressure decrease Δp_M (equation (30)] is a function:

$$\Delta p_M = \frac{2\Pi M_M}{q_{Mt}\,\eta_{Mm}\,\eta_{Mp}}$$

with: $\quad \eta_{Mm} = f(M_{Mm}, M_M) = f(M_M, n_M, \nu)$
because: $\quad M_{Mm} = f(M_M, n_M, \nu)$
and: $\qquad \eta_{Mp} = f(\Delta p_{Mp}, \Delta p_{Mi}) = f(Q_M, \Delta p_{Mi}, \nu)$
because: $\quad \Delta p_{Mp} = f(Q_M, \nu)$.

After replacing in equation (44) η_{Mm} with formula (11), η_{Mv} with formula (23) and η_{Mp} with formula (37), we obtain an expression describing the efficiency η_M as a product of individual efficiencies described by losses and parameters deciding of their values and where at the same time Δp_{Mi} and Q_M are functions of the losses.

$$\eta_M = f(M_M, n_M, \nu) = \eta_{Mm}\eta_{Mv}\eta_{Mp} =$$
$$= \frac{M_M}{M_M + M_{Mm}}\,\frac{q_{Mt} n_M}{q_{Mt} n_M + Q_{Mv}}\,\frac{\Delta p_{Mi}}{\Delta p_{Mi} + \Delta p_{Mp}} \qquad (46)$$

where: $\quad M_{Mm} = f(M_M, n_M, \nu)$ [equation (2)]
$\qquad\qquad Q_{Mv} = f(\Delta p_{Mi}, n_M, \nu)$ [equation (14)]
$\qquad\qquad \Delta p_{Mp} = f(Q_M, \nu)$ [equation (25)]

with: $\qquad \Delta p_{Mi} = \dfrac{2\Pi(M_M + M_{Mm})}{q_{Mt}}$ [equation (6)]

and: $\qquad Q_M = q_{Mt} n_M + Q_{Mv}$ [equation (16)].

Decrease Δp_{Mi} of pressure indicated in the working chambers [equation (6)] is a function of the loading torque M_M and torque M_{Mm} of mechanical losses in the „shaft – working chambers" assembly. Capacity Q_M in the motor channels [equation (16)] is a function of motor shaft speed n_M and the intensity Q_{Mv} of volumetric losses in the working chambers.

Formula (46) shows a direct dependence of the torque M_{Mm} of mechanical losses in the „shaft – working chambers" assembly on the torque M_M and on the motor shaft rotational speed n_M as well as on the working fluid viscosity ν.

Formula (46) presents a complex dependence of the intensity Q_{Mv} of volumetric losses in the working chambers on the shaft loading torque M_M and on the torque M_{Mm} of mechanical losses in the „shaft – working chambers" assembly (decrease Δp_{Mi} of pressure indicated in the working chambers depends on M_M and M_{Mm} and has direct impact on Q_{Mv}) and also on the shaft speed n_M (influencing in diversified way the torque M_{Mm} of mechanical losses and intensity Q_{Mv} of volumetric losses). The intensity Q_{My} of volumetric losses depends on diversified impact of the working fluid viscosity ν: indirectly by impact of ν on the torque M_{Mm} of mechanical losses in the „shaft – working chambers" assembly and directly by impact of ν on intensity Q_{Mv} of losses in the chambers.

Formula (46) presents also a complex dependence of losses Δp_{Mp} of working fluid pressure in the channels on the shaft rotational speed n_M and on intensity Q_{Mv} of volumetric losses in the working chambers. The intensity Q_{Mv} of losses influences the motor capacity Q_M [equation (16)] and at the same time Q_{Mv} depends in a complex way on the shaft loading torque M_M and on the torque M_{Mm} of mechanical losses in the „shaft – working chambers" assembly. Pressure losses Δp_{Mp} in the channel are also dependent on the diversified impact of the working fluid viscosity ν: indirectly by impact of ν on the torque M_{Mm} of mechanical losses in the „shaft – working chambers" assembly and by impact of ν on the intensity Q_{My} of volumetric losses in the working chambers and directly by impact of ν on the losses Δp_{Mp} of pressure in the channels.

ANALYSIS OF THE PRESENTED DEFINITIONS AND RELATIONS

1. The power P_{Mc} consumed by the motor is a sum of motor shaft useful power P_{Mu} and powers of three different energy losses in the motor. The losses occur in series increasing power stream in the opposite direction to the direction of power flow. In effect, the power stream in the motor increases from the shaft useful power P_{Mu} to the working fluid power P_{Mc} consumed by the motor:

$$P_{Mc} = P_{Mu} + \Delta P_{Mm} + \Delta P_{Mv} + \Delta P_{Mp}$$

Mechanical losses (and power ΔP_{Mm}) occur in the „shaft – working chambers" assembly, volumetric losses (and power ΔP_{Mv}) occur in the working chambers, pressure losses (and power ΔP_{Mp}) occur in the motor channels.

2. Figure 1 presents a diagram of the direction of increasing power stream in a hydraulic motor. Direction of the increase of power stream is opposite to the direction of power flow in the motor. The diagram replaces the Sankey diagram of distribution of power flowing in a power transmission system. The use of Sankey diagram for description of power stream in the power transmission systems is a basic cause of errors in evaluation of losses in the power flow. The Sankey diagram suggests determination of losses in a system as a function of input parameters of that system. The suggestion can be noticed in the method of hydraulic motor investigations and in the related evaluations of losses and the motor energy efficiency. But the input parameters of the system depend on the losses.

3. Torque M_{Mm} of mechanical losses in the „shaft – working chambers" assembly should be evaluated as a function M_{Mm} = $f(M_M, n_M, \nu)$, i.e. as a function of the motor shaft loading torque M_M and the shaft rotational speed n_M and also as a function of a working fluid viscosity ν.
   The picture of torque M_{Mm} of mechanical losses in the motor, presented in literature and in the industrial practice as a function $M_{Mm} = f(\Delta p_M, n_M, \nu)$, i.e. as a direct dependence on the decrease Δp_M of pressure in the motor, is incorrect because it bears the impact of the mechanical losses and also of volumetric losses in the working chambers and pressure losses in the motor channels.

4. Intensity Q_{Mv} of volumetric losses in the motor working chambers should be evaluated as a function $Q_{Mv} = f(\Delta p_{Mi}, n_M, \nu)$, i.e. a function of decrease Δp_{Mi} of pressure indicated in the working chambers and of motor shaft rotational speed n_M and also as a function of the working fluid viscosity ν.
   The picture of intensity Q_{Mv} of volumetric losses, presented in literature and in industrial practice as a function $Q_{Mv} = f(\Delta p_M, n_M, \nu)$, i.e. as a direct dependence on the decrease Δp_M of pressure in the motor, is incorrect, because it bears the impact of the pressure losses in the motor channels.
   Similarly, the picture of intensity Q_{Mv} of volumetric losses as a function $Q_{Mv} = f(M_M, n_M, \nu)$, i.e. as a direct dependence on the motor shaft loading torque M_M, is also incorrect, because it bears the impact of the mechanical losses in the „shaft – working chambers" assembly.

5. Pressure losses Δp_{Mp} in the motor channels should be evaluated as a function $\Delta p_{Mp} = f(Q_M, \nu)$, i. e. a function of motor capacity Q_M and of working fluid viscosity ν.
   The picture of pressure losses Δp_{Mp}, presented sometimes in literature and in the industrial practice as a function $\Delta p_{Mp} = f(n_M, \nu)$, i.e. as a direct dependence on the motor shaft rotational speed n_M, is incorrect because it bears the impact of mechanical losses in the „shaft – working chambers" assembly and the impact of volumetric losses in the motor working chambers.

6. The torque M_{Mm} of mechanical losses in the „ shaft – working chambers" assembly and the so called „torque" of pressure losses Δp_{Mp} in the motor channels cannot make up a „sum" and also that „sum" cannot be evaluated as directly dependent on the same chosen parameters (which is practiced in literature and in industry), because those losses are of different character and are dependent on different parameters [$M_{Mm} = f(M_M, n_M, \nu)$, $\Delta p_{Mp} = f(Q_M, \nu)$].

7. The impact of working fluid viscosity ν on:
   – torque M_{Mm} of mechanical losses in the „shaft – working chambers" motor assembly
   – intensity Q_{Mv} of volumetric losses in the motor working chambers
   – pressure losses Δp_{Mp} in the motor channels
   is differentiated.

The dependence of particular kinds of losses on the working fluid viscosity ν should be presented in expressions describing dependence of those losses on other parameters which have a direct impact on them [$M_{Mm} = f(M_M, n_M, \nu)$, $Q_{Mv} = f(\Delta p_{Mi}, n_M, \nu)$, $\Delta p_{Mp} = f(Q_M, \nu)$].

8. The overall efficiency of the motor (with determined theoretical capacity q_{Mt} per one shaft revolution), in the ($0 \leq \overline{\omega}_M \langle \overline{\omega}_{Mmax}$, $0 \leq \overline{M}_M \langle \overline{M}_{Mmax}$) range of hydraulic motor shaft speed and torque coefficients and in the $\nu_{min} \leq \nu \leq \nu_{max}$ range of working fluid viscosity, must be evaluated only as a function $\eta_M = f(M_M, n_M, \nu)$, i.e. as a function of the required motor shaft torque M_M, required shaft rotational speed n_M and as a function of the working fluid viscosity ν. Torque M_M and speed n_M are parameters required by the motor driven machine (device), independent of the motor and of the motor losses. The working fluid viscosity ν is also independent of the motor and of the motor losses. At the same time those parameters (M_M, n_M, ν), in a direct or indirect way, have an impact on the motor mechanical, volumetric and pressure losses and also on the internal parameters deciding of the losses: on pressure decrease Δp_{Mi} indicated in the working chambers and deciding of the capacity Q_{Mv} of volumetric losses in the working chambers as well as on the motor capacity Q_M directly deciding of the pressure losses Δp_{Mp} in the motor channels.

9. The motor overall efficiency η_M, as a function of the motor shaft torque M_M and speed n_M and as a function of the working fluid viscosity ν, is a product of the motor mechanical efficiency η_{Mm}, volumetric efficiency η_{Mv} and pressure efficiency η_{Mp}:

$$\eta_M = f(M_M, n_M, \nu) = \frac{P_{Mu}}{P_{Mc}} = \eta_{Mm}\,\eta_{Mv}\,\eta_{Mp}$$

Each of the three efficiencies, as a factor of the product describing the overall efficiency, is evaluated as a function of parameters having a direct impact on the respective losses and as a function of a parameter to which those losses are „added".

10. The mechanical efficiency:

$$\eta_{Mm} = \frac{P_{Mu}}{P_{Mi}} = \frac{M_M}{M_M + M_{Mm}} = f(M_M, n_M, \nu)$$

must be evaluated as a function of parameters which have a direct impact on the torque $M_{Mm} = f(M_M, n_M, \nu)$ of mechanical losses in the „shaft – working chambers" assembly, i.e. a function of the required motor shaft torque M_M and a function of the required shaft rotational speed n_M as well as a function of the working fluid viscosity ν. At the same time, the mechanical efficiency η_{Mm} is directly a function of the shaft torque M_M because the torque M_{Mm} of mechanical losses is „added" to the torque M_M, causing decrease of power transmission efficiency in the assembly.

11. The volumetric efficiency:

$$\eta_{Mv} = \frac{P_{Mi}}{P_{Mci}} = \frac{q_{Mt}\,n_M}{q_{Mt}\,n_M + Q_{Mv}} = f(\Delta p_{Mi}, n_M, \nu)$$

must be evaluated as a function of parameters which have a direct impact on the intensity Q_{Mv} of volumetric losses in the working chambers, i.e. a function of pressure decrease Δp_{Mi} indicated in the chambers and as a function of the required motor shaft rotational speed n_M as well as a function of the working fluid viscosity ν. At the same time, the volumetric efficiency η_{Mv} is directly a function of the shaft rotational speed n_M, because the intensity
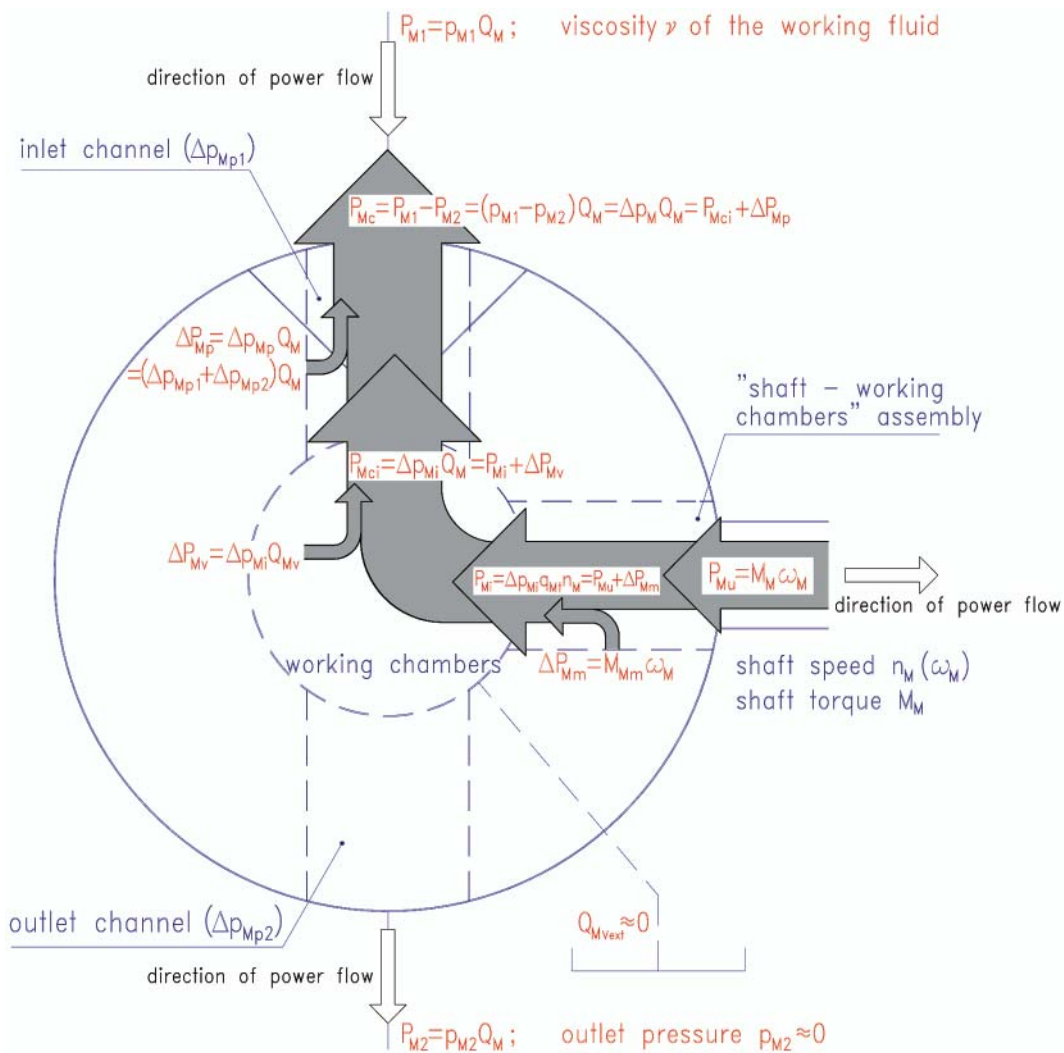
Fig. 1. *Diagram of the direction of increasing power stream in a rotational hydraulic motor; direction of the increase of power stream is opposite to the direction of power flow in the motor. Power stream increases from the motor useful power P_{Mu} required on the motor shaft by the driven machine (device) to power P_{Mc} consumed and required by the motor from the working fluid. The increase of power stream is an effect of the power of losses in the motor: power ΔP_{Mm} of mechanical losses in the „shaft – working chambers" assembly, power ΔP_{Mv} of volumetric losses in the working chambers and power ΔP_{Mp} of pressure losses in the motor channels. Powers ΔP_{Mm}, ΔP_{Mv} and ΔP_{Mp} of the losses are functions of the output parameters of the motor assembly where the losses occur and diversified functions of the working fluid viscosity v: power ΔP_{Mm} of mechanical losses is a function of torque M_M and shaft speed n_M (ω_M) required of the motor by the driven machine (device) and a function of the working fluid viscosity v, power ΔP_{Mv} of volumetric losses is a function of the decrease Δp_{Mi} of pressure indicated in working chambers (torque M_{Mi} indicated in the chambers) and of the shaft rotational speed n_M as well as a function of the working fluid viscosity v, power ΔP_{Mp} of pressure losses is a function of motor capacity Q_M and of the working fluid viscosity v. Power P_{Mi} indicated in the working chambers: $P_{Mi} = P_{Mu} + \Delta P_{Mm}$, power P_{Mci} of the working fluid consumed in the working chambers: $P_{Mci} = P_{Mu} + \Delta P_{Mm} + \Delta P_{Mv}$, power P_{Mc} of the working fluid consumed by the motor: $P_{Mc} = P_{Mu} + \Delta P_{Mm} + \Delta P_{Mv} + \Delta P_{Mp}$. The diagram replaces the Sankey diagram of distribution of power in transmission systems, causing incorrect loss evaluation during the hydraulic motor energy investigations.*

Q_{Mv} of volumetric losses is „added" to the product of theoretical capacity q_{Mt} per one shaft revolution and speed n_M, causing decrease of power transmission efficiency in the chambers.

If we wish to present the motor volumetric efficiency η_{Mv} as a factor in the product $\eta_{Mm} \eta_{Mv} \eta_{Mp}$ describing the motor overall efficiency η_M, i.e. to present η_{Mv} as a complex dependence on the parameters (M_M, n_M, v) describing the overall efficiency η_M and as a dependence on the mechanical losses in the motor, the intensity $Q_{Mv} = f(\Delta p_{Mi}, n_M, v)$ of volumetric losses in the chambers should be determined with:

$$\Delta p_{Mi} = \frac{2\Pi (M_M + M_{Mm})}{q_{Mt}}$$

and with torque M_{Mm} of mechanical losses in the „shaft – working chambers" assembly as a function of $M_{Mm} = f(M_M, n_M, v)$.

12. The pressure efficiency:

$$\eta_{Mp} = \frac{P_{Mci}}{P_{Mc}} = \frac{\Delta p_{Mi}}{\Delta p_{Mi} + \Delta p_{Mp}} = f(\Delta p_{Mi}, Q_M, v)$$

must be evaluated as a function of parameters which have a direct impact on the pressure losses Δp_{Mp} in the motor channels, i.e. as a function of the motor capacity Q_M and a function of the working fluid viscosity v. At the same time, the pressure efficiency η_{Mp} is directly a function of the pressure decrease Δp_{Mi} indicated in the motor working chambers, because pressure losses Δp_{Mp} in the motor channels are „added" to the pressure decrease Δp_{Mi}, causing decrease of power transmission efficiency in the channels.

If we wish to present the motor pressure efficiency η_{Mp} as a factor in the product $\eta_{Mm} \eta_{Mv} \eta_{Mp}$ describing the motor overall efficiency η_M, i.e. to present η_{Mp} as a complex dependence on the parameters (M_M, n_M, v) describing the

overall efficiency η_M and as a dependence on the mechanical and volumetric losses in the motor, the pressure losses $\Delta p_{Mp} = f(Q_M, \nu)$ in the channels should be determined with $Q_M = q_{Mt} n_M + Q_{Mv}$, the intensity $Q_{Mv} = f(\Delta p_{Mi}, n_M, \nu)$ of volumetric losses in the chambers should be determined with:

$$\Delta p_{Mi} = \frac{2\Pi (M_M + M_{Mm})}{q_{Mt}}$$

and with torque M_{Mm} of mechanical losses in the „shaft – working chambers" assembly determined as a function of $M_{Mm} = f(M_M, n_M, \nu)$.

13. Therefore, the picture of the characteristics of overall efficiency as a product $\eta_{Mm} \eta_{Mv} \eta_{Mp}$ of efficiencies correctly described by the characteristics of mechanical efficiency $\eta_M = f(M_M, n_M, \nu)$, volumetric efficiency $\eta_{Mv} = f(\Delta p_{Mi}, n_M, \nu)$ and pressure efficiency $\eta_{Mp} = f(\Delta p_{Mi}, Q_M, \nu)$ is complex.

CONCLUSIONS

1. The methods of investigation of the rotational hydraulic motor losses and energy efficiency, used in the scientific research and in industrial practice, give incorrect results because:
   – losses and efficiencies are evaluated as functions of parameters which depend on those losses or which have no direct impact on the losses,
   – the mechanical, volumetric and pressure losses and the corresponding efficiencies are presented as directly dependent on the same parameters, although each of those losses is a function of different parameters and is a different function of the working fluid viscosity ν.

2. In the investigations of the hydraulic motor (pump and a hydrostatic transmission system) losses and energy efficiency it is necessary to use as a guide the diagram of the direction of increasing power stream from the hydraulic motor shaft to the pump shaft.

3. The complex method of evaluation of the motor overall efficiency $\eta_M = f(M_M, n_M, \nu)$ as a product $\eta_{Mm} \eta_{Mv} \eta_{Mp}$ of three efficiencies correctly described by the characteristics of mechanical efficiency $\eta_{Mm} = f(M_M, n_M, \nu)$, volumetric efficiency $\eta_{Mv} = f(\Delta p_{Mi}, n_M, \nu)$ and pressure efficiency $\eta_{Mp} = f(\Delta p_{Mi}, Q_M, \nu)$ should be replaced by a method of evaluation of the motor efficiency based on the defined coefficients k_i of the motor and the motor driving system energy losses. The proposed motor efficiency evaluation is performed as a part of the energy efficiency evaluation of the hydrostatic driving system where the motor is used.

4. The evaluation method of the hydraulic motor (and also of the pump and of the hydrostatic driving system) energy efficiency is based on the mathematical models of losses where each type of losses is a function of parameters influencing directly the losses and independent of those losses.
   Evaluated are the loss coefficients k_i relating the hydraulic motor (pump and system) mechanical, volumetric and pressure losses to the reference values: driving system nominal pressure p_n, pump theoretical capacity Q_{Pt}, motor theoretical rotational speed n_{Mt} and theoretical torque M_{Mt}. The loss coefficient k_i are determined at the working fluid reference viscosity ν_n. Also the impact is determined of the

viscosity ratio ν/ν_n (viscosity changing in the $\nu_{min} \leq \nu \leq \nu_{max}$ range) on the value of loss coefficients k_i.
The method allows to evaluate the values and proportions of mechanical, volumetric and pressure losses in the motor (pump, driving system) and their dependence on the fluid viscosity ν.
The knowledge of coefficients k_i of the mechanical, volumetric and pressure losses allows to obtain, by applying a numerical method, a picture of the overall efficiency $\eta_M = f(\overline{\omega}_M, \overline{M}_M)$ of the motor (pump and system) in the $(0 \leq \overline{\omega}_M \langle \overline{\omega}_{Mmax}, \ 0 \leq \overline{M}_M \langle \overline{M}_{Mmax})$ motor operating field and for the selected ratio ν/ν_n of fluid viscosity.
Simultaneously, the $(0 \leq \overline{\omega}_M \langle \overline{\omega}_{Mmax}, \ 0 \leq \overline{M}_M \langle \overline{M}_{Mmax})$ motor (pump and system) operating field is determined for a selected ν/ν_n ratio of the working fluid viscosity to the reference viscosity.
It is assumed that the method is precise and simple in use. It reduces the necessary laboratory investigations of pumps and hydraulic motors. Il allows to seek energy saving displacement machine designs. It also allows to evaluate the drive energy efficiency and to seek energy saving structures of hydrostatic transmission systems.

BIBLIOGRAPHY

1. Paszota Z.: *Graphical presentation of the power of energy losses and power developed in the elements of hydrostatic drive and control system. Part I – Rotational hydraulic motor speed series throttling control systems*. Chapter in the monograph: „*Research, design, production and operation of hydraulic systems*" (in Polish), Adam Klich, Edward Palczak and Andrzej Meder editors. „Cylinder" Library. Komag Mining Mechanisation Centre, Gliwice 2008

2. Paszota Z.: *Graphical presentation of the power of energy losses and power developed in the elements of hydrostatic drive and control system. Part II – Rotational hydraulic motor speed parallel throttling control and volumetric control systems*. Chapter in the monograph: „*Research, design, production and operation of hydraulic systems*" (in Polish), Adam Klich, Edward Palczak and Andrzej Meder editors. „Cylinder" Library. Komag Mining Mechanisation Centre, Gliwice 2008

3. Paszota Z.: *Direction of increase of power stream in the hydrostatic drive and control system. Graphical presentation of the power of energy losses and power developed in the elements of hydrostatic drive and control system. Part I – Rotational hydraulic motor speed series throttling control systems*. (in Polish), Napędy i sterowanie, scientific monthly, No 10 (114), October 2008

4. Paszota Z.: *Direction of increase of power stream in the hydrostatic drive and control system. Graphical presentation of the power of energy losses and power developed in the elements of hydrostatic drive and control system. Part II – Rotational hydraulic motor speed parallel throttling control and volumetric control systems*. (in Polish), Napędy i sterowanie, scientific monthly, No 11 (115), November 2008

5. Paszota Z.: *Graphical presentation of the power of energy losses and power developed in the elements of hydrostatic drive and control system. Part I – Rotational hydraulic motor speed series throttling control systems*. Polish Maritime Research 03/2008

6. Paszota Z.: *Graphical presentation of the power of energy losses and power developed in the elements of hydrostatic drive and control system. Part II – Rotational hydraulic motor speed parallel throttling control and volumetric control systems*. Polish Maritime Research 04/2008

7. Paszota Z.: *The operating field of a hydrostatic drive system*. Chapter in the monograph: „*Research, design, production and operation of hydraulic systems*" (in Polish), Adam Klich, Antoni Kozieł and Edward Palczak editors. „Cylinder" Library. Komag Mining Mechanisation Centre, Gliwice 2009

8. Paszota Z.: *Parameters of the energy efficiency investigations of pumps and hydraulic motors. The operating field of a hydrostatic drive system*. (in Polish), Napędy i sterowanie, scientific monthly, No 11 (127), November 2009

9. Paszota Z.: *The operating field of a hydrostatic drive system parameters of the energy efficiency investigations of pumps and hydraulic motors*. Polish Maritime Research 04 / 2009

10. Technical matter of the Hägglunds Company: Product Manual VIKING EN397-3a 1999

11. Technical matter of the Bosch Rexroth AG Company: RE 91 604/06.03 I AGVM

12. Technical matter of the Parker Hannifin Company: Catalogue HY30-8223/UK

13. Technical matter of the SAUER DANFOSS Company: Technical Information 520L0440·Rev AD·Dec 2009

14. Technical matter of the LABORATOIRE HYDRO LEDUC Company: Efficiency M series motors

---

CONTACT WITH THE AUTHOR

Prof. Zygmunt Paszota
Faculty of Ocean Engineering
and Ship Technology
Gdansk University of Technology
Narutowicza 11/12
80-233 Gdansk, POLAND
e-mail: zpaszota@pg.gda.pl

Assessing the applicability of new refrigerants in marine cooling systems

Bogusław Zakrzewski, Assoc. Prof.
Tomasz Łokietek, Ph.D.
West Pomeranian University of Technology, Szczecin

ABSTRACT

The article assesses the applicability of new refrigerants, being possible substitution for Freon 22, in marine refrigeration and air-conditioning systems. A collection of technical data on the physical properties of the new refrigerants is presented. Suggestions are made about certain energetic and ecological profits which can be gained when using energetically efficient refrigerants with low GWP values. The results of the TEWI comparison analysis for selected refrigerants are also included.

Keywords: TEWI, ODP, GWP, heat pump, air conditioning, cooling installations, refrigerant, R22 substitute, energetic efficiency, R41, R152a, R218, R227ea, RC318, R600a, R290, R1270

INTRODUCTION

The applicability of the refrigerants R41, R152a, R218, R227ea, RC318, R600a, R290, and R1270 in cooling installations was analysed based on the assessment of the use of these substances in the heat pump cycle, for devices operating in the heating mode. The medium used in the reference heat pump installation was R22, due to its favourable thermodynamic properties, along with low energy consumption of the devices filled with this medium. Indeed, many substances which are used as substitutes for Freon 22 reveal higher energy consumption and GWP. The main criterion used for assessing the applicability of the substances, referred to as refrigerants – refrigerating media, is their influence on the environment. The Carnot cycle is considered here the reference for real cycles realised using the media being homogeneous substances, such as Freon R22 and its substitutes.

ECOLOGICAL CRITERIA FOR THE SELECTION OF REFRIGERANTS

Present tendencies in manufacturing of the cooling devices and installations are closely connected with the use of new effective refrigerants. These refrigerants should also meet the requirements concerning atmosphere protection [4]. Ecological problems with the use of older refrigerants have led to the situation in which the chemical industry offers a large and still growing number of new substances, with a guaranty of their favourable thermal, flow and ecological characteristics. Unfortunately, we cannot be sure that no unexpected and

unfavourable phenomena will be observed in the future, some time after these substances start being practically used [4]. In the Annex to the standard PN-EN 378 [3] the majority of the new refrigerants are taken into account, including criteria of the assessment of their influence on the environment.

We all are aware that the Earth's atmosphere should be protected. It was particularly evident for the signatories of the "Montreal Protocol" of 1987, as a consequence of the increasing area of holes in the ozone layer in previous years. Consequently, the signatories agreed on substantial reduction of the emission of CFCs until 2000. Poland signed and ratified the Montreal Protocol in 1990, and in 1996 the Act No. 176 was adopted according to which Republic of Poland signs the London and Copenhagen Annex to the Montreal Protocol. Initially, the negative effect of the halogen derivative compounds to the Earth's atmosphere was described by two coefficients. The first is the Ozone Depletion Potential, ODP, which characterizes the effect of a substance on the intensity of ozone decomposition, while the second is the newly introduced GWP (Global Warming Potential) factor, calculated in the relation to CO_2 for which it is equal to 1 (Tab. 1). The carbon dioxide reveals a relatively low potential for creating the greenhouse effect, but its amounts emitted to the atmosphere are so huge that they contribute in about 50% to this effect. On the other hand, despite their small volumetric proportions in the atmosphere, vestigial gases, such as methane and halogen derivative compounds of CFC and HFC type, contribute in nearly 20% to the creation of this phenomenon [4]. Unfortunately for many Freon 12 and Freon 22 substitutes, which are expected to be safe for the ozone layer, reveal high GWP values, close to those revealed

by the withdrawn Freons. The GWP value is estimated for the time of 100 years, as the stability of the existence of the given substance in the atmosphere is to be taken into account.

The sole information about GWP of the refrigerants turned out insufficient, as it did not take into account differences in the amount of driving energy consumed by the devices working with different substances. That is why the new factor includes the total level of CO_2 "emission" taking also into account refrigerant losses and the energy used for driving the device. The energy consumed for driving the cooling devices leads to the emission of CO_2, the amount of which depends on the energy source. For instance, the combustion of different fuels generates different volumes of CO_2. Also when the energy is generated without combustion, we will obtain different values

Tab. 1. ODP and GWP factors describing ecological threat of selected refrigerants to the environment [3]

Item	Name of substance	Refrigerant	Chemical formula	ODP value (R11 = 1)	GWP value (C0$_2$ = 1, 100-years period)
1	Chlorodifluoromethane	R22	CHF_2Cl	0.06	1700
2	Fluoromethane	R41	CHF_3	0.00	97
3	1,1-difluroethane	R152a	$C_2H_4F_2$	0.00	140
4	1,1,1,2,3,3,3-Heptafluoropropane	R227ea	C_3HF_7	0.00	2900
5	Octofluoropropane	R218	C_3F_8	0.00	7000
6	Octofluorocyclobutane	RC318	C_4F_8	0.00	8700
7	2-metylopropane	R600a	C_4H_{10}	0.00	3
8	Propane	R290	C_3H_8	0.00	3
9	Propylene	R1270	C_3H_6	0.00	3

Tab. 2. Physicochemical properties of selected refrigerants [7]

Item	Refrigerant	R22	R41	R152a	R218	R227ea	RC318	R600a	R290	R1270
1	Molecular weight [g/mol]	86.468	34.033	66.051	188.02	170.03	200.03	58.122	44.096	42.08
2	Freezing point [°C]	-157.42	-143.33	-118.59	-160.15	-126.8	-39.8	-159.59	-187.67	-185.2
3	Boiling point [°C]	-40.81	-78.123	-24.023	-36.83	-16.45	-5.975	-11.67	-42.09	-47.69
4	Density of liquid (25°C) [kg/m³]	1190.7	574.26	899.47	1325.7	1388.9	1498.3	549.86	492.08	504.47
5	Density of vapour (25°C. 1.013bar) [kg/m³]	3.5859	1.4027	2.7583	7.8513	7.1423	8.4270	2.4396	1.8314	1.7443
6	Critical temperature [°C]	96.145	44.13	113.26	71.95	101.65	115.23	134.67	96.675	92.42
7	Critical pressure [MPa]	4.99	5.897	4.5168	2.671	2.926	2.7775	3.64	4.2471	4.6646
8	Critical density [kg/m³]	523.84	316.51	368	627.98	573	619.97	224.35	218.5	223.39
9	Heat of vaporisation (1.013bar) [kJ/kg]	233.75	488.82	329.92	105.20	131.42	116.75	365.95	425.83	439.16
10	Thermal conductivity of liquid (25°C) [mW/mK]	83.479	115.25	97.975	44.753	59.402	65.136	88.998	93.621	110.70
11	Thermal conductivity of vapour (1.013bar) [mW/mK]	7.0475	10.120	9.4093	8.1634	10.415	10.212	13.208	11.570	10.576
12	Specific heat of liquid (25°C) [kJ/kgK]	C_p = 1.2568 C_V = 0.69086	C_p = 3.7343 C_V = 1.2560	C_p = 1.8 C_V = 1.1379	C_p = 1.16910 C_V = 0.79750	C_p = 1.1748 C_V = 0.82591	C_p = 1.1135 C_V = 0.80403	C_p = 2.4502 C_V = 1.7007	C_p = 2.7367 C_V = 1.6667	C_p = 2.6701 C_V = 1.5521
13	Specific heat of vapour (1.013bar) [kJ/kgK]	C_p = 0.60629 C_V = 0.49043	C_p = 1.1865 C_V = 0.85355	C_p = 0.97657 C_V = 0.81640	C_p = 0.70620 C_V = 0.64870	C_p = 0.76641 C_V = 0.70035	C_p = 0.74488 C_V = 0.69390	C_p = 1.5583 C_V = 1.3817	C_p = 1.4610 C_V = 1.2333	C_p = 1.3210 C_V = 1.0904
14	Viscosity of liquid (25°C) [µPa s]	164.39	77.997	163.16	166.92	239.46	362.88	150.16	96.948	94.479
15	Viscosity of vapour (1.013bar) [µPa s]	9.6967	7.0552	9.4093	9.7823	9.9046	10.230	6.5810	6.3092	6.3554
16	Cp/Cv (vapour) [25°C. 1.013bar]	1.1847	1.2927	1.1549	1.0655	1.0150	1.0642	1.1053	1.1359	1.1569

of the factor describing the volume of the produced carbon dioxide [kg CO_2/1kWh]. Its assumed values are the following: burned coal z = 1.12; fuel oil z = 0.94; natural gas z = 0.57; wind, water and nuclear power plants z = 0.00. For Poland it is assumed that z ~ 0.7 – 0.8 [4].

Analysing different solutions and refrigerants used for instance in marine cooling installations we can assess the TEWI (Total Equivalent Warming Impact) factor for them and select those revealing its lowest values.

Cooling installations and/or heat pumps contribute to the creation of the greenhouse effect, mostly in an indirect way via CO_2 emission connected with the production of the energy used by their driving systems. Since this energy is most frequently generated in Europe in electric power plants in which mineral fuel is burned, each kilowatt hour of the electric power is connected with the approximate emission of 0.4 ÷ 1.2 kg of CO_2 to the atmosphere, depending on a country.

In this way, the consumption of the driving energy by the cooling system contributes to the creation of the greenhouse effect during the entire time of system operation. Consequently, we should attempt not only to use substances revealing low GWP, which reduces part connected with the emission, but also tend to obtain the highest possible thermodynamic efficiency. An important feature of the present pro-ecological solutions is the use of highly effective compressors, fans, pumps, or other subsystems of the cooling systems or heat pumps.

For simplicity purposes, it was assumed in the present analysis that the installations are identically filled with the medium and the level of leakage is in constant proportion to the installation filling. In practice, leakage flows of the refrigerant are different for different devices and substances, and the risk of their appearance is especially high in cooling installations which are spread over a large area.

A high worldwide effort is made to reduce the emission of greenhouse gases, as a result of which some legal regulations were adopted. Since 2007, on the EU territory the Directive [6] on some fluorinated greenhouse gases is in force, which imposes severe limits to be complied with in the cooling and air conditioning engineering. (Directive no 842/2006 of May 17, 2006, Polish text published in the EU Official Journal No. L161/ of June 14, 2006).

The Total Equivalent Warming Impact (TEWI) factor is calculated from the formula [3]:

$$TEWI = GWP \cdot L \cdot n + GWP \cdot m \cdot (1\text{-}f) + n \cdot E \cdot z$$

where:
GWP - Global Warming Potential, in relation to CO_2 [-]
L   - amount of the substance emitted to the atmosphere [kg/year]
n   - device's operating time [years]
m   - amount of the refrigerant in the installation [kg]
f   - dimensionless number assessing the recovery ratio [-]
E   - energy consumed by the device in one year (E = t_R N), [kWh]
z   - CO_2 emission divided by the scaling energy unit [kgCO_2/kWh]
N   - heat pump driving power [kW]
t_R - annual time of operation [h].

Sample TEWI calculation for a heat pump

For comparison purposes, the TEWI factor for the heat pump installation was calculated taking into account the following refrigerants: R22, R41, R152a, R218, R227ea, RC318, R600a, R290, and R1270. The operating parameters and technical data of the installation were the following: mass

of refrigerant in the installation m = 5kg, annual emission of the substance L = 1kg, operating time of the installation n = 15 years, annual time of operation t_R = 6000 h, medium recovery ratio f = 0.5, heating power of the heat pump Q_{pc} = 25kW, z = 0.94 kg CO_2/kWh. The assumed identical filling of the installation and similar emission in case of each refrigerant are some simplification of the real situation.

The calculations of a single-stage cycle with SLHE (suction-liquid line heat exchanger) were performed based on the assumptions collected in Tab. 3. The analysed refrigeration cycle is shown in Fig. 1.
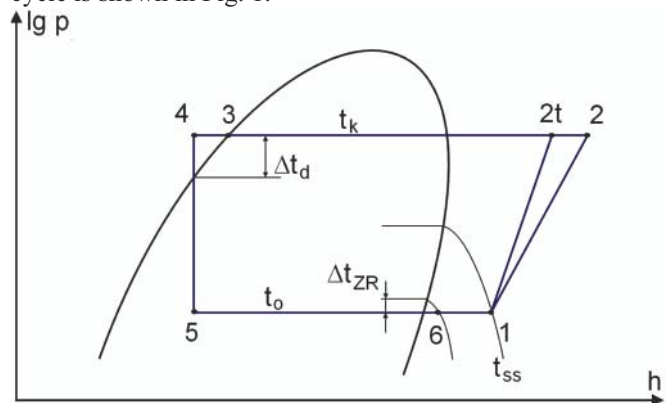
Fig. 1. Single-stage cycle with SLHE in the lgp-h diagram: t_o – evaporation temperature, t_k – condensation temperature, Δt_{ZR} – superheating of vapour in the evaporator, Δt_d – extra cooling of liquid in extra cooler, t_{ss} - temperature of vapour at compressor's suction side

***Tab. 3.** Initial calculation data*

Data of calculation	
Evaporation temperature t_o [°C]	2
Condensation temperature t_k [°C]	40
Superheating of vapour in the evaporator Δt_{ZR} [K]	4
Sub-cooling of liquid in the SLHE Δt_d [K]	Resulting from SLHE efficiency 0.80
Temperature of vapour at compressor suction side t_{ss} [°C]	20
SLHE efficiency η_{WR} [-]	0.8
Isentropic efficiency of compression η_{iz} [-]	0.85
Compressor's mechanical efficiency η_m [-]	0.9

Tab. 4 collects the results of the TEWI calculations for the following refrigerants: R41, R152a, R218, R227ea, RC318, R600a, R290, R1270 and R22.

Fig. 2 shows the relative TEWI factor calculated for the refrigerants: R41, R152a, R218, R-227ea, RC318, R600a, R290 and R1270, taking R22 (100%) as the reference. After assuming identical conditions for: the heating power, filling of the installation with the medium, the scale of leakage, and the operating time, the calculations have led to nearly 21% reduction of the TEWI factor for **R600a** compared to R22. The second favourable refrigerant was R152a, which revealed the TEWI factor lower by 19% than R22. Similar TEWI results were also obtained for the refrigerants R290 and R1270, for which TEWI decrease amounted to 18 and 17%, respectively.

Refrigerant	q_k [kJ/kg]	m [kg/s]	N [kW]	COP	GWP*L*n	GWP*m*(1-f)	n*E*z	TEWI [kgCO$_2$]
R41*	319.9	0.078	5.67	4.41	1 455	242.5	479 414	481 112
R152a	319.0	0.078	4.32	5.78	2 100	350	365 774	368 224
R218	83.7	0.299	4.60	5.44	105 000	17 500	389 140	511 640
R227ea	121.7	0.205	4.32	5.79	43 500	7 250	365 434	416 184
RC318**	111.7	0.224	4.29	5.82	130 500	21 750	363 136	515 386
R22	211.6	0.118	4.46	5.60	25 500	4 250	377 465	407 215
R600a	364.98	0.0685	4.22	5.93	45	7.5	356 777	356 829
R290	381.89	0.0655	4.39	5.69	45	7.5	371 752	371 805
R1270	385.3	0.065	4.46	5.60	45	7.5	377 643	377 696

* - not mentioned in the list in prPN-EN 378, ** - missing safety group in Table E1 in prPN-EN 378 -1
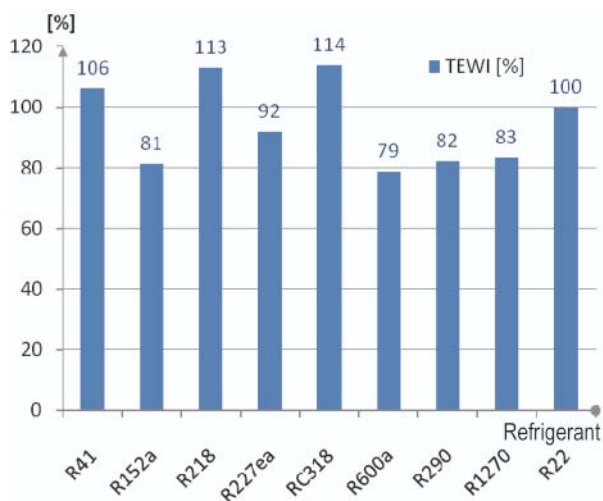
Fig. 2. *Total heat pump TEWI factor for refrigerants: R41, R152a, R218, R-227ea, RC318, R600a, R290, R1270 and R22*
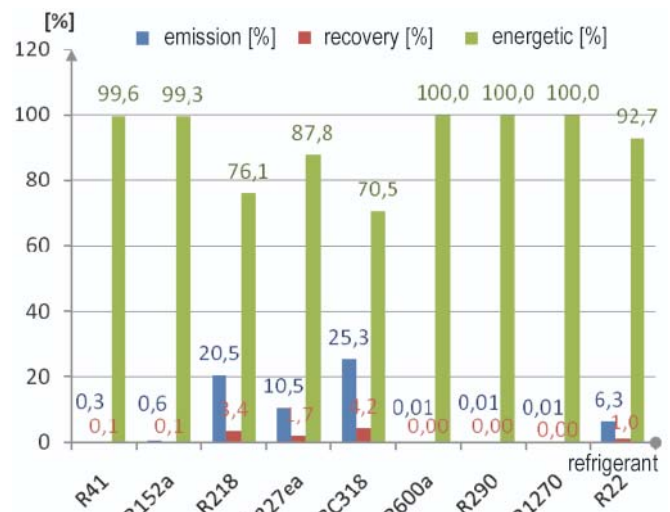
Fig. 3. *TEWI components for R41, R152a, R218, R-227ea, RC318, R600a, R290, R1270 and R22*

The last favourable result in this group was the refrigerant R227ea which revealed lower TEWI by 8%. The remaining refrigerants have higher TEWI values: R41 by 6%, R218 by 13%, and RC318 by 14 % with respect to the referential TEWI factor of R22.

Fig. 3 shows that the proportion of the energetic component in the TEWI factor amounts to 100% for R600a, R290 and R1270, 99.6% for R41, and 99.3 % for R-152a. In those cases the emission and recovery components do not exist or are negligibly small, below 1% of the total TEWI value. For the remaining refrigerants the emission component and the recovery component contribute to a much larger extent: 29.5 % for RC318, 23,9 % for R218, and 12.2% for R227ea.

COMBUSTIBILITY OF REFRIGERANTS

It has been known [2] that the refrigerants R218 and R-227ea are not combustible under the atmospheric pressure and in temperatures not exceeding 80°C (except R152a). However, the tests [5] have also proved that even R22 becomes combustible at the pressure exceeding 5,15 bar and in regular ambient temperature when it mixes with the air to the concentration equal to or higher than 65 per cent. Consequently,

these substances should be used in the way protecting against the creation of air mixtures, during leakage examination, for instance. In general, we should not accept conditions for possible creation of such high-concentration mixtures at pressures exceeding the atmospheric pressure.

The refrigerants R600a, R290 and R1270 belong to the group of media revealing increased combustibility (the lower combustibility limit is lower than 3.5% of the volumetric concentration in air). Moreover, R152a is a combustible medium, which was proved in relevant tests. At lower temperatures, higher pressure is required for the refrigerant to become combustible. That is why these refrigerants should not be mixed with air to examine the leakage flows. The problem of combustibility of the refrigerants and the resultant demand for relevant protection of the installation is an important, but fully realisable issue. It is also noteworthy that R717 (NH$_3$) is in common use in land cold stores, and even in marine refrigeration plants, despite their health threat and combustibility in certain mixtures with air.

Below given is the classification of the refrigerants R41, R152a, R218, R-227ea, RC318, R600a, R290 and R1270 with the reference to the safety groups of these substances according to prPN-EN 378-1 [3]

Tab. 5. *Classification of selected refrigerants by safety group (Annex E to prPN-EN 378-1)*

Refrigerant	Safety group (PN-EN-378)	Fluid group according to PED	Practical concentration limit[1] (kg/m^3)	ATEL/ODL[2] (kg/m^3)	Combustibility LFL[3] (kg/m^3)	Self-ignition temperature (°C)
R41	4	4	4	4	4	4
R152a	A2	1	0.026	0.14	0.13	455
R218	A1	2	0.44	0.44	-	-
R227ea	A1	2	0.49	0.49	-	-
RC318	4	2	0.81	0.81	-	-
R600a	A3	1	0.0086	0.06	0.043	460
R290	A3	1	0.008	0.09	0.038	470
R1270	A3	1	0.008	0.10	0.040	455

1 - lower combustibility limit,

2 - acute toxicity exposure limit ATEL or oxygen defect limit ODL,

3 - lower combustibility limit ,

4 - missing data (according to PN-EN 378, the standard does not refer to substances without attributed safety group)

CONCLUSIONS

The obtained results reveal that differences up to 35% can be obtained when calculating the TEWI factor for a heat pump with different media used by it. Therefore this factor can be considered an applicable and relatively simple criterion for assessing the performance of refrigerators or heat pumps. The refrigerants which occupy top ranks in this analysis are: **R600a, R152a, R290, R1270 and R227ea**; the results of their comparison are better than those obtained for R22. According to [1], R152a is a long-term substitute for R12 and R22; while R600a is a long-term substitute for R12, and R290 and R1270 are long-term substitutes for R22 and R502.

1. Unfortunately, despite their good properties for air conditioning, wider use of R600a, R152a, R290, and R1270 is limited because of their high combustibility (R152a - group A2, remaining – group A3). These media have a very low TEWI factor, which suggests that they are likely to be used in individual design solutions.

   The problem of protection against the danger resulting from their high combustibility can be solved in many cases using relatively simple design means without excessive rise of costs. In this case controlling the filling of the installation is necessary (it should be done following the regulations of the standard PN-EN 378-1 Annex C, C3). When the device is situated in the open area, it does not create serious threat. R717 (NH_3) is used in land cold stores and marine refrigeration plants.

2. The use of R227ea is also a correct choice, as its TEWI factor is relatively low. However, high value of the GWP factor, equalling 2900, may result, in the future, in prohibition of the use of this medium [6].

3. Refrigerants R41, R218, RC318 are less favourable taking into account the TEWI values. They also have low value of the cycle performance, COP. Another disadvantage of R41 is very low critical temperature, equalling to 44.5°C. Moreover, there are no data on the safety group (the medium is not classified in the standard worked out in 2009!), which may suggest that no company submitted it for classification, or there are no relevant tests to allow this medium to be used. The data are also missing on the safety group for RC318.

4. R218 and RC318 reveal high TEWI factors, they are also the substances with high GWP factor ($GWP_{R218} = 7000$, $GWP_{RC318} = 8700$), which practically eliminates them from wider use.

BIBLIOGRAPHY

1. Bitzer: *Refrigerants*. Report. Issue 15 (in Polish). A-501-15PL
2. Bonca Z., Butrymowicz D., Hajduk T., Targański W.: *New refrigerants and coolants*. Handbook (in Polish). IPPU Masta. Gdansk, 2004
3. PN-EN 378: *Refrigerating installations and heat pumps. Requirements concerning safety and environment protection* (in Polish)
4. Maczek K.: *Conditions for applications of refrigerators and heat pumps* (in Polish). Chłodnictwo, no. 3, 2000
5. Farbwerke Hoechst AG Frigen-Informationsdienst: *Frigen 22 - Fibel für die Kälte und Klimatechnik*, 1972
6. European Parliament and Council directive 842/2006 of May 17, 2006, on some fluorinated greenhouse gases
7. REFPROP, *Reference Fluid Thermodynamic and Transport Properties*. NIST Standard Reference Database 23, Version 7.0. E.W. Lemmon, M.O. McLinden, M.L. Huber. USA, 2002.

CONTACT WITH THE AUTHORS
Boguslaw Zakrzewski, Assoc. Prof.
Tomasz Lokietek, Ph.D.
West Pomeranian University of Technology, Szczecin
Faculty of Marine Technology
Al. Piastow 41
71-065 Szczecin, POLAND
e-mail: boguslaw.zakrzewski@zut.edu.pl

Problems of welding in shipbuilding - an analytic-numerical assessment of the thermal cycle in HAZ with three dimensional heat source models in agreement with modelling rules

Part II
An analytical assessment of thermal cycle by used C-I-N and D-E heat sources models

Eugeniusz Ranatowski, Prof
University of Technology and Life Science, Bydgoszcz

ABSTRACT

This part is continuation of PART I. The basis of this analytic solution are the Fourier - Kirchhoff partial differential equation with appropriated boundary conditions. For a plate with optional thickness, the radiative heat transfer on both surfaces is taken into account. It is assumed that moving C-I-N or D-E heat sources during a very short period of time, generate an impulse of energy inducing an instantaneous thermal field in the plate area and the analytic solution is received by used Fourier transformation. These fields are being continuously summed up to obtain resultant thermal field $\left(T = \int_0^t dT(t')\right)$. Finally, the temperature fields generated by C-I-N and D-E heat sources in both stationary and moving co-ordinates systems are established.

Keywords: welding; shipbuilding; welding in shipbuilding; thermal cycle; heat affected zone; heat source model

LINEAR ANALYTICAL HEAT FLOW SOLUTION FOR A PLATE WITH OPTIONAL THICKNESS AND RADIATIVE HEAT TRANSFER ON SURFACES BY C-I-N HEAT SOURCE MODEL

Energy heat transport in HAZ is mainly progressed by thermal conduction and can be described by F–K partial differential equation.

Here is the way how the solution for temporary temperature fields is received. The integral transformation method is being used.

HS power input in volume showed by eq. (12) – part I in impulse form is described as:

$$q_v = \frac{Q \cdot \delta(t)}{\pi \cdot [1 - \exp(-K_z \cdot s)]} \cdot k \cdot K_z \cdot$$
$$\cdot \exp[-k(x^2 + y^2) - K_z \cdot z] \cdot [1 - u(z - s)] \tag{1}$$

or

$$q_v = q_{vMAX} \cdot \delta(t) \cdot$$
$$\cdot \exp[-k(x_0^2 + y_0^2) - K_z \cdot z_0] \cdot [1 - u(z - s)] \tag{2}$$

Putting it into F-K equation the following form is received[1]:

$$\frac{\partial^2 T}{\partial x_0^2} + \frac{\partial^2 T}{\partial y_0^2} + \frac{\partial^2 T}{\partial z_0^2} + \frac{q_{vMAX} \cdot \delta(t)}{\lambda} \cdot$$
$$\cdot [1 - u(z - s)] \cdot \exp[-k(x_0^2 + y_0^2) - K_z \cdot z_0] = \frac{1}{a} \frac{\partial T}{\partial t} \tag{3}$$

Boundary conditions:

$$T(x_0, y_0, z_0, t = 0) = T_0 = 0 \tag{3a}$$

$$\frac{\partial T}{\partial x_0} = 0 \text{ when } x_0 \to \infty, x_0 \to -\infty \tag{3b}$$

$$\frac{\partial T}{\partial y_0} = 0 \text{ when } y_0 \to \infty, y_0 \to -\infty \tag{3c}$$

$$\lambda \cdot \frac{\partial T}{\partial z_0} = \alpha_0 \cdot T \text{ when } z_0 = 0 \tag{3d}$$

$$\lambda \cdot \frac{\partial T}{\partial z_0} = \alpha_0 \cdot T \text{ when } z_0 = g \tag{3e}$$

Graphic interpretation of the above conditions is shown in Fig. 1.
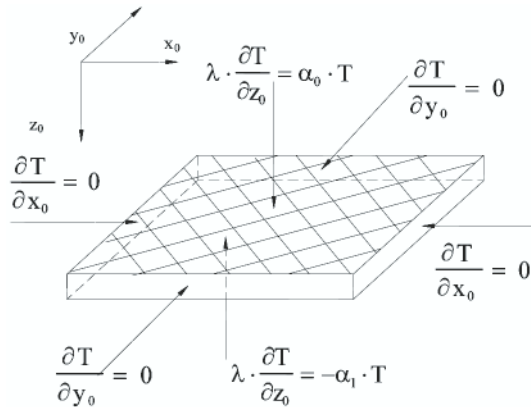
Fig. 1. *Graphic interpretation of boundary conditions*

The x_0, y_0 and z_0 variable transformations for equation (3) are executed with use the classic Fourier transformation. Transformation module for x_0 is described as[2]:

$$K(r, x_0) = \exp(i \cdot p \cdot x_0) \qquad (4)$$

The integration range is $(-\infty, +\infty)$. The equation (3) after multiplying by (4) looks like:

$$\int_{-\infty}^{+\infty} \frac{\partial^2 T}{\partial x_0^2} \cdot e^{i \cdot p \cdot x_0} dx_0 + \int_{-\infty}^{+\infty} \frac{\partial^2 T}{\partial y_0^2} \cdot e^{i \cdot p \cdot x_0} dx_0 +$$

$$+ \int_{-\infty}^{+\infty} \frac{\partial^2 T}{\partial z_0^2} \cdot e^{i \cdot p \cdot x_0} dx_0 + \int_{-\infty}^{+\infty} \frac{\partial^2 T}{\partial x_0^2} \cdot \frac{q_{vMAX} \cdot \delta(t)}{\lambda} \cdot \qquad (5)$$

$$\cdot [1 - u(z-s)] \cdot \exp[-k(x_0^2) - K_z \cdot z_0] dx_0 = \int_{-\infty}^{+\infty} \frac{1}{a} \frac{\partial T}{\partial t} \cdot dx_0$$

Transforming operation:

$$\int_{-\infty}^{+\infty} \frac{\partial^2 T}{\partial x_0^2} \cdot e^{i \cdot p \cdot x_0} dx_0 =$$

$$= \frac{\partial T}{\partial x_0} \cdot e^{i \cdot p \cdot x_0} \Big|_{-\infty}^{+\infty} - i \cdot p \cdot \int_{-\infty}^{+\infty} \frac{\partial T}{\partial x_0} \cdot e^{i \cdot p \cdot x_0} dx_0 =$$

$$= \frac{\partial T}{\partial x_0} \cdot e^{i \cdot p \cdot x_0} \Big|_{-\infty}^{+\infty} - i \cdot p \cdot \left(T \cdot e^{i \cdot p \cdot x_0} \Big|_{-\infty}^{+\infty} - i \cdot p \cdot \right.$$

$$\left. \cdot \int_{-\infty}^{+\infty} T \cdot e^{i \cdot p \cdot x_0} dx_0 \right) = \frac{\partial T}{\partial x_0} \cdot e^{i \cdot p \cdot x_0} \Big|_{x_0 = \infty} - \frac{\partial T}{\partial x_0} \cdot \qquad (5a)$$

$$\cdot e^{i \cdot p \cdot x_0} \Big|_{x_0 = -\infty} - i \cdot p \cdot T \cdot e^{i \cdot p \cdot x_0} \Big|_{x_0 = \infty} +$$

$$+ i \cdot p \cdot T \cdot e^{i \cdot p \cdot x_0} \Big|_{x_0 = -\infty} + i^2 \cdot p^2 \cdot$$

$$\cdot \int_{-\infty}^{+\infty} T \cdot e^{i \cdot p \cdot x_0} dx_0 = 0 - 0 - 0 + 0 +$$

$$+ (-p^2 \cdot \int_{-\infty}^{+\infty} T \cdot e^{i \cdot p \cdot x_0} dx_0) = -p^2 \cdot \overline{T}$$

Transforming operations for: y_0, z_0, and t variables.
These are obviously transformations for variables other than x_0, which simplifies the counting.

Therefore for y_0, z_0 variable we'll obtain

$$\int_{-\infty}^{+\infty} \frac{\partial^2 T}{\partial y_0^2} \cdot e^{i \cdot p \cdot x_0} dx_0 =$$

$$= \frac{\partial^2}{\partial y_0^2} \int_{-\infty}^{+\infty} T \cdot e^{i \cdot p \cdot x_0} dx_0 = \frac{\partial^2}{\partial y_0^2} \overline{T} \qquad (5b)$$

$$\int_{-\infty}^{+\infty} \frac{\partial^2 T}{\partial z_0^2} \cdot e^{i \cdot p \cdot x_0} dx_0 =$$

$$= \frac{\partial^2}{\partial z_0^2} \int_{-\infty}^{+\infty} T \cdot e^{i \cdot p \cdot x_0} dx_0 = \frac{\partial^2}{\partial z_0^2} \overline{T} \qquad (5c)$$

and for t variable:

$$\int_{-\infty}^{+\infty} \frac{\partial T}{\partial t} \cdot e^{i \cdot p \cdot x_0} dx_0 = \frac{\partial}{\partial t} \int_{-\infty}^{+\infty} T \cdot e^{i \cdot p \cdot x_0} dx_0 = \frac{\partial}{\partial t} \overline{T} \quad (5d)$$

Transforming operation for:

$$\frac{q_{vMAX} \cdot \delta(t)}{\lambda} \cdot [1 - u(z-s)] \cdot$$

$$\cdot \exp[-k(x_0^2 + y_0^2) - K_z \cdot z_0]$$

where:

$$q_{vMAX} = \frac{k \cdot K_z \cdot Q}{\pi \cdot [1 - \exp(-K_z \cdot s)]}$$

$$\int_{-\infty}^{+\infty} \frac{q_{vMAX} \cdot \delta(t)}{\lambda} \cdot [1 - u(z-s)] \cdot$$

$$\cdot \exp[-k(x_0^2 + y_0^2) - K_z \cdot z_0] \cdot e^{i \cdot p \cdot x_0} dx_0 =$$

$$= \sqrt{\frac{\pi}{k}} \frac{q_{vMAX} \cdot \delta(t)}{\lambda} \cdot [1 - u(z-s)] \cdot \qquad (5e)$$

$$\cdot \exp\left[-k(\frac{p^2}{4k} + y_0^2) - K_z \cdot z_0 \right]$$

and finally after first transformation the following is received:

$$-p^2 \cdot \overline{T} + \frac{\partial^2}{\partial y_0^2} \overline{T} + \frac{\partial^2}{\partial z_0^2} \overline{T} + \sqrt{\frac{\pi}{k}} \frac{q_{vMAX} \cdot \delta(t)}{\lambda} \cdot$$

$$\cdot [1 - u(z-s)] \cdot \exp\left[-k(\frac{p^2}{4k} + y_0^2) - K_z \cdot z_0 \right] = \frac{1}{a} \cdot \frac{\partial}{\partial t} \overline{T} \qquad (6)$$

Similarly like for x_0, this classic Fourier transformation we will use for y_0 transformation.
Transformation module for y_0 is described as:

$$K(r, y_0) = \exp(i \cdot p \cdot y_0) \qquad (7)$$

The integration range is $(-\infty, +\infty)$. The equation (6) after multiplying by (7) and transforming looks like:

$$-p^2 \cdot \overline{\overline{T}} - q^2 \cdot \overline{\overline{T}} + \frac{\partial^2 \overline{\overline{T}}}{\partial z_0^2} + \frac{q_{vMAX} \cdot \pi \cdot \delta(t)}{\lambda \cdot k} \cdot \qquad (8)$$

$$[1 - u(z-s)]) \exp\left(-\frac{p^2}{4 \cdot k} - \frac{q^2}{4 \cdot k} - K_z \cdot z_0 \right) = \frac{1}{a} \frac{\partial \overline{\overline{T}}}{\partial t}$$

Finally, transformation module for z_0 is described as:

$$K(r, z_0) = \cos(r \cdot z_0) + \frac{\alpha_0}{\lambda \cdot r} \cdot \sin(r \cdot z_0) \qquad (9)$$

Therefore:

$$-(p^2 + q^2 + r^2) \cdot \overline{\overline{\overline{T}}} + \int_0^g \frac{q_{vMAX} \cdot \pi \cdot \delta(t)}{\lambda \cdot k} \cdot$$

$$\cdot [1 - u(z - s)] \cdot \exp\left(-\frac{p^2}{4 \cdot k} - \frac{q^2}{4 \cdot k} - K_z \cdot z_0\right) \cdot \quad (10)$$

$$\cdot \cos(r \cdot z_0) + \frac{\alpha_0}{\lambda \cdot r} \cdot \sin(r \cdot z_0) dz_0 = \frac{1}{a} \frac{\partial \overline{\overline{\overline{T}}}}{\partial t}$$

and

$$-(p^2 + q^2 + r^2) \cdot \overline{\overline{\overline{T}}} + \int_0^g \frac{q_{vMAX} \cdot \pi \cdot \delta(t)}{\lambda \cdot k} \cdot$$

$$\cdot \exp\left(-\frac{p^2}{4 \cdot k} - \frac{q^2}{4 \cdot k} - K_z \cdot z_0\right) \cdot$$

$$\qquad (11)$$

$$\cdot \int_0^g \exp(-K_z \cdot z_0) \cdot \cos(r \cdot z_0) +$$

$$+ \frac{\alpha_0}{\lambda \cdot r} \cdot \sin(r \cdot z_0) dz_0 = \frac{1}{a} \frac{\partial \overline{\overline{\overline{T}}}}{\partial t}$$

Let's find:

$$\int_0^s \exp(-K_z \cdot z_0) \cdot \cos(r \cdot z_0) + \frac{\alpha_0}{\lambda \cdot r} \cdot$$

$$\qquad (12)$$

$$\cdot \sin(r \cdot z_0) dz_0 = D$$

$$D = \exp(-K_z \cdot s) \cdot$$

$$\cdot \frac{-K_z \cdot \cos(r \cdot s) \cdot \lambda \cdot r + r^2 \cdot \sin(r \cdot s) \cdot}{(K_z^2 + r^2) \cdot \lambda \cdot r}$$

$$\qquad (12a)$$

$$\frac{\cdot \lambda - \alpha_0 r \cdot \cos(r \cdot s) - \alpha_0 K_z \cdot \sin(r \cdot s)}{1} + \frac{K_z \cdot \lambda + \alpha_0}{(K_z^2 + r^2) \cdot \lambda}$$

$r_1, r_2, r_3, ..., r_n$ are roots of :

$$\cot(r \cdot g) = \frac{\lambda^2 r^2 - \alpha_0 \alpha_1}{\lambda \cdot r \cdot (\alpha_0 + \alpha_1)} \qquad (12b)$$

So, the following is received:

$$-(p^2 + q^2 + r^2) \cdot \overline{\overline{\overline{T}}} + \frac{q_{vMAX} \cdot \pi \cdot \delta(t)}{\lambda \cdot k} \cdot$$

$$\cdot \exp\left(-\frac{p^2}{4 \cdot k} - \frac{q^2}{4 \cdot k}\right) \cdot D = \frac{1}{a} \frac{\partial \overline{\overline{\overline{T}}}}{\partial t}$$

$$\qquad (13)$$

The solution of (13) is Green function corresponding to differential operator:

$$\frac{d}{dt} + a \cdot (p^2 + q^2 + r^2)$$

The Green's functions solution is as follows:

$$\overline{\overline{\overline{T}}} = \frac{a \cdot Q \cdot K_z \cdot u(t)}{\lambda \cdot (1 - \exp(-K_z \cdot s))} \cdot \exp\left(-\frac{p^2}{4 \cdot k} - \frac{q^2}{4 \cdot k}\right) \cdot$$

$$\cdot D \cdot \exp[-a \cdot (p^2 + q^2 + r^2) \cdot t]$$

$$\qquad (14)$$

In order to obtain solution for T(x, y,z, t) - the reverse transformations must be provided.

At first, reverse transformations with specified modules for "x_0" and "y_0" will be executed.

The reverse transformations modules are as follows:

$$R(p, x_0) = \frac{1}{2\pi} \cdot \exp(-i \cdot p \cdot x_0) \qquad (15)$$

$$R(q, y_0) = \frac{1}{2\pi} \cdot \exp(-i \cdot q \cdot y_0) \qquad (16)$$

The integration range is $(-\infty, +\infty)$ for both: "p" and "q" variables.

In turn, the equation (14) after multiplying by (16) and "p" retransformation looks like:

$$\overline{\overline{T}} = \frac{a \cdot Q \cdot K_z \cdot u(t) \cdot D}{\sqrt{\pi} \cdot \lambda \cdot [1 - \exp(-K_z \cdot s)]} \cdot$$

$$\cdot \exp\left(-\frac{q^2}{4 \cdot k} - a \cdot (q^2 + r^2) \cdot t - \frac{x_0^2}{4 \cdot a \cdot t + 1}\right)$$

$$\qquad (17)$$

Then, the equation (17) after multiplying by (16) and "q" retransformation looks like:

$$\overline{T} = \frac{Q \cdot K_z \cdot k \cdot u(t)}{\pi \cdot c_\gamma \cdot (1 - \exp(-K_z \cdot s) \cdot (1 + 4 \cdot a \cdot t \cdot k)} \cdot$$

$$\cdot D \cdot \exp\left[-a \cdot r^2 \cdot t - \frac{k \cdot (x_0^2 + y_0^2)}{1 + 4 \cdot a \cdot t \cdot k}\right]$$

$$\qquad (18)$$

where:

$$c_\gamma = c_p \cdot \rho$$

The last transformation for "z_0" variable is defined as:

$$T = \sum_{i=1}^{\infty} \overline{T}_i R_i (r, z_0) \qquad (19)$$

with z_0 retransformation module:

$$R_i(r, z_0) = B_i \cdot C_i$$

and B_i, C_i, values are in agreement with (23a) and (23b).

Finally, HS impulse temperature field is:

$$T = \frac{Q \cdot K_z \cdot k \cdot u(t)}{\pi \cdot c_\gamma \cdot (1 - \exp(-K_z \cdot s) \cdot (1 + 4 \cdot a \cdot t \cdot k)} \cdot$$

$$\cdot \exp\left[-\frac{k \cdot (x_0^2 + y_0^2)}{1 + 4 \cdot a \cdot t \cdot k}\right] \cdot$$

$$\qquad (20)$$

$$\cdot \sum_{i=1}^{\infty} B_i C_i D_i \cdot \exp(-a \cdot r^2 \cdot t)$$

Total temperature distribution from moving HS can be achieved by summing HS impulse results on its movement path:

$$T(t) = \int_0^t dT(t') \qquad (21)$$

Therefore, in stationary co-ordinates system:

$$dT = \frac{Q \cdot K_z \cdot k \cdot u(t)}{\pi \cdot c_\gamma \cdot [1 - \exp(-K_z \cdot s) \cdot (1 + 4 \cdot a \cdot (t - t') \cdot k)]} \cdot$$

$$\cdot \exp\left[-\frac{k \cdot [(x_0 - v \cdot t')^2 + y_0^2]}{1 + 4 \cdot a \cdot (t - t') \cdot k}\right] \sum_{i=1}^{\infty} B_i \cdot C_i \cdot D_i \cdot \quad (22)$$

$$\cdot \exp(-a \cdot r^2 \cdot (t - t')$$

$$T = \int_0^t dt \frac{Q \cdot K_z \cdot k \cdot u(t)}{\pi \cdot c_\gamma \cdot [1 - \exp(-K_z \cdot s)] \cdot [1 + 4 \cdot a \cdot (t - t') \cdot k]} \cdot$$

$$\cdot \exp\left[-\frac{k \cdot [(x_0 - v \cdot t')^2 + y_0^2]}{1 + 4 \cdot a \cdot t \cdot k} \right] \cdot \sum_{i=1}^\infty B_i \cdot C_i \cdot D_i \cdot$$

$$\cdot \exp[-a \cdot r^2 \cdot (t - t')] \quad (23)$$

where:

$$B_i = \cos(r_i \cdot z_0) + \frac{\alpha_0}{\lambda \cdot r_i} \cdot \sin(r_i \cdot z_0) \quad (23a)$$

$$C_i = \frac{2 \cdot r_i^2}{\left(\frac{\alpha_0^2}{\lambda^2} + r_i^2 \right) \cdot \left(g + \frac{\alpha_1 \cdot \lambda}{\alpha_1^2 + r_i^2 \cdot \lambda^2} \right) + \frac{\alpha_0}{\lambda}} \quad (23b)$$

$$D_i = \exp(-K_z \cdot s) \cdot \frac{[-K_z \cdot \cos(r_i \cdot s) \cdot \lambda \cdot r_i + r_i^2 \cdot \sin(r_i \cdot s) \cdot}{(K_z^2 + r_i^2) \cdot \lambda \cdot r_i}$$

$$\frac{\cdot \lambda - \alpha_0 \cdot r_i \cdot \cos(r_i \cdot s) - \alpha_0 \cdot K_z \cdot \sin(r_i \cdot s)] \cdot}{1} + \quad (23c)$$

$$+ \frac{K_z \cdot \lambda + \alpha_0}{(K_z^2 + r_i^2) \cdot \lambda}$$

$r_1, r_2, r_3 \dots r_i$ are roots of :

$$ctg(r_i \cdot g) = \frac{\lambda^2 \cdot r_i^2 - \alpha_0 \cdot \alpha_1}{\lambda \cdot r_i \cdot (\alpha_0 + \alpha_1)} \quad (23d)$$

In moving co-ordinates system, $x = x_0 - vt$, $y = y_0$, $z = z_0$ (Fig. 1, part I):

$$T = \int_0^t dt \frac{Q \cdot K_z \cdot k \cdot u(t)}{\pi \cdot c_\gamma \cdot [1 - \exp(-K_z s)] \cdot [1 + 4 \cdot a \cdot (t - t') \cdot k]} \cdot$$

$$\cdot \exp\left[-\frac{k \cdot [(x + v \cdot (t - t'))^2) + y^2]}{1 + 4 \cdot a \cdot (t - t') \cdot k} \right] \cdot \quad (24)$$

$$\cdot \sum_{i=1}^\infty B_i C_i D_i \cdot \exp[-a \cdot r^2 \cdot (t - t')]$$

$$B_i = \cos(r_i \cdot z) + \frac{\alpha_0}{\lambda \cdot r_i} \cdot \sin(r_i \cdot z) \quad (24a)$$

where:
C_i, D_i, r_i - values are represented by same equations as for stationary system.

The equations (23), (24) for assessment of the temperature fields in both stationary and moving coordinates systems have far more extended form than classical analytical solution of Rosenthal-Rykalin. Certainly it results from accepted heat source model C-I-N and characterising it parameters like: Q, k, K_z, u(z–s). Furthermore, important elements of received solution are such parameters as: B_i, C_i, D_i. Their values also depend on such physical parameters as: λ, α, α_0 and roots r_i from equation (23d). However eq. (23), (24) have correct forms of solutions from mathematical and physical points of view but they have too compound mathematical form and they are hard for direct analytical account. Besides, analytical form of solution makes calculation impossible when taking into consideration non-linear form of thermal process under welding. So, above-mentioned affirmations make necessity of modification of analytical solution. This is possible through employment of hybrid analytical-numerical method. Present analytical form of solution defined by equations (23), (24) makes also impossible direct employment of numeric method for solution of these equations and assessment of the temperature fields.

LINEAR ANALYTICAL HEAT FLOW SOLUTION FOR PLATE WITH OPTIONAL THICKNESS AND RADIATIVE HEAT TRANSFER ON SURFACES BY USED D-E HEAT SOURCE MODEL

Similarly are estimated temperature fields for D-E heat source model but in a little complicated manner. At the beginning we must establish two partial differential heat flow equations for two different "quadrants" of another ellipsoids (Fig. 5, part I) at the same boundary conditions-equations (3a) ÷ (3e):
- $x > 0$, (Fig. 5, part I)

$$\frac{\partial^2 T}{\partial x_0^2} + \frac{\partial^2 T}{\partial y_0^2} + \frac{\partial^2 T}{\partial z_0^2} + \frac{q_v f_f}{\lambda} = \frac{1}{\alpha} \frac{\partial T}{\partial t} \quad (25a)$$

- $x < 0$, (fig. 5, part I)

$$\frac{\partial^2 T}{\partial x_0^2} + \frac{\partial^2 T}{\partial y_0^2} + \frac{\partial^2 T}{\partial z_0^2} + \frac{q_v f_r}{\lambda} = \frac{1}{\alpha} \frac{\partial T}{\partial t} \quad (25b)$$

In stationary coordinate system the x_o, y_o and z_o variable transformations for equations (25a), (25b) are executed in agreement with Fourier transformation as follows:
a. for variable x_0 with transformation module $K(p, x_0) = e^{-ipx_0}$ we will receive:
- $x_0 > 0$

$$-p^2 \overline{T} + \frac{\partial^2 \overline{T}}{\partial y_0^2} + \frac{\partial^2 \overline{T}}{\partial z_0^2} + \frac{6f_f \cdot Q \cdot \delta(t)}{\pi \lambda bc} \cdot$$

$$\cdot \exp\left(\frac{-3a_1^2 (y_0^2 c^2 + z_0^2 b^2)}{a_1^2 b^2 c^2} - \frac{p^2 a_1^2}{12} \right) = \frac{1}{\alpha} \frac{\partial \overline{T}}{\partial t} \quad (26a)$$

- $x_0 < 0$

$$-p^2 \overline{T} + \frac{\partial^2 \overline{T}}{\partial y_0^2} + \frac{\partial^2 \overline{T}}{\partial z_0^2} + \frac{6f_r \cdot Q \cdot \delta(t)}{\pi \lambda bc} \cdot$$

$$\cdot \exp\left(\frac{-3a_2^2 (y_0^2 c^2 + z_0^2 b^2)}{a_2^2 b^2 c^2} - \frac{p^2 a_2^2}{12} \right) = \frac{1}{\alpha} \frac{\partial \overline{T}}{\partial t} \quad (26b)$$

b. for variable y_0 with transformation module $K(p, x_0) = e^{-ipx_0}$ we will receive:
- for $x_0 > 0$

$$-p^2 \overline{\overline{T}} - q^2 \overline{\overline{T}} + \frac{\partial^2 \overline{\overline{T}}}{\partial z_0^2} + \frac{2\sqrt{3} f_f \cdot Q \cdot \delta(t)}{\sqrt{\pi} \lambda c} \cdot$$

$$\cdot \exp\left[-\frac{3z^2}{c^2} - \frac{1}{12} \left(p^2 a_1^2 + \frac{1}{12} q^2 b^2 \right) \right] = \frac{1}{\alpha} \frac{\partial \overline{\overline{T}}}{\partial t} \quad (27a)$$

- for $x_0 < 0$

$$-p^2 \overline{\overline{T}} - q^2 \overline{\overline{T}} + \frac{\partial^2 \overline{\overline{T}}}{\partial z_0^2} + \frac{2\sqrt{3} f_r \cdot Q \cdot \delta(t)}{\sqrt{\pi} \lambda c} \cdot$$

$$\cdot \exp\left[-\frac{3z_0^2}{c^2} - \frac{1}{12} (p^2 a_2^2 + q^2 b^2) \right] = \frac{1}{\alpha} \frac{\partial \overline{\overline{T}}}{\partial t} \quad (27b)$$

c. for variable z_0 with transformation module $K(r, z_0) = \cos r z_0 + \dfrac{\alpha_0}{\lambda r} \sin r z_0$ we will receive:

- for $x_0 > 0$

$$\overline{\overline{\overline{T}}}(-p^2 - q^2 - r^2) + \frac{2\sqrt{3} f_f \cdot Q \cdot \delta(t)}{\sqrt{\pi} \lambda c} \cdot$$

$$\exp\left[-\frac{1}{12}(p^2 a_1^2 + q^2 b^2) \right] \cdot \qquad (28a)$$

$$\cdot \int_0^g \left[\cos(r z_0) + \frac{\alpha_0}{\lambda r} \sin(r z_0) \right] \cdot e^{-\frac{3 z_0^2}{c^2}} dz_0 = \frac{1}{\alpha} \frac{\partial \overline{\overline{\overline{T}}}}{\partial t}$$

- for $x_0 < 0$

$$\overline{\overline{\overline{T}}}(-p^2 - q^2 - r^2) + \frac{2\sqrt{3} f_r \cdot Q \cdot \delta(t)}{\sqrt{\pi} \lambda c} \cdot$$

$$\cdot \exp\left[-\frac{1}{12}(p^2 a_2^2 + q^2 b^2) \right] \cdot$$

$$\cdot \int_0^g \left[\cos(r z_0) + \frac{\alpha_0}{\lambda r} \sin(r z_0) \right] \cdot e^{-\frac{3 z_0^2}{c^2}} dz_0 = \frac{1}{\alpha} \frac{\partial \overline{\overline{\overline{T}}}}{\partial t} \quad (28b)$$

During the Fourier transformation for the „z_0" variable it appears in eq. (28a) and (28b) the integral:

$$\int_0^g \left(\cos(r z_0) + \frac{\alpha_0}{\lambda r} \sin(r z_0) \right) \cdot \exp\left(-\frac{3 z_0^2}{c^2} \right) dz_0 \quad (29)$$

The above integral can't be solved immediately but an algorithm can be used to obtain a satisfactory approach. In order to obtain the solution, the function $\exp(-3 z_0^2/c^2)$ may be written[1]:

$$\exp\left(-\frac{3 z_0^2}{c^2} \right) = 1 + \sum_{n=1}^{nlast} \frac{\left(-\dfrac{3}{c^2} z^2 \right)^n}{\left[\displaystyle\prod_{n=1}^{m} (n) \right]} = \qquad (30)$$

$$= \mathrm{approx}(z, c, nlast)$$

In particular, nlast may be small when calculating for thin plates with quite large z-semi axis, see Fig. 2.
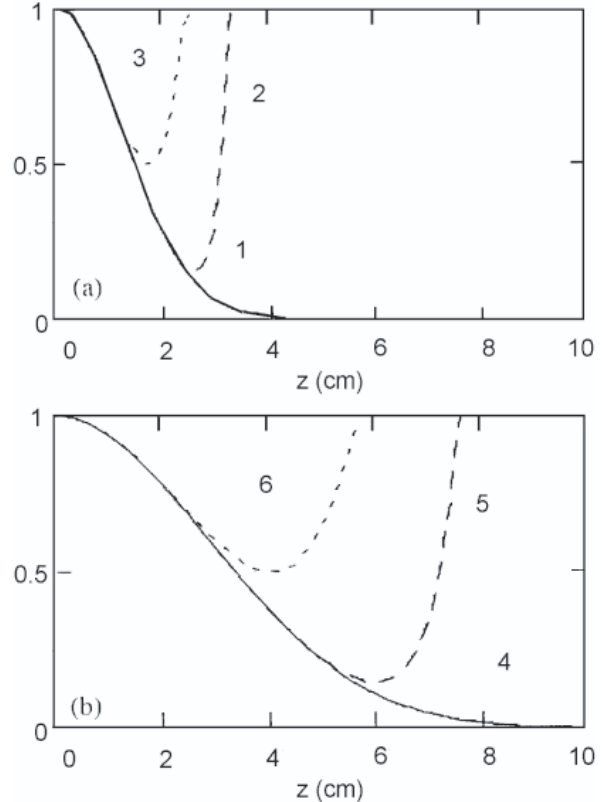
Fig. 2. Graphs representing convergence of exp(-3z²/c²) and its approx function (30) with various nlast and c values: **1.** exp(-3z²/c²), c = 3; **2.** approx(z, c, nlast), c = 3, nlast = 6; **3.** approx(z, c, nlast), c = 3, nlast = 2; **4.** approx(z, c, nlast), c = 7; **5.** approx(z, c, nlast), c = 3, nlast = 6; **6.** approx(z, c, nlast), c = 7, nlast = 2

In general, a source of given c and plates with large thickness, require a high nlast parameter which makes the whole calculation longer. For example, analysing a plate with thickness g = 5 cm, penetrated by a "double ellipsoid configuration of source" with c = 2 cm, the approx function must be used with nlast = 13 (or larger) and is equal to:

$$\mathrm{approx} = 1 - \frac{3}{c^2} \cdot z^2 + \frac{9}{(2 \cdot c^4)} \cdot z^4 - \frac{9}{(2 \cdot c^6)} \cdot z^6 + \frac{27}{(8 \cdot c^8)} \cdot z^8 - \frac{81}{(40 \cdot c^{10})} \cdot z^{10} \ldots +$$

$$+ \frac{81}{(80 \cdot c^{12})} \cdot z^{12} - \frac{243}{(560 \cdot c^{14})} \cdot z^{14} + \frac{729}{(4480 \cdot c^{16})} \cdot z^{16} - \frac{243}{(4480 \cdot c^{18})} \cdot z^{18} \ldots + \qquad (31)$$

$$+ \frac{729}{(44800 \cdot c^{20})} \cdot z^{20} - \frac{2187}{(492800 \cdot c^{22})} \cdot z^{22} + \frac{2187}{(1971200 \cdot c^{24})} \cdot z^{24} - \frac{6561}{(25625600 \cdot c^{26})} \cdot z^{26}$$

So, a Fourier transformation for the z variable can be easily found:

$$\int_0^g \left[\cos(r \cdot z) + \frac{\alpha_0}{\lambda r} \sin(r \cdot z_0) \right] \cdot \mathrm{aprox}(z, c, nlast) dz \qquad (32)$$

The integral equation (32) is computed with the use of computer symbolic calculation. The result is usually very long. This expression is signed as E_i^1 to perform the rest operations.

Through execution the reverse transformation for specified modules for x_0, y_0, z_0 in the same way as previously for C-I-N H-S model the temporary temperature field generated by a pulsed "double ellipsoid configuration of source" is finally achieved as follows:

$$T = \left(\frac{q \cdot f_f \cdot 3\sqrt{3}}{\pi \cdot \sqrt{\pi} \frac{\lambda}{\alpha} c_f \sqrt{(12 \cdot \alpha \cdot t + a_f^2)(12\alpha t + b_f^2)}} \cdot \exp\left[-\left(\frac{x_0^2}{4\alpha t + \frac{1}{3}a_f^2} + \frac{y_0^2}{4\alpha t + \frac{1}{3}b_f^2} \right) \right] \right) +$$

$$+ \left(\frac{q \cdot f_r \cdot 3\sqrt{3}}{\pi \cdot \sqrt{\pi} \frac{\lambda}{\alpha} c_r \sqrt{(12 \cdot \alpha \cdot t + a_r^2)(12\alpha t + b_r^2)}} \cdot \exp\left[-\left(\frac{x_0^2}{4\alpha t + \frac{1}{3}a_r^2} + \frac{y_0^2}{4\alpha t + \frac{1}{3}b_r^2} \right) \right] \right) \cdot \tag{33}$$

$$\cdot \sum_{i=1}^{\infty} B_i C_i E_i \cdot \exp(-\alpha \cdot r_i^2 \cdot t)$$

Using an additivity method, we may achieve the summary temperature field generated by moving heat source as follows:
- stationary co-ordinates system:

$$T(x_0, y_0, z_0) = \int_0^t \left(\frac{q \cdot f_f \cdot 3 \cdot \sqrt{3}dt}{\pi \cdot \sqrt{\pi} \cdot \frac{\lambda}{a} \cdot c_f \cdot \sqrt{([12 \cdot a \cdot (t-t') + a_f^2] \cdot [12 \cdot a \cdot (t-t') + b_f^2])}} \cdot \right.$$

$$\cdot \exp\left[-\left(\frac{(x_0 - v \cdot t')^2}{4 \cdot a \cdot (t-t') + \frac{1}{3}a_f^2} + \frac{y_0^2}{4 \cdot a \cdot (t-t') + \frac{1}{3}b_f^2} \right) \right] + \frac{q \cdot f_r \cdot 3 \cdot \sqrt{3}dt'}{\pi \cdot \sqrt{\pi} \cdot \frac{\lambda}{a} \cdot c_r \cdot \sqrt{([12 \cdot a \cdot (t-t') + a_r^2] \cdot [12 \cdot a \cdot (t-t') + b_r^2])}} \cdot$$

$$\left. \cdot \exp\left[-\left(\frac{(x_0 - v \cdot t')^2}{4 \cdot a \cdot (t-t') + \frac{1}{3}a_r^2} + \frac{y_0^2}{4 \cdot a \cdot (t-t') + \frac{1}{3}b_r^2} \right) \right] \right) \cdot \sum_{i=1}^{\infty} B_i \cdot C_i \cdot E_i \cdot \exp[-a \cdot r_i^2 \cdot (t-t')]$$

$$\tag{34}$$

- moving co-ordinates system: $x = x_0 - vt$, $y = y_0$, $z = z_0$:

$$T(x, y, z) = \int_0^t \left(\frac{q \cdot f_f \cdot 3 \cdot \sqrt{3}dt}{\pi \cdot \sqrt{\pi} \cdot \frac{\lambda}{a} \cdot c_f \cdot \sqrt{([12 \cdot a \cdot (t-t') + a_f^2] \cdot [12 \cdot a \cdot (t-t') + b_f^2])}} \cdot \right.$$

$$\cdot \exp\left[-\left(\frac{[x + v \cdot (t-t')]^2}{4 \cdot a \cdot (t-t') + \frac{1}{3}a_f^2} + \frac{y^2}{4 \cdot a \cdot (t-t') + \frac{1}{3}b_f^2} \right) \right] + \frac{q \cdot f_r \cdot 3 \cdot \sqrt{3}dt'}{\pi \cdot \sqrt{\pi} \cdot \frac{\lambda}{a} \cdot c_r \cdot \sqrt{([12 \cdot a \cdot (t-t') + a_r^2] \cdot [12 \cdot a \cdot (t-t') + b_r^2])}} \cdot$$

$$\left. \cdot \exp\left[-\left(\frac{[x + v \cdot (t-t')]^2}{4 \cdot a \cdot (t-t') + \frac{1}{3}a_r^2} + \frac{y^2}{4 \cdot a \cdot (t-t') + \frac{1}{3}b_r^2} \right) \right] \right) \cdot \sum_{i=1}^{\infty} B_i \cdot C_i \cdot E_i \cdot \exp[-a \cdot r_i^2 \cdot (t-t')]$$

$$\tag{35}$$

where:

$$E_i = \int_0^g \left(\cos(r_i \cdot z) + \frac{\alpha_0}{\lambda \cdot r} \cdot \sin(r_i \cdot z) \right) \cdot \text{approx}(z, c, \text{nlast}) dz \tag{36}$$

$$\text{approx}(z, c, \text{nlast}) = 1 + \sum_{n=1}^{\text{nlast}} \frac{\left(-\frac{3}{c^2} \cdot z^2 \right)}{\prod_{i=1}^{m} n} \tag{37}$$

Equations (34), (35) have a similar features as previously determined equations (23), (24) for assessment of the temperature fields in both stationary and moving coordinates systems. Both solutions have been given for three dimensional C-I-N and D-E heat source models but with different thermal characteristic. Especially it is obliged to differentiate low or high concentration of energy of heat sources.

Remaining comments concerning manner of solutions of equations (34), (35) and their results are the same as presented previously for equation (23), (24). The employment of method of hybrid account exists also in this case. That is the main purpose of the III part of this work. For further calculations it is chosen the analytic-numerical method.

CONCLUSIONS

In this paper the new temperature evaluation during welding of a plate with optional thickness is presented. Furthermore, the radiative heat transfer on both surfaces is taken into account. In these calculations we used the following heat source models: cylindrical-involution-normal (C-I-N) and double ellipsoidal configuration of source (D-E). By using the Fourier transformation method, the temperature fields generated by above heat sources in both stationary and moving co-ordinates system are presented. The algebraic forms of analytic solutions presented by equations requires **discretising** in order to make possible numerical calculation.

NOMENCLATURE

$\overline{T}, \overline{\overline{T}}, \overline{\overline{\overline{T}}}$ — the temperature transformation
$K(r, x_0), K(r, y_0), K(r, z_0)$ — transformations modules for x_0, y_0, z_0
$R(r, x_0), R(r, y_0), R(r, z_0)$ — reverse transformations modules
c_γ — volumetric heat, $[J\,K^{-1}\,cm^{-3}]$
c_p — specific heat, $[J\,K^{-1}kg^{-1}]$
ρ — mass density, $[kg\,cm^{-3}]$
$\prod\limits_{i=1}^{m} n$ — performs iterated multiplication of n over i = 1, .., m-1, [m]

B_i, C_i — values are in agreement with (23a) and (23b)
nlast — natural positive number as large as is necessary to achieve the required approximation
HAZ — Heat Affected Zone
C-I-N — Cylindrical-Involution-Normal heat source model
D-E — Double-Ellipsoidal heat source model
HS — Heat Source.

BIBLIOGRAPHY

1. E. Ranatowski, A. Poćwiardowski: *Mathematical Modelling of Weld Phenomena 5*, (ed H. Cerjak),pp. 725-742. 2000. London
2. G.A. Korn, T.M. Korn: *Mathematics for scientists and engineers*. McGraw – Hill Book Company. Copyright for Polish edition by PWN. Part I, pp. 144-146. 1983. Warsaw
3. Benker: Practical use of Mathcad: *Solving of Mathematical Problems*. Springer-Verlag. Berlin Heidelberg. 1999.

CONTACT WITH THE AUTHOR

Prof. Ranatowski Eugeniusz
Faculty of Mechanical Engineerig,
University of Technology and Life Science,
Prof. S. Kaliskiego 7
85-763 Bydgoszcz, POLAND
e-mail: ranatow@utp.edu.pl

Boundary element modelling of wave diffraction by interaction with wave-offshore structure and dredged region

S. D. Kim, Ph.D.
Chung-Ang University, South Korea
H. J. Lee, Ph.D.
Colorado State University, USA

ABSTRACT

The purpose of this study is to estimate the wave height at the front face of breakwater (Refracted breakwater and Straight breakwater), when dredging like the submarine pit is performed in the distant offshore from outer breakwater. The wave field of the problem is considered to be two dimensional planes and the configuration of the pit region is designated by a single horizontal long-rectangular system. The numerical approach uses the Green function based on the boundary integral approach. The results of the present numerical works are illustrated by applying the normal and inclined incidence. It is shown that in the case of normal incidence, the ratio of wave height reduction at the front face of both types of breakwaters is approximately more than 20% due to the effect of the submarine pit on the sea bed. Furthermore, regardless of the type of breakwater and the difference in incident wave angles, the ratio of wave height was shown to be reduced.

Keywords: Submarine pit; Green function; boundary integral approach; breakwater

INTRODUCTION

Study of wave diffraction by submarine pits has important application to coastal engineering. The purpose of this study is to investigate the reduction effect of wave height by submarine pit using depth-discontinuity. The early studies on the interaction of incident waves with a dredged region has been investigated by Newman (1965), Hilay (1969), Lee and Ayer (1981), Miles (1982), Kirby and Dalrymple (1983), Ting and Raichlen (1986), and Kirby et al. (1987). In all of these studies, the pit region was assumed to be infinitely long and the problem was restricted to the horizontal and vertical coordinates.

Later, Williams (1990) and McDougal et al. (1996) presented the numerical model for involving two horizontal planes in the case of single or multiple pits. The 3D (three dimensional) model, which is based on the Airy wave theory, was then investigated by Williams and Vazquez (1991) to analyze wave diffraction through a single pit. Recently, modeling diffraction of random waves by submarine pits has been investigated by Kim (2007). However, the focus in all of these studies were restricted to interaction of only one or two aspects, which occurred over pit (or trench) with discontinuity water depth.

The present study is about the interaction of wave, which is propagated over pit with discontinuity water depth. This study investigates the affect of this wave on the font face of breakwater systems (refracted and straight breakwater) when a pit is dredged. The wave interaction is connected to three boundary problems: the interaction of discontinuity water depth boundary and pit boundary, discontinuity water depth boundary within pit and breakwater boundary, and pit boundary and breakwater boundary. The problem is considered in a two dimensional plane, and the configuration of the dredging region on sea bed is a single-long rectangular type. The numerical simulation is performed by using the solution of the boundary integral equation based on the Green function.

In order to verify the present numerical model, comparisons made with the results of absolute and approximation solution presented by Koji and Mutsuo (1976) for regular wave diffraction at the front face of refracted breakwater without pit. Upon comparison, the present numerical simulation and the research by Koji and Mutsuo (1976) fell into relative agreement.

Decreasing effects of diffracted wave field in vicinity of breakwater due to a pit with discontinuity water depth were shown. The present study can provide information to design the dredge line of the outer breakwater that is distant from this dredge line. This study can also be effectively utilized for wave interaction by pit and be applicable to coastal engineering.

THEORETICAL DEVELOPMENT

The geometry of the problem is presented in Fig. 1. The fluid domain can be separated into three regions: the interior pit region with uniform depth d, the refracted breakwater, and the exterior fluid region with uniform depth h. The boundary
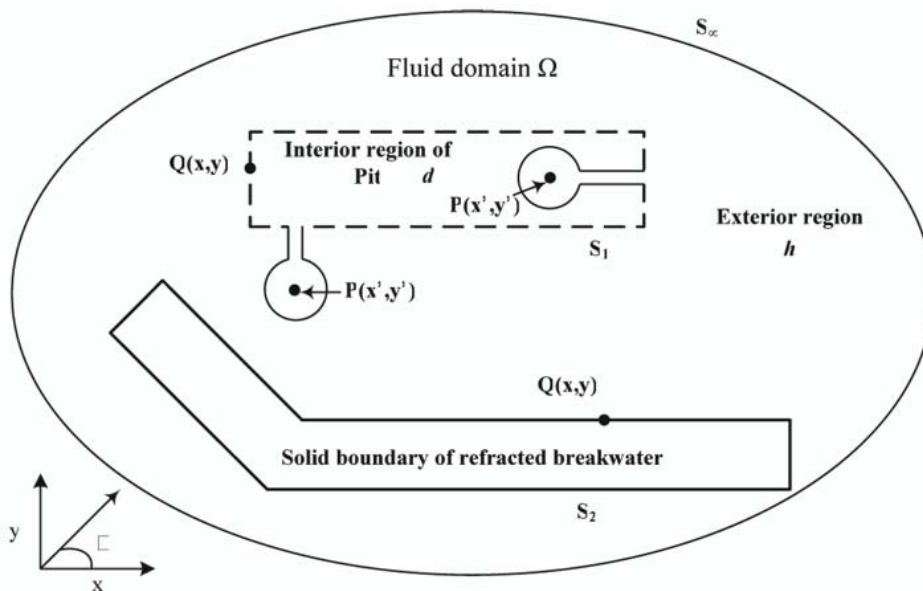
Fig. 1. Definition sketch for fluid domain and boundaries

regions express S_1 (pit boundary) and S_2 (breakwater region), respectively. In Fig. 1 the Cartesian coordinates are designated as having the origin at a corner of the breakwater. The x- and y- are directed in the horizontal plane and the z-axis is directed vertically upward from at the equilibrium water surface.

The fluid region is taken to be inviscid and incompressible, and the flow irrotational, then it will be assumed that the fluid motion may be described in terms of a velocity potential $\phi_j(x, y, z, t) = Re[\Phi_j(x, y, z)e^{-i\omega t}]$ for $j = 1, 2$. This potential must satisfy Laplace's equation, $\nabla^2\Phi_j = 0$. It is subject to the usual boundary conditions on the free surface and seabed, and the solution of velocity potential can be given following forms:

$$\Phi_1(x, y, z) = \Psi_1\cosh[k_1(z + d)] \quad \text{on } S_1 \qquad (1)$$

$$\Phi_2(x, y, z) = \Psi_2\cosh[k_2(z + h)] \quad \text{on } S_2 \qquad (2)$$

where, d is the water depth within the interior pit region, and h is the water depth of the exterior fluid region. The subscript 1 represents the pit region; subscript 2 represents the exterior fluid region, and the wave numbers $k_j(j = 1, 2)$ are defined by:

$$\omega^2 = gk_1\tanh(k_1 d) \quad \text{on} \quad S_1 \qquad (3)$$

$$\omega^2 = gk_2\tanh(k_2 h) \quad \text{on} \quad S_2 \qquad (4)$$

where:
ω - angular frequency
g - gravitational acceleration.

The governing equations in each of the fluid regions should be satisfied by the Helmholtz equation.

$$\frac{\partial^2\Psi}{\partial x^2} + \frac{\partial^2\Psi}{\partial y^2} + k_j^2\Psi = 0 \; ; j = 1, 2 \qquad (5)$$

Continuity of mass flux and pressure across the fluid interface between the interior pit region (S_1) and the exterior region (S_2) requires the following conditions to be satisfied:

$$d\frac{\partial\Psi_1}{\partial n} = h\frac{\partial\Psi_2}{\partial n} \quad \text{on } S_1 \qquad (6)$$

$$\Psi_1 = \Psi_2 \quad \text{on } S_1 \qquad (7)$$

Finally, the scattered component of the fluid potential in the S_3 is subject to a radiation or far-field boundary condition at large radial distances r, which may be written as:

$$\lim_{r\to\infty}\sqrt{r}\left(\frac{\partial}{\partial r} - ik_j\right)(\Psi_3 - \Phi_1) = 0 \; ; j = 1, 2 \qquad (8)$$

where Φ_I is the incident potential function and is given by:

$$\Phi_I(x, y, z) = -\frac{igH_I}{2\omega}\frac{\cosh[k_2(z + h)]}{\cosh(k_2 h)} \qquad (9)$$

Green's function $G_j(P, Q)$, $j = 1, 2$ may now be expressed for each region as:

$$G_j(P, Q) = \frac{i\pi}{2}H_0^{(1)}(k_j R) \; ; j = 1, 2 \qquad (10)$$

where, $H_0^{(1)}$ is the Hankel function of the first kind of order zero, P and Q have the coordinate of (x', y') and (x, y) on the boundary(S_1, S_2), respectively, and $R = \sqrt{(x'-x)^2 + (y'-y)^2}$.

Applying Green's second identity to Ψ_j and extending to full regions ($S_1 + S_2 + S_3$), boundary integral equations can be yielded as Eq. (11) and Eq. (12).

$$\Psi_2(P) + \frac{1}{\pi}\int_{S_1+S_2+S_3}\left[\Psi_2(Q)\cdot\frac{\partial G_j}{\partial n}(P, Q) - G_j(P, Q)\cdot\frac{\partial\Psi_2}{\partial n}(P)\right]dS_j = 0 \qquad ; j = 1, 2 \quad (11)$$

$$\Psi_2(P) - 2\Phi_1(P) - \frac{1}{\pi}\int_{S_1+S_2+S_3}\left[\Psi_2(Q)\cdot\frac{\partial G_j}{\partial n}(P, Q) - G_j(P, Q)\cdot\frac{\partial\Psi_2}{\partial n}(P)\right]dS_j = 0 \; ; j = 1, 2 \quad (12)$$

The scattered wave has no effect on the imaginary boundary line (S_3), and applying boundary condition of (6) and (7) proposed by Williams (1990) and McDougal et al. (1996) to Eq. (11) and (12), and Eq. (11) and (12) become:

$$\Psi_2(P) + \frac{1}{\pi}\int_{S_1}\left[\Psi_2(Q)\cdot\frac{\partial G_1}{\partial n}(P,Q) - \frac{h}{d}G_1(P,Q)\cdot\frac{\partial\Psi_2}{\partial n}(P)\right]dS_1 + \tag{13}$$

$$+ \frac{1}{\pi}\int_{S_2}\left[\Psi_2(Q)\cdot\frac{\partial G_2}{\partial n}(P,Q) - \frac{h}{d}G_2(P,Q)\cdot\frac{\partial\Psi_2}{\partial n}(P)\right]dS_2 = 0$$

$$\Psi_2(P) - 2\Phi_1(P) - \frac{1}{\pi}\int_{S_1}\left[\Psi_2(Q)\cdot\frac{\partial G_1}{\partial n}(P,Q) - \frac{h}{d}G_1(P,Q)\cdot\frac{\partial\Psi_2}{\partial n}(P)\right]dS_1 + \tag{14}$$

$$+ \frac{1}{\pi}\int_{S_2}\left[\Psi_2(Q)\cdot\frac{\partial G_2}{\partial n}(P,Q) - \frac{h}{d}G_2(P,Q)\cdot\frac{\partial\Psi_2}{\partial n}(P)\right]dS_2 = 0$$

The free surface elevation in each region can be obtained using Eq. (15):

$$\eta_j = -\frac{1}{g}\frac{\partial\Psi_j}{\partial t} \qquad ; j = 1, 2 \tag{15}$$

in which $\eta(x, y, t) = \text{Re}\{\Delta_j(x, y)e^{-\omega t}$, where Δ_j is the spatial component of surface elevation in fluid region. Finally, the diffraction coefficient of regular wave, K_d is defined as:

$$K_d = \left|\Psi_j(x', y')\right| \tag{16}$$

NUMERICAL RESULTS AND ANALYSIS

Validation of the numerical model

A computer program has been developed to implement the above theory for regular wave diffraction at the vicinity of breakwater by pit on the sea bed. To verify the present numerical results of the wave height at the front face of refracted breakwater, these were compared with the absolute and approximate solutions presented by Koji and Mutsuo (1976). The conditions of calculation and configuration of refracted breakwater in regular waves without pit by Koji and Mutsuo (1976) are defined as incident wave angle $\theta = 45°$, angle of refracted breakwater $\beta = 135°$, reflection coefficient $K_r = 0.8$, and length of breakwater = 2L ($L_1 + L_2 = 2L$), respectively.

Fig. 2 shows a comparison of the results at the front face of refracted breakwater for the diffraction coefficient of regular waves (CD line) obtained by the present numerical model and those of Koji and Mutsuo (1976) . In a comparison from fig. 2, it is noticed that reasonable agreement is shown in the three cases for the refracted breakwater, but the diffraction coefficient at the front face of refracted breakwater by the present numerical model is a little bit higher than the results of Koji and Mutsuo (1976). They had performed their studies

at the infinite refracted breakwater but the present numerical model has been investigated at the finite refracted breakwater, so in the case of finite breakwater, the wave interface has been occurred by phase difference and interaction between incident waves and reflect waves.

Numerical examples

Numerical examples are presented to investigate the influences by rectangular submarine pit at the front face of refracted and straight breakwaters with different incident wave angle.

In this study, the condition of calculations are water depth of the vicinity of breakwater h = 7 m, water depth within submarine pit region h = 14 m, the refracted angle within the refracted breakwater $\beta = 160°$, and incident wave angle $\theta = 90°$ and $\theta = 135°$ for the regular wave, respectively. Figs 3 and 4 present the results for the diffraction coefficient obtained by the present numerical model with and without submarine pit at the front face (CD line) of refracted and straight breakwater, respectively.

In the case of normal incident wave angle $\theta = 90°$, wave height reduction of refracted breakwater due to submarine pit at

Fig. 2. Comparison of wave diffractions of present study with those of approximate and absolute solutions at the front face of refracted breakwater
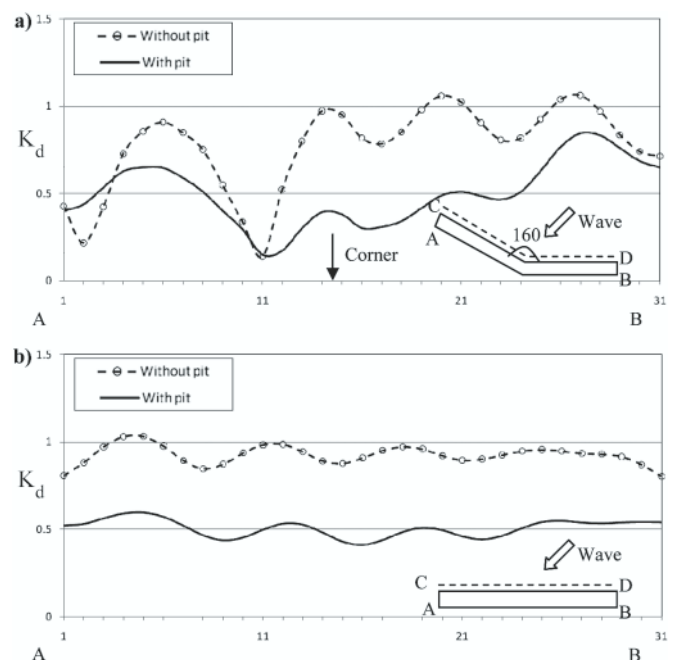
Fig. 3. Wave height distributions at the front face of breakwater systems with or without pit (incident wave angle $\theta = 90°$)

the offshore sea bed as shown in fig. 3(a) can be observed at the vicinity of corner side. The wave height reduction at the vicinity of the corner side is shown to be the largest. This means that the wave energy is concentrated on the corner of the refracted breakwater, and by using the pit, the wave energy is subdued thus reducing damage on the breakwater. Fig. 3(b) shows that the straight breakwater is reduced in the entire region. This reduction is 26.5% less than the numerical results for the case without submarine pit for the refracted breakwater, and 41.7% for straight breakwater.

As for the case of inclined wave angle θ = 135°, wave height reduction due to pit can be estimated 12.6% for refracted breakwater and 5.0% for straight breakwater. As shown in figs 4(a) and (b), reduced wave height is expressed at the front face of breakwater except at the left side of each breakwater. Table 1 presents the effect of added pit on the reduction in wave height line CD.

From these analyses, we find out that the overall reduction of wave height may be observed at the vicinity of breakwater with an appropriately set submarine pit.
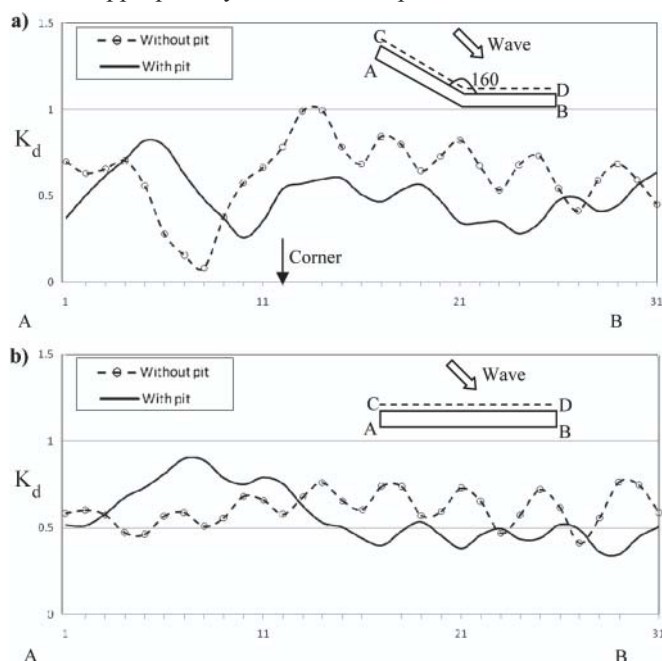
Fig. 4. *Wave height distributions at the front face of breakwater systems with or without pit (incident wave angle θ = 135°)*

Tab. 1. The ratio of reduction in wave height

Type of breakwater \\ Incident wave angle	Refracted breakwater	Straight breakwater
θ = 90°	26.5%	41.7%
θ = 135°	12.6%	5.0%

Fig. 5 presents the contours of the wave height ratios near the breakwaters due to regular diffraction wave with two case of breakwater. We can derive from the results that a dredging pit may provide an excellent means of protection from a wave attack. It can be seen that wave energy is weakened by discontinuity water depth (dredging). The results from numerical simulation for wave diffraction indicate that the present model is appreciable to estimate the wave field at the vicinity of breakwater when a pit is dredged on the offshore sea bed.
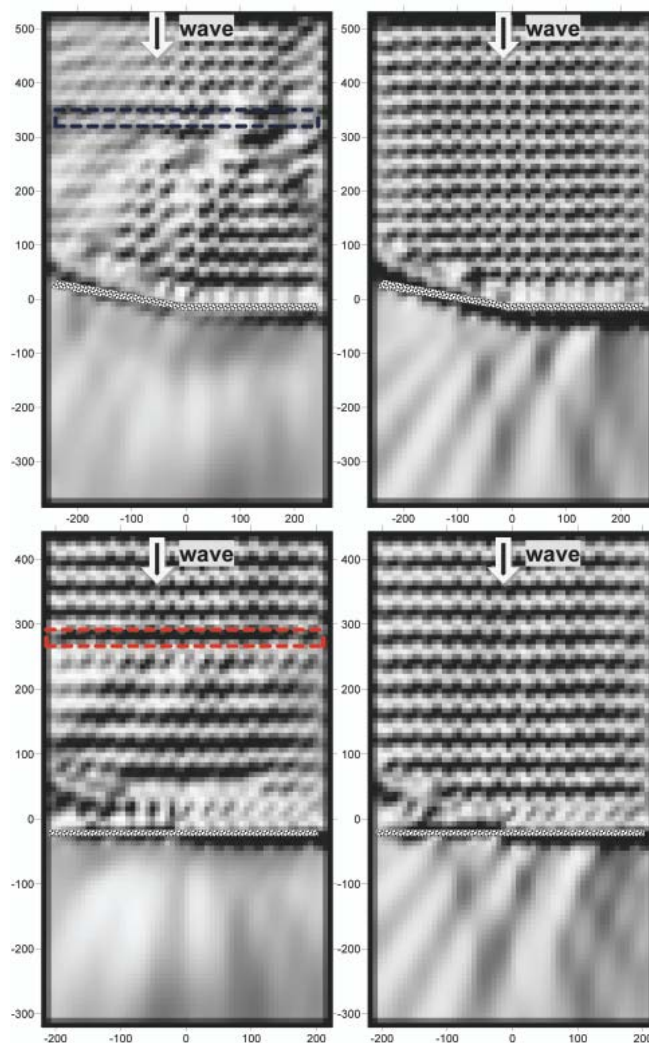
Fig. 5. *Diffraction contour plots at the vicinity of breakwaters with or without pit*

CONCLUSIONS

- The purpose of this study was to estimate the decreasing effects of diffracted wave fields around breakwater when the dredging work (pit) is performed at the offshore sea bed. This study is about the composite interaction for the three problems: dredging boundaries, depth discontinuity of pit, and breakwater boundaries. The boundary conditions are established for those problems and applied to the boundary integral equation.
- Results for the incident wave conditions have been presented to illustrate the wave height distribution of the wave field near breakwater by the influence of the pit. The results of present numerical model have been compared with those from published calculations and present numerical simulations that show relative agreement with published data for diffraction.
- Through the present numerical simulations the wave height reduction of refracted and straight breakwater with different incident wave angle due to submarine pit at the offshore sea bed can be observed.
- It is noticed that the results from the present numerical model accurately provides the diffracted wave height of vicinity of breakwater systems, when the pit is dredged on the offshore sea bed, and so may be extended to apply with confidence in breakwater planning and design applications.

BIBLIOGRAPHY

1. HILAY N.: *Water waves over a rectangular channel though a reef*. Journal of Waterways and Harbor Division, ASCE, 95(1):77-94, 1969.
2. Kim S.D.: *Multidirectional random wave diffraction in a harbor with partial-reflecting boundary by placing submarine pit*. Ph.D. Thesis, Chung-Ang University, South Korea, 2007.
3. KIRBY J.T. and DALRYMPLE R.A.: Propagation of obliquely incident water waves over a Trench. Journal of Fluid Mechanics, 133: 47-63, 1983.
4. KIRBY J.T., DALRYMPLE R.A. and SEO S.N.: *Propagation of obliquely incident water waves over a trench*. Part 2. Current flowing along the trench, Journal of Fluid Mechanics, 176: 95-116, 1987.
5. KOJI K. and MUTSUO O.: *A study of wave height distribution along a breakwater with a corner*. Report of the Port & Harbor Research Institute, 15(2): 55-88, 1976.
6. LEE J.J. and AYER R.M.: *Wave propagation over a rectangular trench*. Journal of Fluid Mechanics, 110: 335-347, 1981.
7. MCDOUGAL W.G., WILLIAMS A.N. and FURUKAWA K.: *Multiple-pit breakwaters, Journal of Waterway*. Port, Coastal and Ocean Engineering, ASCE, 122(1): 27-33, 1996.
8. MILES J.W.: *On surface wave diffraction by a trench*. Journal of Fluid Mechanics, 115: 315-25, 1982.
9. NEWMAN J.N.: *Propagation of water waves over an infinite step*. Journal of Fluid Mechanics, 23: 399-415, 1965.
10. TING C.K.F. and RAICHLEN F.: *Wave interaction with a rectangular trench*. Journal of Waterway. Port, Coastal and Ocean Engineering, ASCE, 112, 454-460, 1986.
11. WILLIAMS A.N.: *Diffraction of long waves by rectangular pit*. Journal of Waterway, Port, Coastal and Ocean Engineering, ASCE, 116(4): 459-469, 1990.
12. WILLIAMS A.N. and VAZQUEZ J.H.: *Wave interaction with a rectangular pit*. Journal of Offshore Mechanics and Arctic Engineering, 113: 193-198, 1991.

CONTACT WITH THE AUTHORS

Sung Duk Kim, Ph.D.
Department of Civil & Environmental Engineering,
Chung-Ang University, South Korea.
Donjak Gu, Heukseok-Dong 221, Seoul, South Korea
Phone: +82-2-820-5253, fax: +82-2-820-5253,
e-mail: soungdoug@hotmail.com

Ho Jin Lee (Corresponding author), Ph.D.
Department of Civil & Environmental Engineering,
Colorado State University, USA.
Fort Collins, CO 80523, USA
e-mail: leehojin74@gmail.com

Study on Hybrid Filtering Solution for Marine Electric Network

Xiao-Yan Xu, Prof.
Shanghai Maritime University, Shanghai 200135, China
Janusz Mindykowski, Prof.
Gdynia Maritime University
C. L. Philip Chen, Prof.
University of Macau, Macau, China

ABSTRACT

This paper presents a Hybrid APF/PFC/PPF Circuit (active power filtering and power factor correction circuit aided by shunt passive filter) for harmonic suppression and power factor correction in a marine electric network. By employing the proposed hybrid circuit, marine electric power network voltage and current can be maintained as being sinusoidal, and the power factor is close to 1. The effectiveness of the proposed method that is applied to a marine electric network is demonstrated through a simulation experiment. The results show that the expected performances are achieved.

Keywords: Electrical engineering, marine vehicle power systems, power system harmonics,
power system measurements, quality control

INTRODUCTION

Recently, application of power electronic devices to marine systems has been wider and wider, which can be seen from the fact that the number of power electronic devices equipped in ships is increasing very quickly and the capacity of these devices in ships is becoming larger and larger. As a result, in a ship, electrical power energy consumed by power electronic devices occupies a continuously increasing proportion of the gross electrical energy produced by the ship. But harmonics produced by power electronic devices such as frequency converters or soft starters cause distortion of the current waveform and voltage waveform of the electric network, as well as having a remarkable influence on safety and capacity in the choice of electric network, which makes harmonic pollution in a marine electric network more and more serious and difficult to estimate [11, 16]. Furthermore, impedances of generators designed for ships are relatively higher than those of overland power sources, which worsens current distortion in marine electric networks. Another problem of marine electrical power quality is a low power factor. The selected capacity of ship equipment is usually very conservative and its power factor during routine operation is correspondingly lower since a marine electric network is a kind of low capacity isolated network when compared with an electric network that operates on shore. But the reliability of ship operation plays a vital role in safety of navigation, which leads to a substantial safety consideration in the design of a marine electric network. This is evident in the rules of marine electric network power quality issued by the majority of shipping classifications in the world, which are not less strict, or are even stricter, than the rules of public electric network power quality issued in international standards [4, 13, 14, 17]. For example, the limit of stable voltage adjusting rate is between +2.5% and –2.5% as ruled by the China Classification Society, and the limit of stable voltage fluctuation is 3.3% in IEC EMC 61000-3-11 [4, 5]. As another example, the limit of total voltage harmonic distortion (THD_v) is 5% as shown in the national standards of low voltage (0.38kV) public electric network of China, while comparatively, the mentioned parameter ruled by DNV (Det Norske Veritas – Norwegian classification society) and ABS (the American Bureau of Shipping) is 5% too. But the fact is, it is more difficult to obtain an improvement of the power quality of a marine electric network than that of an overland electric network due to the characteristics of marine electric networks [10].

Hitherto, the majority of achievements in the field of product design for power quality improvement have been restricted to overland electric networks. There is still a lack of reports showing significant progress of power quality improvement technology applied to ship electric networks. Nevertheless, even considering the practical products which have been applied to overland electric networks, their applied effect has not been satisfactory due to the limitation of control effect and the accuracy of measurement of the electric network in the aspects of active power, reactive power, power factor and high order harmonics. That is, it is reasonable to design a new circuit for a marine electric network to depress harmonics and correct the power factor under the consideration of characteristics of a marine electric network.

HYBRID APF/PFC/PPF CIRCUIT

Definitions of harmonic distortion and power factor

Normally, distorted power, based on Budeanu's concept, is defined as [18]:

$$D = \sqrt{S^2 - P^2 - Q^2} \qquad (1)$$

The most popular parameters describing the above-mentioned distortions are the total harmonic distortion coefficients THD_V and THD_I, voltage and current respectively, as shown in formulas (2) and (3).

$$THD_V = \frac{\sqrt{\sum_{n=2}^{n_{max}} V_n^2}}{V_1} \qquad (2)$$

$$THD_I = \frac{\sqrt{\sum_{n=2}^{n_{max}} I_n^2}}{I_1} \qquad (3)$$

where V_1 is root mean square value of the fundamental harmonic, n is order of harmonics, and V_n is harmonic voltage when the order is n. Normally, THD_V and THD_I are obtained when n_{max} is 40 or 50, where n_{max} is the highest harmonic order in the process of defining THD_V or THD_I.

The definition of power factor is shown in formula (4), where total power factor λ is the arithmetic product of displacement power factor λ_φ and the distortion power factor λ_D. Formulas (5) and (6) show the definitions of λ_φ and λ_D respectively. The total power factor λ can be described as formula (7), where S_1 is the apparent power under fundamental frequency, P is active power, Q is reactive power, D is distorted power and S is apparent power.

$$\lambda = \lambda_\varphi \cdot \lambda_D \qquad (4)$$

$$\lambda_\varphi = \frac{P}{S_1} \qquad (5)$$

$$\lambda_D = \frac{S_1}{S} = \frac{V_{1rms}}{V_{rms}} \cdot \frac{I_{1rms}}{I_{rms}} = \frac{1}{\sqrt{1 + THD_V^2}\sqrt{1 + THD_I^2}} \qquad (6)$$

$$\lambda = \frac{P}{S} = \frac{P}{\sqrt{P^2 + Q^2 + D^2}} \qquad (7)$$

The design of harmonic suppression and power factor correction solutions for ship use aims to minimize the quantities of Q and D in equation (7) to improve the total power factor λ in the marine electric network environment [9].

Design of Hybrid APF/PFC/PPF Circuit

In this paper, the designed Hybrid APF/PFC/PPF Circuit is a combination of SAPF (series active power filter) and active PFC (power factor correction circuit) aided by a shunt passive filter, which is shown in Fig. 1.

Application of this design takes into consideration that a marine electrical power system is very different from a land power system, because of its character, i.e. an isolated power system, where the capacity of a heavy load in a ship is comparable to that of a ship electrical power station. Moreover, the impedance of generators designed for ships is higher than that of a land power source, which worsens voltage deviations in marine electric networks. Also a heavy load gives an electric network a great impact and causes a considerable voltage drop and frequency oscillations of the electric network at the moment it is switched on. At the same time, power electronic devices generally are used in ship systems and cause distortion of current, and in consequence, voltage waveforms. Taking into account the complexity of the considered matter, it means that the load variation range and variation frequentness, and many kinds of disturbances covering the current as well as the voltage character (including their harmonics) must be considered. At the moment to mitigate harmonics, mainly passive power filters (PPF), and rarely parallel active power filters (APF) in marine technology are used. To improve the dynamic properties of a marine electrical power station and to reduce the power of filtering circuits, a hybrid filter concept for marine electric networks was investigated.

A new type of hybrid solution for a marine electric network was considered as a study and research for the general case of a marine electric network, including voltage sensitive (in the meaning of voltage quality) loads as well as voltage non-sensitive loads. Both of them may be easily appointed in the marine networks, e.g. all computer-aided control, alarm and monitoring systems are strongly sensitive voltage loads, while in contrast the heaters are voltage non-sensitive loads. On the
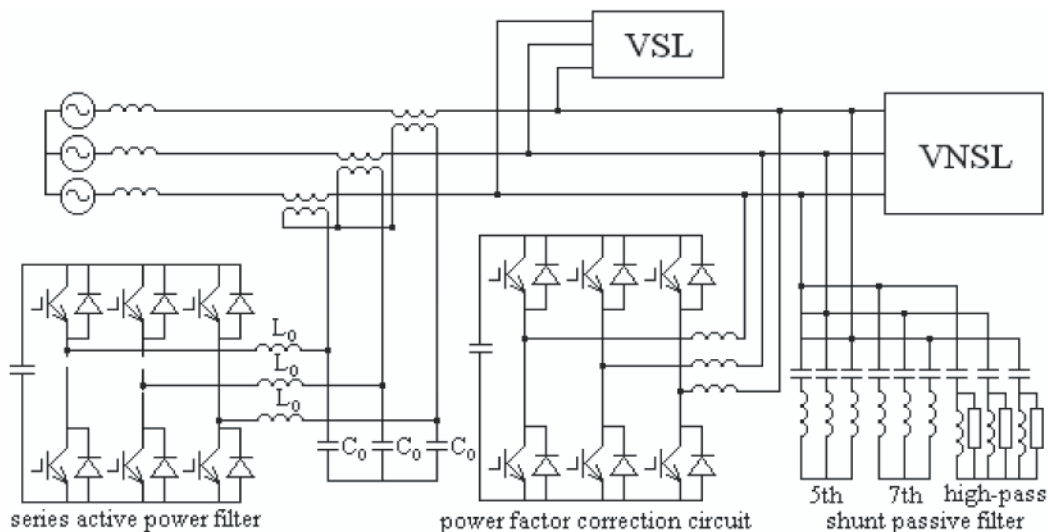
Fig. 1. Configuration of Hybrid APF/PFC/PPF Circuit

other hand, power converters generate mainly current, but also voltage harmonics, so they generally require a compensation voltage and current harmonics.

In Fig. 1, the SAPF and shunt PF constitute a combined system of series active power filter and shunt passive filter. Based on the following two reasons, the combined series active power filter is designed to be included in the Hybrid APF/PFC/PPF Circuit. Firstly, the capacity of a marine power station, as well as the capacity of a single generator contained in a power station, becomes higher and higher, but due to the characteristics of a marine generator, source voltage harmonics are rather considerable when compared with those that can be found in an overland network. The SAPF is first of all a controlled voltage source, and it is connected in series between an electrical power supplier and a linear load. The authors have distinguished two kinds of load: one is the voltage sensitive load (VSL) and the second is the voltage non-sensitive load (VNSL). The SAPF can compensate voltage harmonics and improve quality of voltage supplied to the voltage sensitive load (VSL). That is, the SAPF is suitable for harmonic suppression in distorted supply voltages [3]. Secondary, large rated cycloconverters and thyristor converters are more and more frequently applied to marine systems whose capacity occupies an incremental percentage of the total capacity of electrical power. When the combined system of shunt passive and series active power filter is applied, the shunt PF acts as the main bearer to fulfil the task of current filtering, while the series APF does not act rather as a harmonic compensator but mainly as a harmonic isolator. It decreases source harmonics flowing into the shunt PF and causing resonance. Also the required rating of the series active filter will be reduced to less than 1%, as compared with the rating of a 3-phase 6-pulse thyristor converter or cycloconverter, that is, the required rating of series APF is much smaller than that of a conventional shunt APF [12]. Thereby, application of a combined system of shunt passive and series active power filter results in better filtering characteristics and lower initial and running costs. In the SAPF shown in Fig. 1, L_0 and C_0 constitute a set of a small capacity filter which is used to suppress high frequency pulsating voltage and current caused by the high frequency switching of the converter.

A combined system of shunt passive and series active power filter is not sufficient for marine electric network application. There are two reasons to develop this filter structure. As mentioned in the first paragraph of this work, the problem of a low power factor may cause a serious problem in ship electric networks and even cause breakdown of an electrical power station during the starting process of bulk load. SAPF is able to improve the operational environment mainly for loads generating voltage harmonics. In contrast, a shunt APF is very effective in depression network current harmonics, usually generated by a non-linear load. Furthermore, the effect of network current harmonic mitigation is not so effective due to the inherent deficiencies of shunt PF, which, undoubtedly, contributes to suppressing the majority of current harmonics. In the authors' opinion a solution is to include an active PFC (power factor correction) circuit in the Hybrid APF/PFC/PPF Circuit. The active PFC circuit is expected to solve the problem of the low power factor in the electric network, and simultaneously acts as a current harmonic filter to suppress network current harmonics additionally. Taking that into consideration, the active PFC circuit is located between the SAPF and the shunt PF.

While both the combined system of shunt passive, the series active power filter and the active PFC circuit are concerned, each of these works as a supplementary means of the other one, and they work together to suppress harmonics and compensate reactive power at the same time more effectively, assuming that superiorities of different types of compensation devices are mutually complementary. It is also anticipated that, for a marine electric network – an independent small capacity electric network in a complex environment and requiring a quick response to harmonics suppression and reactive power compensation – the proposed solution will meet the demand of a marine electric network for high-speed and accurate measurement and management of harmonics and reactive power. Moreover, taking into consideration the possibility of harmonics suppression and reactive power compensation, the suggested solution will lead to the achievement of significant energy saving.

Control algorithm of Hybrid APF/PFC Circuit

The key technology to achieve a rapid and accurate effect of electric power quality compensation in ship electric networks, considering the application of the Hybrid APF/PFC Circuit, is the high operational performance of the SAPF and the active PFC circuit in the Hybrid APF/PFC Circuit due to the complicated operational environment of ship loads and high frequency of a wide range of variation of load operating mode.

For an active power filtering or an active power factor correction circuit, the detection circuit of harmonics and reactive current is an important part that determines its compensation characteristics. Generally speaking, in practical application, there are two major types of harmonics and reactive current detection methods. One is based on series expansion of Fourier Transform [2], while the other is based on the theory of Instantaneous Reactive Power of a 3-phase circuit, also called the p-q method [1]. The former method is able to detect a detailed values of harmonics series or the harmonics of a specified frequency band, which qualifies it for fault diagnosis and protection of the electric network, but its real time operational property of current detection is not satisfactory. The latter method has quite good properties in real time detection but is not able to work effectively when the source voltage is distorted [19]. Nevertheless, the theory of Instantaneous Reactive Power of a 3-phase circuit has been the most used until now in the control of active power filters [15]. Of course, there are quite a number of other types of harmonics detection methods, e.g., the adaptive harmonic current detection method [8] and the predictive current detection method [6]. The fact is that all these proposed methods are still in the stage of research and development and lack practicability. A current detection method based on an improvement of the Instantaneous Reactive Power theory of a 3-phase circuit, which is called the i_p-i_q method, is being developed to effectively detect load current and divide the load current into the fundamental active component, fundamental reactive component and harmonic component with accuracy and real-time property even when the source voltage is distorted or 3-phase unbalanced [19]. Its working principle is expressed concisely in this paper by Fig. 2.

In Fig. 2, voltage vector V_a stands for phase A voltage of power source, with its instantaneous value $v_a = V_m \sin\omega t$, where, V_m is amplitude of phase voltage. It provides a PLL (phase-locked loop) circuit with the phase information of $\sin\omega t$ and $\cos\omega t$, with appropriately defined signs. In this detection and control system, three types of coordinates are involved, among which the "3-phase coordinate" and "αβ coordinate" are static coordinates and the "pq coordinate" is a rotary coordinate with its angular velocity ω – the angular velocity of source voltage. The quantities i_a, i_b, i_c are the detected 3-phase line currents of the electrical power network respectively.
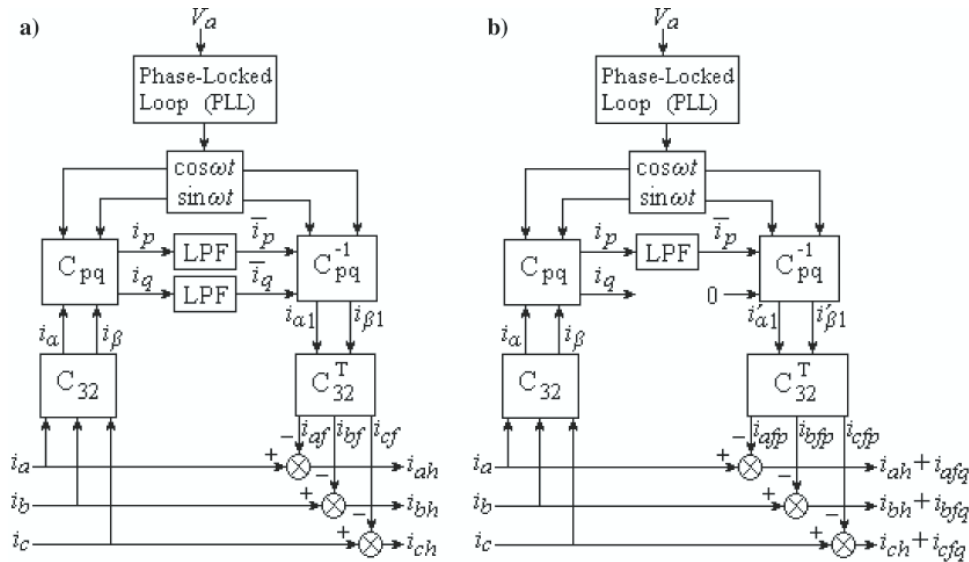
Fig. 2. *Fundamental principle of the compensation current determined by i_p-i_q method,*
***a)** detection of harmonic current, **b)** detection of the sum of harmonic current and reactive current*

In Fig. 2a, i_{ah}, i_{bh}, i_{ch} are the 3-phase harmonic currents respectively and i_{af}, i_{bf}, i_{cf} are the 3-phase fundamental currents respectively. In Fig. 2b, i_{afp}, i_{bfp}, i_{cfp} are the 3-phase fundamental active currents respectively, and i_{afq}, i_{bfq}, i_{cfq} are the 3-phase fundamental reactive currents respectively.

The relationship of the variations in Fig. 2 is:

$$\begin{bmatrix} i_p \\ i_q \end{bmatrix} = C_{pq} \begin{bmatrix} i_\alpha \\ i_\beta \end{bmatrix} = C_{pq} C_{32} \begin{bmatrix} i_a \\ i_b \\ i_c \end{bmatrix} \qquad (8)$$

where:

$$C_{32} = \sqrt{\frac{2}{3}} \begin{bmatrix} 1 & -1/2 & -1/2 \\ 0 & \sqrt{3}/2 & -\sqrt{3}/2 \end{bmatrix}$$

$$C_{pq} = \begin{bmatrix} \cos\omega t & -\sin\omega t \\ -\sin\omega t & -\cos\omega t \end{bmatrix}$$

So the fundamental current is:

$$\begin{bmatrix} i_{af} \\ i_{bf} \\ i_{cf} \end{bmatrix} = C_{32}^T C_{pq}^{-1} \begin{bmatrix} \bar{i}_p \\ \bar{i}_q \end{bmatrix} \qquad (9)$$

where C_{pq}^{-1} is the inverse matrix of C_{pq}, and $C_{pq}^{-1} = C_{pq}$. C_{32}^T is the transposed matrix of C_{32}. The output of LPF (low pass filter), $\bar{i}_p$ and $\bar{i}_q$, are the direct current value of i_p and i_q respectively. I_{af}, i_{bf}, i_{cf} are 3-phase fundamental currents respectively. Afterwards, the compensation current of harmonic current is:

$$\begin{bmatrix} i_{ah} \\ i_{bh} \\ i_{ch} \end{bmatrix} = \begin{bmatrix} i_a \\ i_b \\ i_c \end{bmatrix} - \begin{bmatrix} i_{af} \\ i_{bf} \\ i_{cf} \end{bmatrix} \qquad (10)$$

Based on the aforementioned harmonic signals which are obtained according to the i_p-i_q method, activity of appropriate filters can be fulfilled.

In the designed SAPF/PFC circuit, considering that the conventional source voltage provided by a ship electrical power station is distorted in evidence and even a little bit 3-phase unbalanced in a degree, the i_p-i_q method is applied to determine the compensation current. Furthermore, in Fig. 2b, the channel of current i_q is disconnected, then the signal i_q that goes through the LPF is 0, and the equation (8) becomes:

$$\begin{bmatrix} i_{afp} \\ i_{bfp} \\ i_{cfp} \end{bmatrix} = C_{32}^T C_{pq}^{-1} \begin{bmatrix} \bar{i}_p \\ 0 \end{bmatrix} \qquad (11)$$

where only active current can be found in its output of $i'_{\alpha 1}$ and $i'_{\beta 1}$, that is, the output of transposition of coordinate converter (C_{32}^T) leaves fundamental active current only. The difference in value between the detected current (i_a, i_b, i_c) and the output of C_{32}^T is the sum of fundamental reactive current (i_{afq}, i_{bfq}, i_{cfq}) and harmonic current (i_{ah}, i_{bh}, i_{ch}). At that time, the final result of current calculation in Fig. 2b expresses the sum of harmonic current and fundamental reactive current. When this result acts as the instruction value of the compensation current, the compensation of fundamental reactive current and the compensation of harmonic current are able to be fulfilled simultaneously. Furthermore, since the method of 3-phase asymmetry control is adopted, the negative sequence current produced by the system itself counteracts the input negative sequence current, so that the simultaneous compensation of negative sequence current is realized [7].

The reactive and harmonic current detection algorithm adopted in the active PFC circuit in the Hybrid APF/PFC Circuit is the i_p-i_q method as shown in Fig. 2b, which is under consideration for its function of both power factor correction and harmonic current compensation, and the source voltage is distorted in ship electric networks.

For the SAPF, in order to compensate harmonic voltage accurately and in real time, its harmonic voltage detection algorithm is similar to the harmonic current detection algorithm which is shown in Fig. 2a, where supplied voltage of v_a, v_b, v_c are measured from the output of the power supplier, then v_p and v_q are obtained through matrix transform of C_{32} and C_{pq}, and after the low pass filter, $\bar{v}_p$ and $\bar{v}_q$, which are DC quantities of v_p and v_q corresponding to 3-phase fundamental voltages v_{af}, v_{bf}, v_{cf}, are obtained.

After matrix transform of C_{pq}^{-1} and C_{32}^T, 3-phase fundamental voltages v_{af}, v_{bf}, v_{cf} are detected. Afterwards, harmonic voltages v_{ah}, v_{bh}, v_{ch} are obtained, according to which the 3-phase instruction voltage of the power electronic converters, corresponding to $-v_{ah}$, $-v_{bh}$, $-v_{ch}$, are ascertained and adopted to control the on-off state of the six switching units in the main circuit.

For the shunt passive filter in the Hybrid APF/PFC/PPF Circuit, its parameters are designed according to the L-C Resonance Principle to suppress the 5th and 7th order current

harmonics, as well as higher order current harmonics, caused by the nonlinear load while it operates in rated conditions, since the eigenvalue of harmonics caused by the adopted nonlinear load is 5th and 7th order harmonics, 11th and 13th order harmonics, etc. The operational performance is not so satisfactory if the shunt passive filter operates alone, for a shunt passive filter does not employ any control algorithm and its parameters are fixed.

SIMULATION EXPERIMENTS

The simulated experimental platform of a marine electric network – including the marine synchronous generator, as well as the linear load and nonlinear load – is established. The parameters of the simulated power source are those of a synchronous generator for marine use which is made in Shanghai Electrical Machinery Plant of Shanghai Electric Group Co., Ltd. Its type is TFH-400/6 - Salient-pole synchronous generator. Its nominal data are: 400 kVA, 400 V line voltage, 50 Hz, 1000 rpm. Relevant reactance data are (pu): d-axis reactance (X_d) is 1.728, d-axis transient reactance (X_d') is 0.384, d-axis subtransient reactance (X_d'') is 0.1793, q-axis reactance (X_q) is 0.865, q-axis subtransient reactance (X_q'') is 0.181, leak reactance (X_l) is 0.113. The simulated current harmonic source is a 3-phase nonlinear load which is a 3-phase full-controlled rectification bridge circuit followed by a resistor of 10 Ω, and the trig angle of each of the 6 thyristors in the rectification bridge is 0°. The linear load is a 3-phase RL load with nominated power 20 kVA. In the shunt passive filter, the values of "L" and "C" in each phase are 2 mH and 200 microF respectively in the 5th single-tuned harmonic filter, 2 mH and 100 microF respectively in the 7th single-tuned harmonic filter, and 0.37 mH and 175 microF respectively in the high pass filter, and "R" in each phase of the high pass filter is 5Ω. For the PFC circuit and the SAPF, the capacitor in shunt connection in the DC side of the converter of both the PFC circuit and SAPF is 2 microF, while each phase reactance that connects the PFC circuit and the network, as well as the SAPF and the network,

is 5 mH. Furthermore, for the design of the SAPF, its low-pass-filtering part adopts the second filter module with its cut-off frequency 20 kHz.

The registered voltage waveform and current waveform in the sub-switchboard of the nonlinear load are shown in Fig. 3. In Fig. 3, THD$_V$ of the voltage supplied to the nonlinear load is 4.94%, THD$_I$ of the nonlinear load harmonic current is 30.55%, and the network total power factor is 0.72.

In the simulation experiment, a comparison between the operation of a combined system of shunt passive and series active power filter and the operation of the Hybrid APF/PFC/PPF Circuit is carried out. In the first step of the experiment, only a combined system of shunt passive and series active power filter operates in the simulated marine electric network. The experimental result of the network voltage and current waveforms and their spectrum are shown in Fig. 4. In the second step of the experiment, the Hybrid APF/PFC/PPF Circuit is put into operation in the simulated marine electric network. The experimental result of the network voltage and current waveforms and their spectrum are shown in Fig. 5. In Fig. 4, THD$_V$ of the voltage supplied to the nonlinear load is 3.89%, THD$_I$ of the nonlinear load harmonic current is 12.58%, and the network total power factor is 0.90. In Fig. 5, THD$_V$ of the voltage supplied to the nonlinear load is 3.13%, THD$_I$ of the nonlinear load harmonic current is 6.19%, and the network total power factor is 0.99.

In the simulation experiment, a comparison between the operation of a combined system of shunt passive and series active power filter and the operation of the Hybrid APF/PFC/PPF Circuit is carried out. In the first step of the experiment, only a combined system of shunt passive and series active power filter operates in the simulated marine electric network. The experimental result of the network voltage and current waveforms and their spectrum are shown in Fig. 4. In the second step of the experiment, the Hybrid APF/PFC/PPF Circuit is put into operation in the simulated marine electric network. The experimental result of the network voltage and current
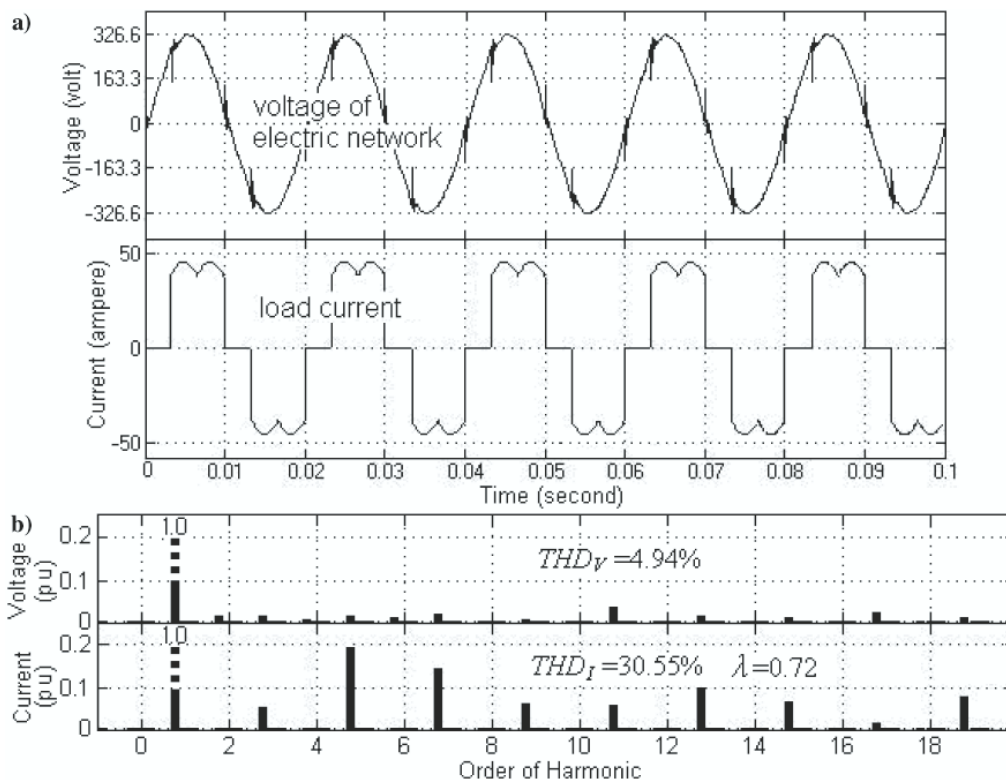
Fig. 3. *Voltage and current waveforms and spectrum of harmonic source,*
a) waveforms of network voltage and nonlinear load current, b) spectrum analysis.
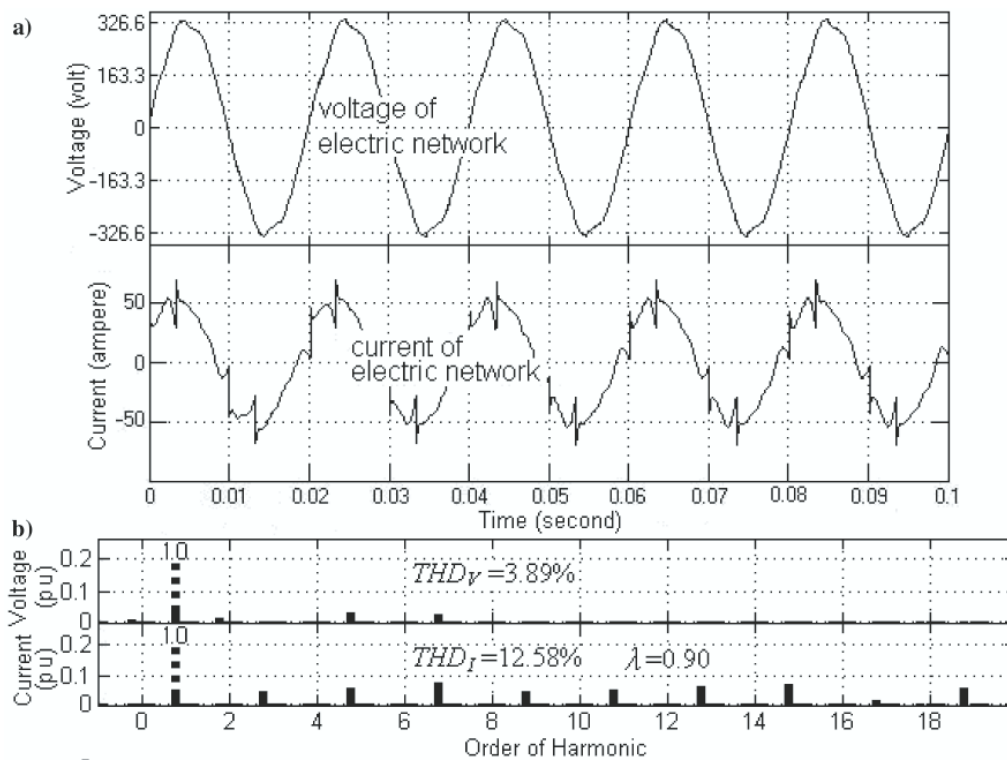
Fig. 4. Voltage and current waveforms and spectrum obtained after the operation of a combined system of shunt passive and series active power filter, a) waveforms of network voltage and current, b) spectrum analysis
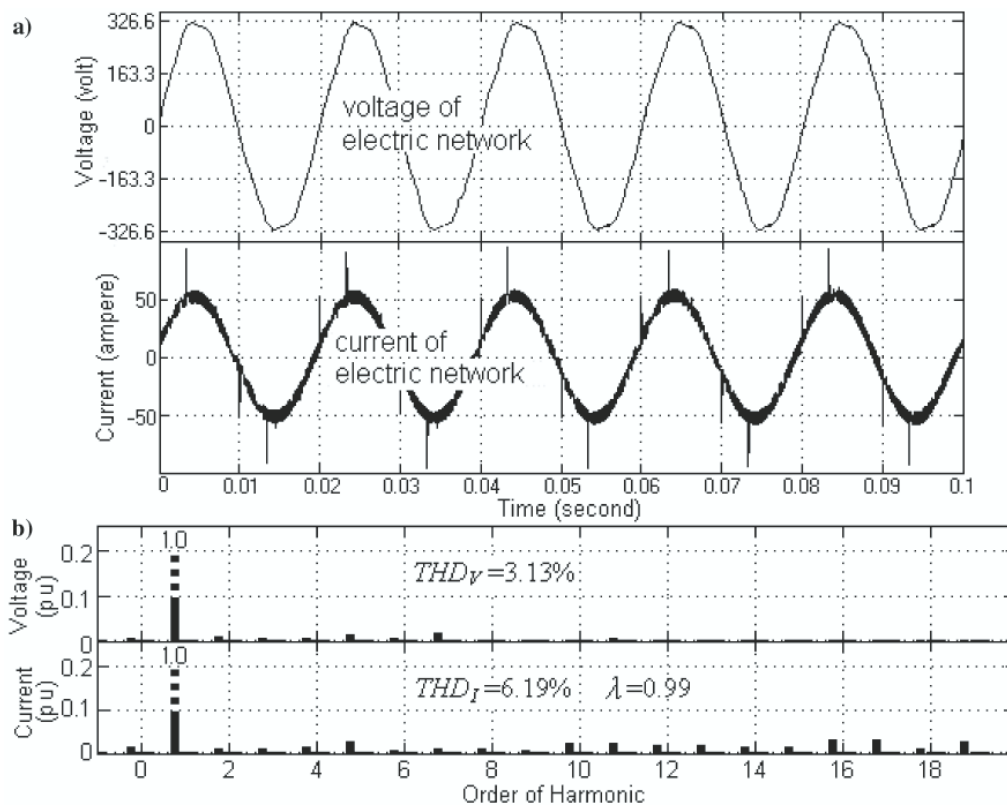
Fig. 5. Voltage and current waveforms and spectrum obtained after operation of the Hybrid APF/PFC/PPF Circuit, a) waveforms of network voltage and current, b) spectrum analysis

waveforms and their spectrum are shown in Fig. 5. In Fig. 4, THD_V of the voltage supplied to the nonlinear load is 3.89%, THD_I of the nonlinear load harmonic current is 12.58%, and the network total power factor is 0.90. In Fig. 5, THD_V of the voltage supplied to the nonlinear load is 3.13%, THD_I of the nonlinear load harmonic current is 6.19%, and the network total power factor is 0.99.

The effectiveness of the filtering circuits under consideration was evaluated not only based on their filtering properties, expressed by related THD values, but also taking into consideration such parameters as max (I_h/I_1), active power factor λ, estimated cost of realization and the influence of $\Delta f = \pm 5\% \, f_n$ (rated frequency) changes on the filtering properties. It was verified that the efficiency of a passive parallel filter (PPF) alone is compromised

when the frequency is deviating. So to improve this situation, a hybrid filter construction should be applied, but at least two criteria must be taken into account at the same time: harmonic mitigation and sensitivity to frequency deviation. The solution based on combined SAPF/PFC/PPF configuration displays the best ability for power quality improvement; however, it is quite an expensive solution and the most susceptible to the marine environment itself. It requires careful design and manufacture of hardware parts in order to be resistant to marine conditions, i.e. vibration, humidity, high temperature.

CONCLUSION

According to the comparison of the experimental results of network voltage and current waveforms and their spectrum in the environment of a simulated marine electric network, it can be concluded that the combined system of shunt passive and series active power filter is able to improve the network harmonics and power factor, but it is not adequately effective in suppressing current harmonics and improving the power factor. In contrast, application of the Hybrid APF/PFC/PPF Circuit gives satisfactory result in both voltage and current harmonics suppression and power factor correction. That is, due to the importance and complicated nature of the problem of marine electrical power quality, application of the designed Hybrid APF/PFC/PPF Circuit to a marine electric network to improve the problem of harmonics and low power factor is a reasonable choice since it shows considerable merits in harmonic suppression and power factor correction in the environment of a marine electric network.

Acknowledgment

BIBLIOGRAPHY

1. Akagi, H., Kanazawa, Y., and Nabae, A.: 'Instantaneous reactive power compensators comprising switching devices without energy storage components', *IEEE Trans. Industry Applications*, 20, (3), pp. 625–630, 1984
2. Arrillaga, J., Watson, N. R., and Chen, S.: '*Power System Quality Assessment*' (UK: John Wiley & Sons, 2000)
3. Chang, G. W., and Chen, W. C.: 'A new reference compensation voltage strategy for series active power filter control', *IEEE Trans. Power Delivery*, 21, (3), pp. 1754-1756, 2006
4. China Classification Society, '*Guide for Harmonic Control in Ocean Ships – in Criterion of steel ocean ship classification and construction (Fascicle No. 4)*' (Beijing: People's communications press, 2001), pp. 4-6, 2001
5. IEC 61000-3-3: '*Electromagnetic Compatibility (EMC)*, Part 3-3: Limits – Limitation of voltage changes, voltage fluctuation and flicker in public low-voltage supply systems, for equipment with rated current <=16A per phase and not subject to conditional connection', 2002
6. Kilic, T., Milun, S., and Petrovic, G.: 'Design and implementation of predictive filtering system for current reference generation of active power filter', *Electrical Power and Energy Systems*, 29, (2), pp. 106–112, 2007
7. Kim S., and Enjeti, P. N.: 'A new hybrid active power filter (APF) topology', IEEE Trans. Power Electronics, 17, (1), pp. 48-54, 2002
8. Luo, S., Hou, Z.: 'An adaptive detecting method for harmonic and reactive currents', *IEEE Trans. Industrial Electronics*, 42, (1), pp. 85-89, 1995
9. Mindykowski, J.: 'Assessment and improvement of electric power quality in ships' modern systems', *Proc. 2003 Int. Marine Electrotechnology Conf. and Exhibition*, Shanghai, China, Sep., pp. 8-21, 2003
10. Mindykowski, J. '*Assessment of Electric Power Quality in Ship System Fitted with Converter Subsystem*' (Gdansk: Press of Shipbuilding and Shipping Ltd, 2003), pp. 1-2, 2003
11. Mindykowski, J., and Tarasiuk, T.: 'Electrical energy quality under ship's conditions'. *Proc. 16th IMEKO World Congress*, Vienna, vol. 7, pp. 245-250, 2000
12. Peng, F. Z., Akagi, H., and Nabae, A.: 'A new approach to harmonic compensation in power systems – a combined system of shunt passive and series active filters', *IEEE Trans. Industry Applications*, 26, (6), pp. 983-990, 1990
13. Pertinent rules and requirements of selected classification institutions: '*ABS*, *DNV*, *IACS*, *LR*, *NKK*, *RS*', (Continuously updated)
14. Lloyd's Register of Shipping: '*Rules and Regulations for Classification of Ships*. Part 6, Electrical Engineering', 1996. updated 1998.
15. Salmeron, P., Herrera, R. S., and Vazquez, J. R.: 'A new approach for three-phase loads compensation based on the instantaneous reactive power theory', *Electric Power Systems Research*, 78, (4), pp. 605–617, 2008
16. Tarasiuk, T., Mindykowski, J., and Xu, X.: 'Facing a problem of electrical energy quality in ship networks – measurement, estimation, control', *J. Shanghai Maritime University*, 24, (3), pp. 193-199, 2003
17. IACS Requirements: '*Test Specification*', 10th Edition (1991), Revision 2.1 (1999), Revision 3 (2000).
18. Wakileh, G. J.: '*Power Systems Harmonics – Fundamentals, Analysis and Filter Design*' (Beijing: China Machine Press, 2003)
19. Yang, J., and Wang, Z.: 'A study on the comparison of two methods used to detect the harmonic currents of three-phase circuits', *Trans. China Electrotechnical Society*, 10, (5), pp. 43-48, 1995

CONTACT WITH THE AUTHORS

Xiao-Yan Xu, Prof.
e-mail: xuxy@shmtu.edu.cn
Department of Mechatronics Engineering, Shanghai Maritime University, Shanghai 200135, China.
Janusz Mindykowski, Prof.
e-mail: janmind@am.gdynia.pl
Faculty of Marine Electrical Engineering,
Gdynia Maritime University,
81-225 Gdynia, POLAND.
C. L. Philip Chen, Prof.
e-mail: Philip.Chen@ieee.org
Faculty of Science and Technology,
University of Macau, Macau, China.

The Ship Handling Research and Training Centre at Ilawa is owned by the Foundation for Safety of Navigation and Environment Protection, which is a joint venture between the Gdynia Maritime University, the Gdansk University of Technology and the City of Ilawa.

Two main fields of activity of the Foundation are:

➲ Training on ship handling. Since 1980 more than 2500 ship masters and pilots from 35 countries were trained at Iława Centre. The Foundation for Safety of Navigation and Environment Protection, being non-profit organisation is reinvesting all spare funds in new facilities and each year to the existing facilities new models and new training areas were added. Existing training models each year are also modernised, that's why at present the Centre represents a modern facility perfectly capable to perform training on ship handling of shipmasters, pilots and tug masters.

➲ Research on ship's manoeuvrability. Many experimental and theoretical research programmes covering different problems of manoeuvrability (including human effect, harbour and waterway design) are successfully realised at the Centre.

The Foundation possesses ISO 9001 quality certificate.

Why training on ship handling?

The safe handling of ships depends on many factors - on ship's manoeuvring characteristics, human factor (operator experience and skill, his behaviour in stressed situation, etc.), actual environmental conditions, and degree of water area restriction.

Results of analysis of CRG (collisions, rammings and groundings) casualties show that in one third of all the human error is involved, and the same amount of CRG casualties is attributed to the poor controllability of ships. Training on ship handling is largely recommended by IMO as one of the most effective method for improving the safety at sea. The goal of the above training is to gain theoretical and practical knowledge on ship handling in a wide number of different situations met in practice at sea.

For further information please contact:
The Foundation for Safety of Navigation and Environment Protection

Head office:
36, Chrzanowskiego Street
80-278 GDAŃSK, POLAND
tel./fax: +48 (0) 58 341 59 19

Ship Handling Centre:
14-200 IŁAWA-KAMIONKA, POLAND
tel./fax: +48 (0) 89 648 74 90
e-mail: office@ilawashiphandling.com.pl
e-mail: office@portilawa.com

GDANSK UNIVERSITY OF TECHNOLOGY

is the oldest and largest scientific and technological academic institution in the Pomeranian region. The history of Gdansk University of Technology is marked by two basic dates, namely: October 6, 1904 and May 24, 1945.

The first date is connected with the beginning of the technical education at academic level in Gdansk. The second date is connected with establishing of Gdansk University of Technology, Polish state academic university. Gdansk University of Technology employ 2,500 staff, 1,200 whom are academics. The number of students approximates 20,000, most of them studying full-time. Their career choices vary from Architecture to Business and Management, from Mathematics and Computer Science to Biotechnology and Environmental Engineering, from Applied Chemistry to Geodesics and Transport, from Ocean Engineering to Mechanical Engineering and Ship Technology, from Civil Engineering to Telecommunication, Electrical and Control Engineering. Their life goals, however, are much the same - to meet the challenge of the changing world. The educational opportunities offered by our faculties are much wider than those of other Polish Technical universities, and the scientific research areas include all of 21st Century technology. We are one of the best schools in Poland and one of the best known schools in Europe – one that educates specialists excelling in the programming technology and computer methods used in solving complicated scientific, engineering, organizational and economic problems.

THE FACULTY OF OCEAN ENGINEERING AND SHIP TECHNOLOGY

The Faculty of Ocean Engineering and Ship Technology (FOEST) as the only faculty in Poland since the beginning of 1945 has continuously been educating engineers and doctors in the field of Naval Architecture and Marine Technology.

The educational and training activities of FOEST are supported by cooperation with Polish and foreign universities, membership in different international organizations and associations, as well as participation in scientific conferences and symposia. Hosting young scientists and students from different countries is also a usual practice in FOEST.

The activities of Faculty departments are related to: mechanics and strength of structures, hydromechanics, manufacturing, materials and system quality, power plants, equipment and systems of automatic control, mostly in shipbuilding, marine engineering and energetic systems.

FOEST is a member of such organizations like WEGEMT; The Association of Polish Maritime Industries and the co-operation between Nordic Maritime Universities and Det Norske Veritas. The intensive teaching is complemented and supported by extensive research activities, the core of which is performed in close collaboration between FOEST staff and industry. We take great care to ensure that the applied research meet both the long term and short term needs of Polish maritime industry. FOEST collaborates with almost all Polish shipyards. Close links are maintained with other research organizations and research institutions supporting the Polish maritime industry, such as Ship Design and Research Centre and Polish Register of Shipping, where several members of the Faculty are also members of the Technical Board.

The Faculty of Ocean Engineering and Ship Technology is a unique academic structure, which possesses numerous highly qualified and experienced staff in all above mentioned specific research areas. Moreover, the staff is used to effective co-operation and exchange of ideas between specialists of different detailed areas. This enables a more integrated and comprehensive treatment of research and practical problems encountered in such a complicated field of activity as naval architecture, shipbuilding and marine engineering.

The staff of the Faculty has strong international links worldwide, being members or cooperating with international organizations like International Maritime Organization IMO, International Towing Tank Conference ITTC, International Ship and Offshore Structures Congress ISSC, International Conference on Practical Design of Ship and other floating Structures PRADS just to name a few.

GDANSK UNIVERSITY OF TECHNOLOGY
Faculty of Ocean Engineering and Ship Technology
11/12 Narutowicza Street, 80-952 Gdansk, Poland
Tel (+48) 58 347 1548 ; Fax (+48) 58 341 4712
e-mail: sekoce@pg.gda.pl

www.oce.pg.gda.pl